SAPIENZA
UNIVERSITÀ DI ROMA

Dipartimento di Chimica e Tecnologie del Farmaco

PhD Thesis

Attractive approach in anticancer therapy: A challenge posed by natural products

Presented by
Elisa De Paolis

Supervisor:
Prof. Dr. Bruno Botta

Dottorato di Ricerca in Scienze Farmaceutiche – XXXI Ciclo

Abstract

This PhD thesis is focused on two main topics:

Part A. Total synthesis, biological evaluation and SAR studies of Smo and Gli antagonists

Hedgehog (Hh) signaling pathway is essential for tissue homeostasis, development and stemness. Since Hh pathway possesses a critical role in cancer initiation, proliferation, metastasis, chemoresistance and in the survival of CSCs, its constituents represent attractive druggable targets for anticancer therapy. With the aim to inhibit the pathway at the upstream receptor Smoothened (Smo) or the downstream effector Gli1, small molecules as emerged as promising anticancer agents.
The natural isoflavone Glabrescione B (GlaB) emerged as the first small molecule binding to Gli1 zinc-finger and debilitating Gli1 activity by interfering with its interaction with DNA.
Here, taking advantage by the versatile isoflavone scaffold, we have designed, synthesized and tested new Hh inhibitors. The rational introduction of defined substitutions on the isoflavone's ring B, led us to identify molecules targeting preferentially Gli1 or Smo. Thanks to a multidisciplinary approach, combining chemical, biological and molecular docking fields, it was possible obtain new insights into the mechanism of action of these molecules. The co-administration of two different isoflavones behaving as Smo and Gli antagonists in primary mudulloblastoma (MB) cells, emphasized the synergistic effects of these agents, hence paving the way to additional and innovative strategies for the pharmacological inhibition of Hh signaling.

Part B. Toward the total synthesis of madangamine B

Marine natural products show increasing interest in biological, ecological, pharmacological and chemical fields. Since their secondary metabolites possess structures not identified in terrestrial organisms, endowed by significant biological activities, they are intriguing candidates as lead compound for drug discovery.

Madangamines (A-F), a class of diazapentacyclic alkaloids, were discovered (A-E) by Andersen and co-workers since 1992 from a sponge of the genus *Haposclerida*, family *Petrosiidae*, collected off Madang, in Papua New Guinea. The same authors reported in 1994 the isolation of madangamine A, found in the marine sponge *Xestospongia ingens*, and few years later they described four new related alkaloids, labelled madangamines B-E. It had to wait until 2005 to reach the isolation of madangamine F from *Pachychalina alcaloidifera*, accomplished by Berlinck and co-workers and reported in 2007.
Pure madangamines A-C and F were isolated as optically active compounds; madangamines D and E were isolated as inseparable mixture.
Until 2014 the absolute configuration of madangamines was only presumed, and it has been hypothesized on the basis of an ingenamine, which is considered a putative precursor of madangamines.

The assignment of the absolute configuration of (+)-madangamine D is based on its first total synthesis by Amat and co-workers. As had been described for the natural products, synthetic madangamine D has been found dextrorotatory, having unambiguous 2*S*, 5*S*, 9*R*, 12*R* absolute configuration of this alkaloid family.
Madangamines A and F exhibited, *in vitro*, μM IC_{50} values against a multitude of cancer cell lines, both human and murine's ones. Thanks to the collaboration with *PharmaMar Company* it was been possible test the activity of madangamine D, that exhibited *in vitro* significant cytotoxic activity against pancreas (GI_{50} 7.4 μg/mL) and colon cancers (GI_{50} 4.4 μg/mL).

Table of Contents

List of Compounds

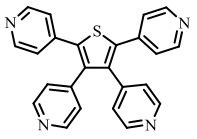

I

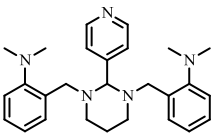

II

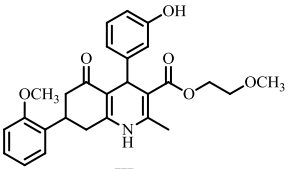

III

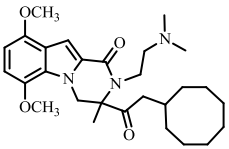

IV

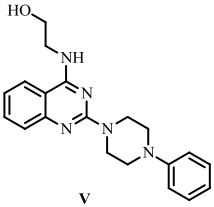

V

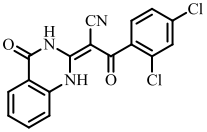

VI

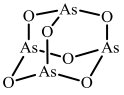

VII

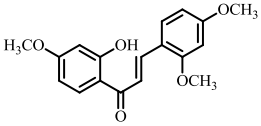

VIII

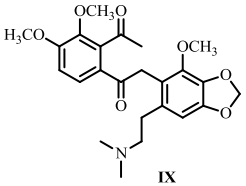

IX

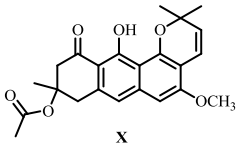

X

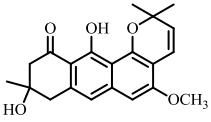

XI

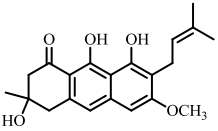

XII

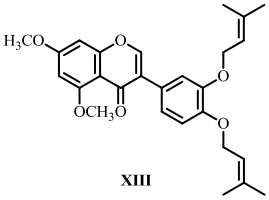

XIII

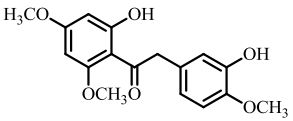

3a

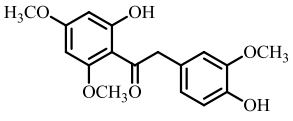

3b

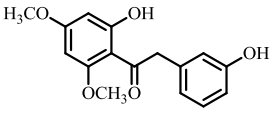

3c

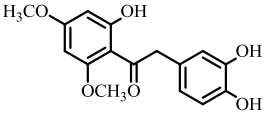

3d

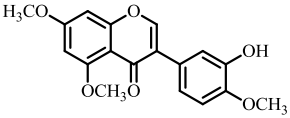

4a

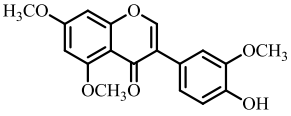

4b

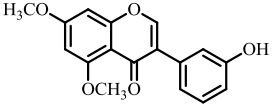

4c

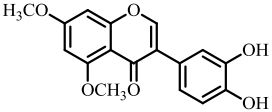

4d

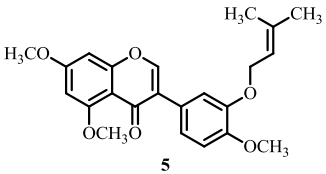

5

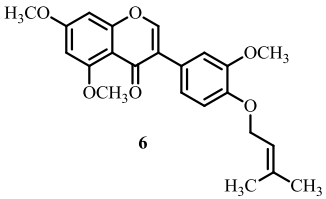

6

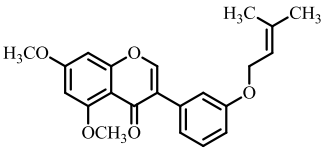

7

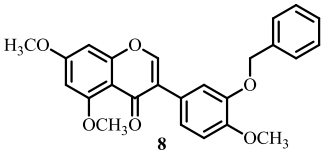

8

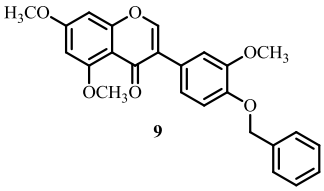

9

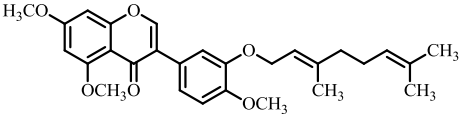

10

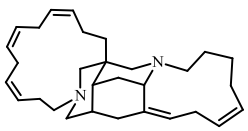

20

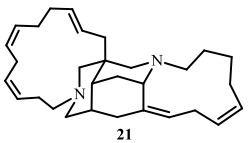

21

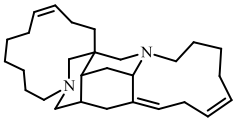

22

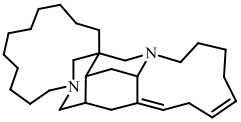

23

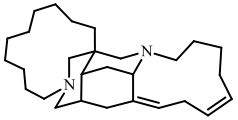

24

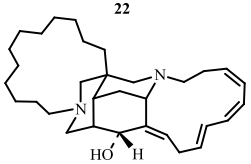

25

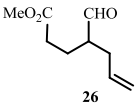

26

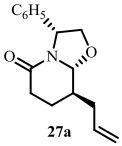

27a

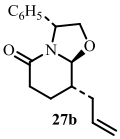

27b

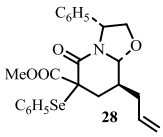

28

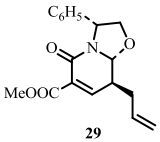

29

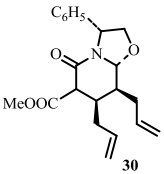

30

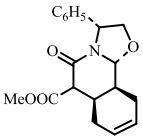

31

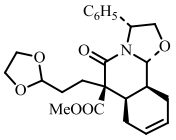

32

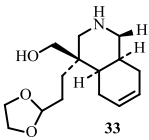

33

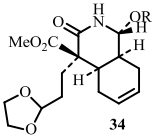

34

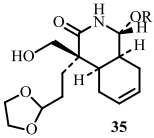

35

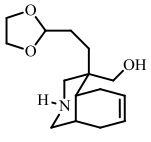

36

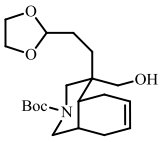

37

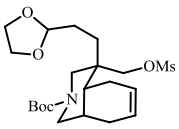

38

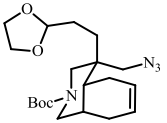

39

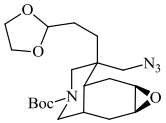

40

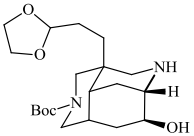

41

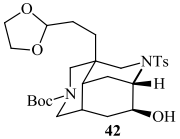

42

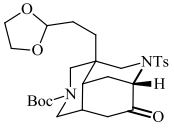

43

44

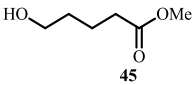

45

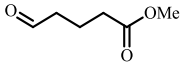

46

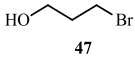

47

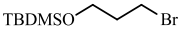

48

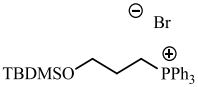

49

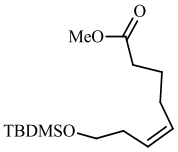

50

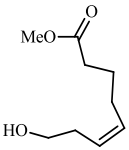

51

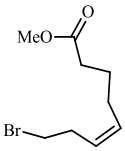

52

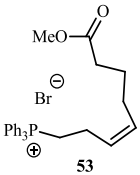

53

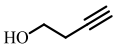

54

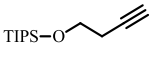

55

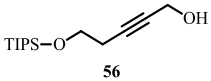

56

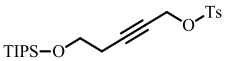

57

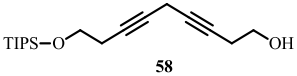

58

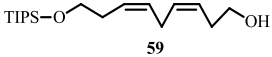

59

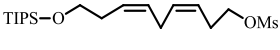

60

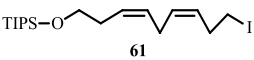

61

62

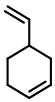

63

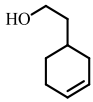

64

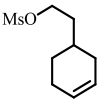

65

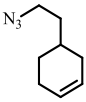

66

67

68

69

List of Abbreviations, Acronyms and Symbols

A

$[a]_D^T$	specific rotation at temperature T at the sodium D line
Å	Ångstrom
Ac	acetyl
ALL	acute lymphoblastic leukemia
AML	acute myeloid leukemia
ATO	arsenic trioxide
Ax	axial

B

BCC	basal cell carcinoma
Boc	*t*-butoxycarbonyl
Bn	benzyl
br	broadened (signal)
Bu	butyl
BuLi	butyl lithium

C

ca.	about, approximately
°C	Celsius degree
Calcd.	calculated
Celite® filtration agent	(90% SiO2, 4% Al2O3, 3.3% Na2O and K2O, 1.3% Fe2O3, 0.5% CaO)
CI	chemical ionization
CK1-α	casein kinase 1 α
13C-NMR	carbon-13 nuclear magnetic resonance
COSY	H-H correlation spectroscopy
m-CPBA	meta-chloroperoxybenzoic acid
CSC	cancer stem cell

D

δ	NMR chemical shift in ppm

ΔG	delta energy
d	doublet or days
Da	Dalton
DCM	dichloromethane
dd	doublet of doublets
Dhh	Desert Hedgehog
dm	doublet of multiplets
DMAP	4-dimethylamino pyridine
DMF	*N*,*N*-dimethylformamide
DMP	Dess–Martin periodinane
DMSO	dimethyl sulfoxide
DNA	deoxyribonucleic acid
dt	doublet of triplets

E

EDA	ethylendiamine
ED_{50}	dose effective in 50% of tests subjects
EI	electron ionization
epi	epimeric
eq.	equatorial
equiv.	equivalent
ESI	electrospray ionization
Et	ethyl
Et_2O	diethyl ether
EtOAc	ethyl acetate
EtOH	ethanol

F

F	phenylalanine
FC	flash chromatography
FDA	Food and Drug Administration
FT-ICR	Fourier transform ion cyclotron resonance
Funct	functionalization

G

g	gram
GI_{50}	half maximal growth inhibitory concentration
GlaB	glabrescione B
Gli	glioma associated oncogene
GSK3-β	glycogen synthase kinase 3 β
GST	glutathione S-transferases

H

H	histidine
h	hour
HCC	hepatocellular carcinoma
HEK	human embryonic kidney
n-Hex	hexane
Hh	hedgehog
HPI	hedgehog pathway inhibitor
HPLC	high-performance liquid chromatography
HRMS	high resolution mass spectrometry
HSQC	H-C heteronuclear single quantum correlation
Hz	Hertz (s^{-1})
^{1}H-NMR	proton nuclear magnetic resonance

I

i	*iso*
IC_{50}	half maximal inhibitory concentration
IGF	insulin-like growth factor
Ihh	indian hedgehog
IL-6	interleukin-6
ImH	imidazole
IR	infrared

J

J	coupling constant

K

K	lysine
KHMDS	Potassium-bis(trismethylsilys)amide
L	
L	lysine
LiAlH4	lithium aluminum hydride
LiHMDS	lithium bis(trismethylsilyl)amide
M	
M	molar/methionine
M^+	molecular ion
μ	micro1
m	multiplet
MB	medulloblastoma
MD	molecular dynamics
MDA	microtubule destabilizing agent
Me	methyl
MEF	mouse embryonic fibroblasts
MeOH	methanol
mg	milligram
MHz	Megahertz
min	minute
mL	milliliter
mM	millimole per liter
mmol	millimole
μL	microliter
Mp	melting point
MS	mass spectrometry
M.S.	molecular sieves
Ms	methanesulfonyl (mesyl)
m/z	mass to charge ratio
N	
n	normal
NaHMDS	sodium bis(trimethylsilyl amide)
NaOAc	sodium acetate
NCI	National Cancer Institute

NEt_3	triethyl amine
ng	nanogram
nM	nanomol per liter
NMR	nuclear magnetic resonance
Nu	nucleophile
O	
o-	orto-
P	
p-	para
PCC	pyridinium chlorocromate
PDC	pyridinium dichromate
PE	petroleum ether
PG	Protecting group
Ph	phenyl
PhD	doctor of philosophy
P_i	inorganic phosphate
PKA	protein kinase A
ppm	parts per million
PPTS	pyridinium *para*-toluenesulfonate
Ptch1	protein patched homolog 1
py	pyridine
Q	
q	quartet
R	
R	arginine
R-	generalized alkyl group or substituent
R_f	retention factor
RCM	Ring Closing Metathesis
RNA	ribonucleic acid
rt	room temperature
S	
s	second or singlet
SAR	structure-activity relationship
sas/ss	Saturated solution

SC	stem cell
SD	standard deviation
Shh	sonic hedgehog
Smo	smoothened
SuFu	suppressor of fused homolog
T	
T	threonine
t	triplet
t	*tert*
TBAI	tetrabutylammonium iodide
TBDMS	*t*-butyldimethylsilyl
td	triples of doublet
THF	tetrahydrofuran
TIPSCl	Triisopropylsilyl chloride
TLC	thin layer chromatography
TMS	trimethylsilyl
TsCl	*p*-toluensulfonyl chloride
U	
USA	United States of America
UV	ultraviolet
V	
VEGF	vascular endothelial growth factor
W	
W	triptofane
WT	wild type
X	
-	-
Y	
-	-
Z	
ZF	zinc finger

Part A

Total synthesis, biological evaluation, and SAR studies of Smo and Gli antagonists

The present part of the thesis deals with a research activity carried out at the Dipartimento di Chimica e Tecnologie del Farmaco at Sapienza Università di Roma, under the supervision of Prof. Bruno Botta.

Chapter A1

General Introduction

A1.1 Natural Products as Anticancer Agents

Modern pharmaceutical research strongly relies on the investigation and identification of innovative lead compounds. In this context, natural products have proven to be extremely promising for anticancer drug discovery.

In the 1950s, the U.S. National Cancer Institute (NCI) established a screening of about 35000 plant samples to rate their growth inhibitory effects against the mouse leukemia cell lines L1210 and P388, respectively. From this screening, paclitaxel (Taxol™), isolated from the bark of the Pacific yew *Taxus brevifolia*, emerged as the most significative drug. By 1985, the NCI carried on that screening against 60 human cancer cell lines, including cell lines derived from solid cancers (i. e. lung, colon, skin, ovary, brain, prostate cancers, leukemia too). In such screening were entailed extracts from plants, animals, microorganisms and co-products derived from microorganisms of marine origin[1]. NCI research to support the discovery of new natural anticancer agents is still ongoing.

To give a practical example of the importance of natural products in anticancer therapy, by 2010, the 52% of the 178 new drugs approved for the treatment of cancers are originated from natural products. In particular, 14% are non-modified natural products, 27% modified natural products, and 11% synthetic compounds obtained after natural product optimization[2]. The latter point emphasizes the

role of natural products as suitable templates for drug design; in fact, even if a natural product is not an effective drug itself, it still may be a good starting material for further improvements.

The major problem encountered during the development of natural products as new drugs is to find out a scalable and inexpensive route to obtain the desired material. Extraction processes allow to achieve very low quantities of natural product. The problem should be overcome by large-scale fermentation, but for some organisms it is not so easy. On the other hand, the chemical synthesis of natural compounds and their analogues could be very effective to solve the abovementioned problems; especially, the total synthesis allows the preparation of natural product derivatives employable for the structure-activity-relationship (SAR) studies, which are very difficult to perform on semi-synthetic intermediates[3].

In conclusion, the abundance of substances driven by plants and marine organisms allows us to exert them as starting products as drug design templates.

A1.2 Inhibition of the Hedgehog Signaling Pathway: a Challenge Posed by Natural products

A1.2.1 Cancer Stem Cells Theory

A1.2.1.1 The Hypotesis

Even if the concept that cancer might arise from a population of stem-like cells was proposed about 150 years ago, only in the last 40 years cancer research has demonstrated that tumor cells are very different. The official definition is[4]:

"A cell within a tumor that possess the capacity
To self-renew and to cause the heterogeneous
Lineages of cancer cell that comprise the tumor[4] *".*

Cancer stem cells (CSCs) can thus be defined experimentally by their ability to regenerate a continuously growing tumor. Heterogeneous populations of cancer cells at various differentiation stages could be the result of both acquired mutations and aberrant but hierarchical differentiation schemes. Cancer is both a differentiation and a proliferation disease, and the 'clonal evolution' and 'cancer stem cell' models might not be mutually exclusive, as initially thought. Owing to genetic instability, the tumor-initiating cells isolated from a clinically detectable tumor would probably have an essentially

different genomic pattern from the initial transformed cells that originated the tumor[5].

CSCs habitually display resistance to traditional chemotherapy and they seem to be responsible of cancer initiation, recurrence and metastasis, due to their asymmetric divisions, ability to drug efflux, immortality, and mesenchymal phenotype. Hence, the possibility to identify and isolate these cells has provided a promising opportunity for novel therapeutic strategies that tender the conventional cancer therapy a tip of the iceberg of anticancer approach. A salient point in this context is that proliferation is not synonymous with self-renewal; a self-renewing cell division results in one or both daughter cells which have essentially the same ability to replicate and generate differentiated cell descents as the parental cell. Stem cells have the ability to undergo a symmetrical self-renewing cell division, causing identical daughter stem cells, which preserve self-renewal capability, or an asymmetrical self-renewing cell division, resulting in one stem cell and more differentiated progenitor cells. As well, it seems that stem cells may divide symmetrically to form two progenitor cells, which could lead to stem cell depletion[4]. This form of division would be a way to deplete the cancer stem population and may constitute a promising strategy to inducing cell death in cancer[4].

A1.2.1.2 Therapeutic Strategies

At the moment, various therapeutic strategies are able to target tumor-initiating cells. Killing these cells can be accomplished by inhibiting their survival pathways or sensitizing them to chemotherapeutic agents. Current failure with cancer treatment is not usually due to the lack of primary response or initial induction of remission, but to relapse or tumor recurrence after therapy, in which tumor-initiating cells seem to play a critical role. If therapies can be targeted against CSCs, this will tender the tumor unable to maintain themselves or grow. The promising approaches to kill tumor-initiating cells include blocking essential self-renewal signaling, inhibiting the survival mechanisms of these cells, or targeting tumor-initiating cell surface markers through antibody-based cytotoxic approaches[6]. Alternatively, differentiating the CSCs might be a successful therapeutic strategy as the bulk of the tumor has limited proliferative potential[7].

Obviously, targeting CSCs alone may not be sufficient to get effective cures or long-term remission for most cancers; a promising solution to eradicate both cancer cells and cancer stem cells is represented by a combined therapy, using both conventional chemotherapeutic drugs with an agent capable to target CSCs. Additionally, since the use of active agents targeting a single hit might lead to resistance phenomena, the most rational solution to target

CSCs is represented by the employment of a multi-target anti CSCs therapy[8] (Figure 1).

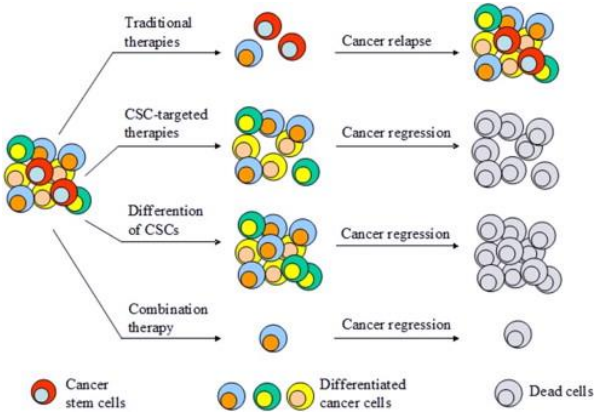

Figure 1 Conventional therapies vs CSCs therapies[9] (Reproduced with permission).

Several signaling pathways that regulate normal stem cells can cause neoplastic proliferation when dysregulated by mutation. In tumor initiating cells those pathways may be constitutively activated or improperly regulated, leading to uncontrolled growth. Developmental signaling pathway responsible for normal stem cell self-renewal, including Wnt, Hedgehog (Hh) and Notch have been shown to be active in several cancers[12] (Figure 2).

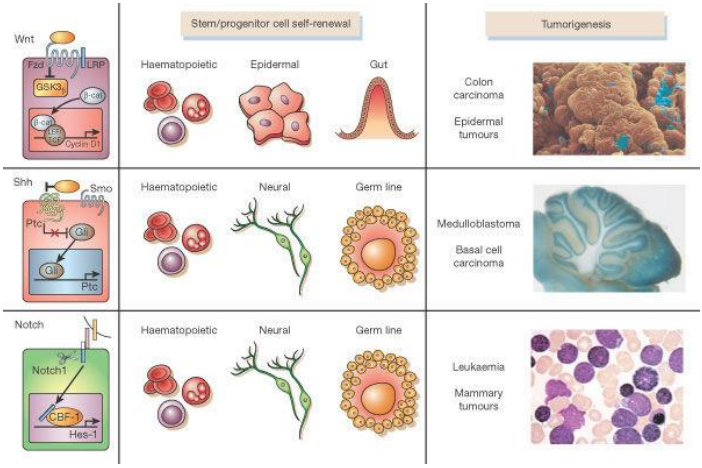

Figure 2 Wnt, Shh and Notch pathways: their contribution in the self-renewal of stem cells and/or progenitors, and in tumorigenesis[10] (Reproduced with permission).

A1.3 The Hedgehog Signaling Pathway

The Hh signaling pathway controls tissue polarity, patterning and stem cell maintenance. In 1980 Christiane Nusslein-Volhard and Eric F. Weischaus identified the Hedgehog gene (Hh) by genetic screens in *Drosophila Melanogaster*. It earned its name from the appearance of embryos with null alleles of Hh, which display a larval of disorganized, hair-like bristles reminiscent of hedgehog spines. The vertebrate genome duplication has resulted its expansion of the Hh genes, which can be classified into: Desert (Dhh), Indian (Ihh) and Sonic (Shh) groups. The Shh activity and effects are the largest studied in vertebrates field.

A1.3.1 The Pathway

The precise mechanism of Hh signaling pathway is not totally understood. Hh pathway activation starts when the ligand Hh, released from the cells through the transmembrane transporter Dispatched, binds the transembrane receptor Patched1 (Ptch1). Constitutively, Ptch1 inhibits the membrane receptor Smoothened (Smo) by preventing its location to the primary cilium (Figure 3a). In the presence of Hh, the Ptch1 loses its inhibitory activity against Smo, Hh-Ptch1 complex is internalized, allowing Smo activation. Translocation of Smo to the primary cilium originates a signaling cascade leading to the activation of glioma associated oncogene (Gli) family of zinc-finger transcription factors (Gli1, Gli2 and Gli3), the final effectors of the pathway. *In vivo*, Gli1 acts predominantly as an activator, Gli3 acts predominantly as repressor and Gli2 possesses both repressive and activator functions. Activated Glis translocate into the nucleus to induce the expression of various specific genes, such as those encoding the D-type cyclins, *c-MYC* (also knowns as *MYC*), *BCL2* and *SNAIL* (also called *SNAI*), which regulate cellular differentiation, proliferation and survival[13, 14]. Moreover, Hh target genes include *Gli1*, *PTCH1*, and the gene encoding Hh-interacting protein[15]. The signaling of Gli is also regulated by several protein mediators (PKA, GSK3-β, CK1-α) including suppressor of fused (SuFu). SuFu behaves as a negative regulator of the Hh pathway by sequestering Gli in the

cytoplasm, thus repressing transcriptional activation by these factors[16, 17] (Figure 3b).

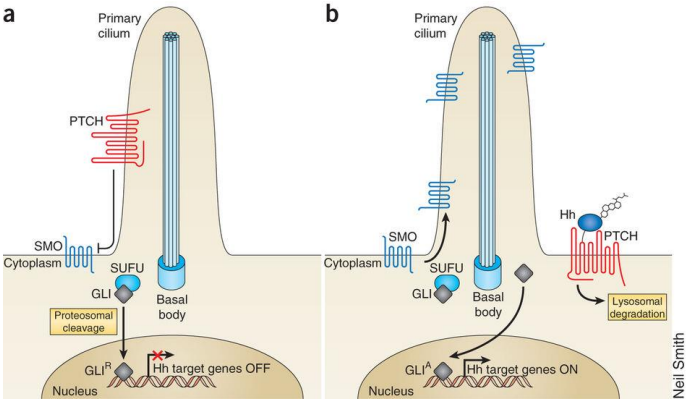

Figure 3 Hh pathway activation. (a) Inactive Hh pathway. (b) Activated Hh pathway[18] (Reproduced with permission).

A1.3.2 Alteration of the Hedgehog Pathway and Cancer

In recent years, several studies emphasized with disarmingly clarity the correlation between the aberrant activation of the Hh pathway and cancer.

Meanwhile during the embryonic phase Hh is fundamental in development and tissue homeostasis, in adults the pathway is activated during tissue repairing[19]. Hh pathway mutation or dysregulation in adults plays a crucial role in the proliferation and differentiation, inducing to tumorigenesis or tumor growth acceleration. Basal cell carcinoma (BCC) and medulloblastoma (MB) are two well-

recognized cancers with mutations in components of the Hh pathway. Inappropriate activation of the Hh signaling pathway has been implicated in the development of several other types of cancer including lung, prostate, breast, and pancreas, as examples[20-22]. According to recent suggestions, it seems that Hh might also promote tumorigenesis by signaling in a paracrine manner from the tumor to surrounding stroma, or in cancer stem cells.

Three basic models have been proposed for the Hh pathway activity in cancer (Figure 4)[13, 23].

- **Type I: ligand-independent**

The first discovered were the type I cancers harbouring Hh pathway-activating mutations which are Hh ligand independent, such as BCCs and MBs (figure 4a). Most of these tumors either had inactivating mutations in Ptch1 (85%) or activating mutations in Smo (10%)[24]. Furthermore, about one third of all medulloblastomas and occasional rhabdomyosarcomas were shown to have inappropriate Hh pathway activation, often due to Ptch1 mutations or sometimes due to SuFu mutations[25, 26]. Since these tumors are ligand independent, Hh pathway inhibitors must act at or below the level of Smo to be effective.

- **Type II: ligand-dependent autocrine mechanism**

Autocrine activation of the Hh pathway in tumor cells through increased Hh ligand expression has been reported in a variety of

tumors, such as lung, breast, stomach and prostate cancers[27] (Figure 4b). The relevance of this mechanism is not clearly understood, and most of these tumors are dissimilar to BCC or MBs; indeed they do not harbor any somatic mutations in the Hh signaling pathway. Rather, they demonstrate an autocrine, ligand-dependent, abnormal Hh pathway activation. Most of these tumors have an elevated expression of the Hh ligand (Shh or Ihh) and/or ectopic Ptch1 and Gli expression within the epithelial compartment. This autocrine tumor growth can be effectively suppressed by various pathway inhibitors such as Hh neutralizing antibodies or Smo antagonists.

- **Type III: ligand-dependent paracrine mechanism**

In contrast to the autocrine model, Bushman and colleagues were the first to propose that at least one model of prostate cancer signals in a paracrine manner to the stroma[28]. In paracrine signaling, Hh produced by the tumor cells is received by the stroma, which feeds other signals back to the tumor to promote its growth or survival (Figure 4c). The precise mechanisms by which the Hh-stimulated stroma positively regulates tumor cell growth are not completely understood.

However, it has been proposed that Hh regulates signaling mediators in the stroma, including insulin-like growth factor (IGF), Wnt, interleukin-6 (IL-6) and vascular endothelial growth factor

(VEGF), which in turn promote tumor growth. Inhibition of this paracrine signaling in epithelial tumors may be of therapeutic value, as specific inhibition of Hh signaling in the stroma did result in growth inhibition of tumor xenografts, although the most effective way of treating these tumors would possibly be to use a combination of a Hh pathway inhibitor to target the stroma and other drugs to target the tumor cells.

- **Tipe IIIb: reverse paracrine mechanism**

Very recently, a "reverse paracrine" signaling model has also been recognized in which Hh is secreted from the stroma and is received by the tumor cells (Figure 4d). In this model, stromal Hh is thought to provide the appropriate microenvironment for potentiating tumor growth and would thus be a suitable therapeutic target as well[27].

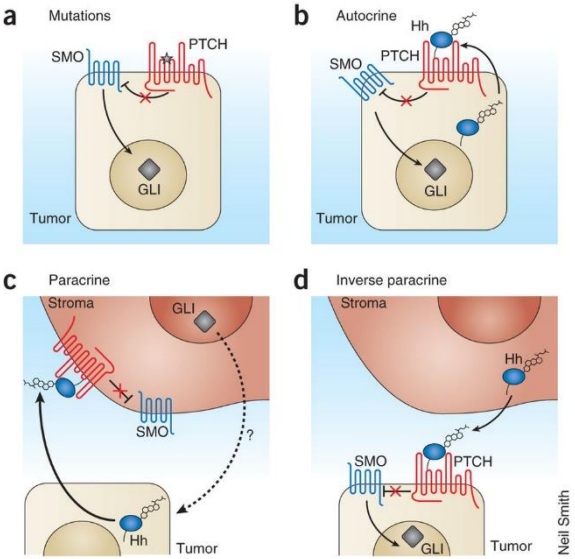

Figure 4 Different models of Hedgehog pathway activation in cancers. (a) Type I ligand-independent cancers. (b) Type II ligand-dependent autocrine cancers. (c) Type III ligand-dependent paracrine cancers. (d) Type IIIb reverse paracrine tumors[18] *(Reproduced with permission).*

A1.4 Hedgehog Pathway and Cancer Stem Cells

Considerably, Hh signaling is active in CSCs of various types of cancer, sustaining the proliferation of these cells, which are considered responsible of tumor relapse and resistance to conventional anticancer therapies. In fact, the Hh pathway controls the functional properties of CSCs, such as self- renewal, survival, metastatic spread, and neoangiogenesis, by the regulation of stemness-determining genes such as *Nanog*, often overexpresses in cancer. Since increasing evidences support the crucial role of the Hh pathway in cancer

initiation, proliferation, metastasis, chemoresistance, and in the survival of CSCs[19, 29], its components represent attractive druggable targets for anticancer therapy.

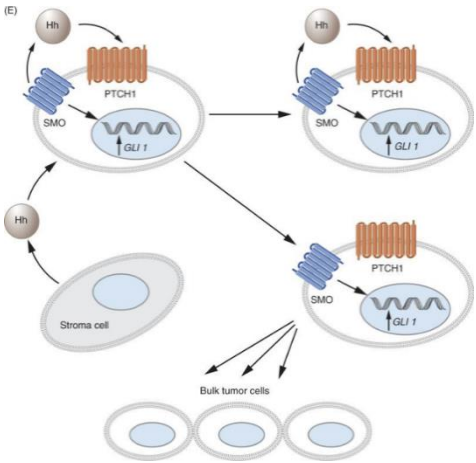

Figure 5 Hedgehog pathway and CSCs.

With the aim to optimize the therapeutic benefit in anticancer treatment, it might be crucial to understand the specific mechanism of Hh activation in cancer desease. Four major modes of Hh inhibition have been exploited therapeutically:

- SMO inhibition;
- Receptor-ligand disruption;
- Inhibition of ligand processing;
- Gli inhibition (Figure 6).

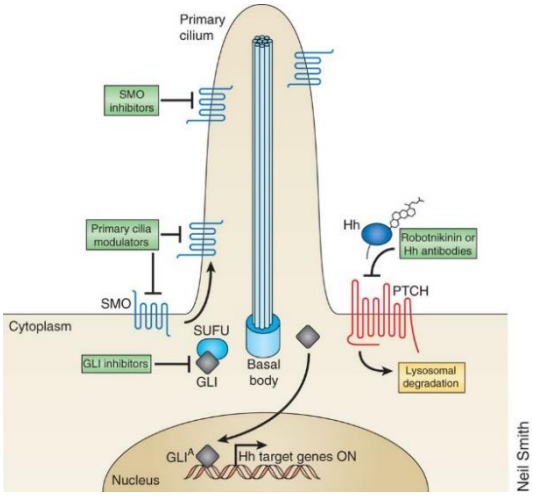

Figure 6 Potential sites for blocking the Hh pathway with therapeutic agents[18] *(Reproduced with permission).*

A1.4.1 Smo Inhibitors

In recent years, drug discovery efforts directed against the Hh pathway and focused predominantly on the development of Smo antagonists. A remarkable number of small molecules of natural, semisynthetic or synthetic origin have been developed and extensively reviewed[30].

The mechanism of Smo regulation during Hh signaling is still obscure. It is well known that Smo is a seven transmembrane protein and exists in conformational switch, converting between an 'open and active' to a 'closed and inactive' form[31, 32]. This equilibrium is controlled by a ligand, whose identity has remained elusive. Among the Smo inhibitors, cyclopamine (natural alkaloid), vismodegib and

sonidegib (approved by FDA in 2012 and 2015, respectively, for treatment of metastatic and locally advanced BCC) are noteworthy.

Despite the initial enthusiasm, clinical development of Smo antagonists has ultimately proved disappointing, due to scarce pharmacokinetics, low selectivity on CSCs, severe side effects, and the emergence of drug resistance[30]. Advanced tumors can evolve resistance through pathway-dependent genetic mechanisms or through compensatory adaptation. Pathway-dependent genetic alterations, discovered in resistant tumors from patients and animal models, directly affect Hh pathway members. In particular, the resistance toward vismodegib originates from genetic alteration at the level of, or downstream from, Smo. Resistance can originate from Smo point mutations that ablate Smo-drug interaction while maintaining Hh pathway avtivation[33] (Figure 7a). These mutations occur in the ligand-binding pocket of Smo. Other genetic aberrations that drive to resistance come from gene duplications of *Gli2* or Hh target gene *cyclin D1* (Figure 7b), able to bypass the requirement of Smo to inappropriately maintain or increase Gli target gene induction. These mutations encourage both Hh pathway activation in the presence of Smo antagonists, and mediate tumor growth.

Compensatory alterations outside the Hh pathway have been individuated to mediate tumor resistance; this is the case in which Hh activation occurs in the absence of a direct genetic mutation or copy number of variation of Hh members, and is epigenetic in nature.

Recently, the development of Hh inhibitors able to modulate targets acting downstream of Smo, or independently by Smo (Gli), might represent a promising therapeutic strategy for the treatment of Hh dependent tumors. This strategy would allow overcoming anti-Smo resistance and adverse effects, which are responsible for more than 50% dropout's rates in Smo antagonists clinical trials.

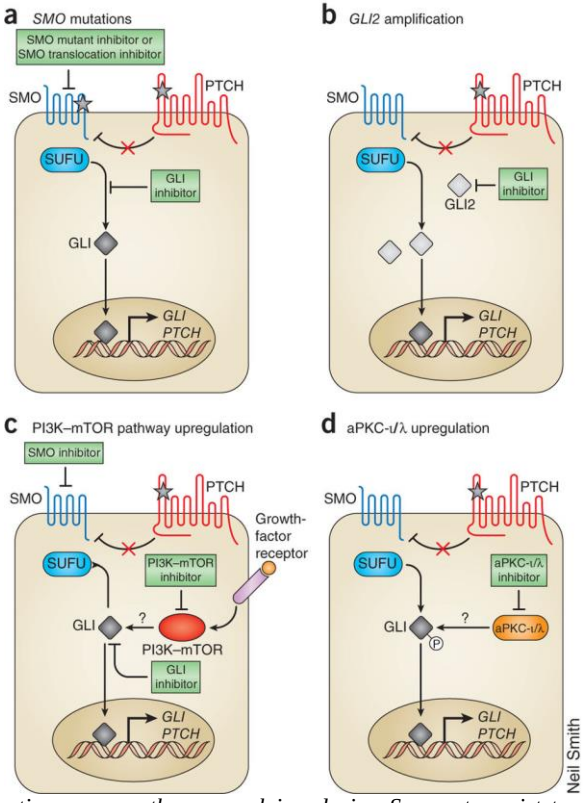

Figure 7 Genetic escape pathways evolving during Smo antagonist treatment and approaches to overcome resistance. (a) Smo point mutations. (b) Gli target gene amplification of Gli2. Compensatory escape pathways including (c) PI3K pathway

up-regulation or (d) inappropriate activation of aPKC-ι/λ[18] (Reproduced with permission).

A1.4.2 Gli Inhibitors

Gli transcription factors (Gli1, activator, Gli2 and Gli3 both activators or repressors) represent the final effectors of the Hh pathway and share common structural features, such as five highly conserved tandem zinc fingers (ZFs), a conserved N-terminal domain, potential protein kinase A (PKA) binding sites, and additional conserved region at the C-terminus.

It is important to consider that, whatever alteration leads to aberrant Hh pathway activation, such as genetic mutations of pathway components or other Smo-dependent or -independent mechanisms, all trigger the down-stream effector of Gli1. For this reason, Gli factors are recently emerging as attractive targets for the development of novel anticancer drugs.

Nowadays, two distinct classes of Gli antagonists have been identified:

- direct Gli antagonists (able to inhibit Gli transcriptional functions through a direct contact);
- indirect Gli antagonists (the inhibition is afforded by arresting of mechanisms that control Gli activities).

The first Gli antagonists discovered by Lauth *et al*. in 2007 were GANT58 (**I**) and GANT61 (**II**)[34] (Figure 8). Compound **II** has become the lead compound in many biological studies, since it proved to

inhibit the Hh pathway in five different human colon carcinoma cell lines and in prostate cancer human xenografts. Recently, the HPIs (Hedgehog Pathway Inhibitors) (**III-VI**) were identified by Chen and co-workers as Gli antagonists[35]. HPI-1 is the most promising compound, and it was encapsulated in a polymeric nanoparticle. Arsenic trioxide (ATO) (**VII**) is a drug approved by FDA for the treatment of promyelocytic leukemia; it resulted effective both *in vivo* and *in vitro* and acts interfering directly with the Gli transcriptional factors[36] (Figure 8). Since 2013, ATO is the protagonist of a clinical trial study, in order to investigate its efficacy in treating patients with BCC.

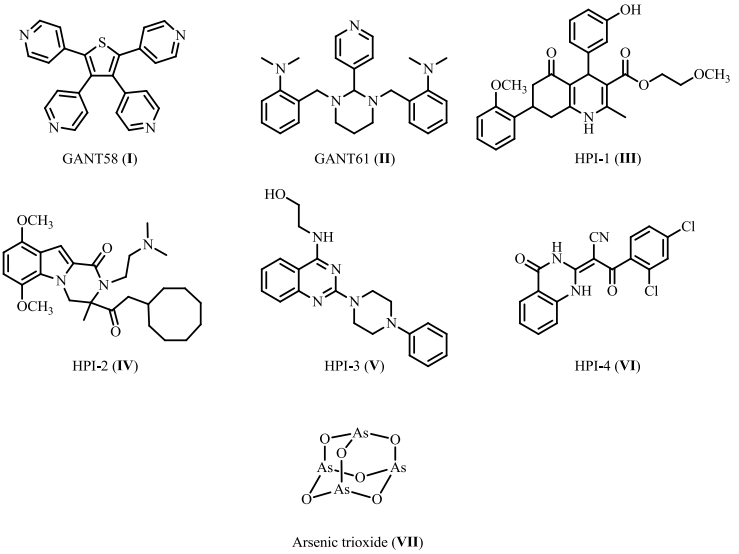

Figure 8 Gli direct antagonists.

In conclusion, Gli transcriptional factors represent the most promising target for the development of new drugs targeting the Hh pathway in tumors. A significant contribution to the discovery of novel Hh inhibitors is given by natural products.

Chapter A2

Hedgehog Pathway: a Druggable Target in Anticancer Therapy

A2.1 Gli1/DNA Interaction: Identification of the Biding Site

The beginning of the investigation on Gli1's active site was based on the available X-ray structure of cobalt ion-coordinated GliZF in complex with DNA[37, 38]. A representative GliZF structure was extracted after molecular dynamics (MD) simulations for further ligand design *in silico* (Figure 9a). Based on MD analysis and X-ray structure, a computational alanine scanning was carried out to verify which basic aminoacidic residues in ZF4 and ZF5 domains are responsible of the thermodynamic stability of the Gli1ZF/DNA adduct[34]. The delta energy (ΔG) of binding to DNA of Gli1 mutants (Figure 10b) and wild-type Gli1ZF (Gli1ZF-WT) (ΔΔG) were calculated. Basic aminoacid residues in ZF4 (K340, K350, R354) and ZF5 (K360, K371, R380 and K381) domains showed the strongest ΔΔG contribution (Figure 9b), suggesting their crucial role in Gli1/DNA interaction[37].

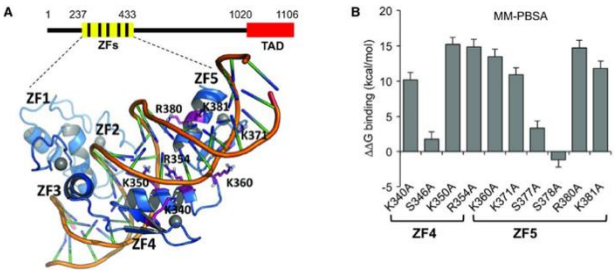

Figure 9 Structure-based analysis of Gli1/DNA complex. (A) Gli1ZF/DNA structure extrapolated from MD analysis. Gli1ZF (blue cartoon), residues involved in binding to DNA (magenta sticks), Zn ions (grey spheres) are shown. (B) Effect of Gli1ZF

mutants on the binding affinity to DNA as predicted by in silico alanine scanning[37] *(Reproduced with permission)*

Mutagenesis studies suggested that the above residues may be involved in Gli1 binding to DNA (Figure 9a). We chose the K350A and K340A mutants, showing the highest and intermediate ΔΔG of binding, respectively , to test their direct interaction with DNA. An electrophoretic mobility shift assay (EMSA) was performed using equal amounts of recombinant GST-Gli1ZF-WT or GST-Gli1ZF-K350A or GST-Gli1ZF-K340A (Figure 10b) and a DNA probe containing Gli-responsive consensus DNA sequence or a mutated version unable to bind Gli1 (Figure 10b). Comparison with the strong DNA binding affinity of the recombinant GST-Gli1ZF-WT confirms that GST-Gli1ZF-K350A was unable to bind DNA, whereas GST-Gli1ZF-K340A did it, albeit to a significantly lower extent (Figure 10b). Notably, these results correlate with the impaired and intermediate transcriptional activity of Gli1ZF-K350A and Gli1ZF-K340A mutants in cell-based assays, respectively (Figure 10a), and suggest that both K350 and K340 are involved in DNA binding and transcriptional activity, although with a different strength.

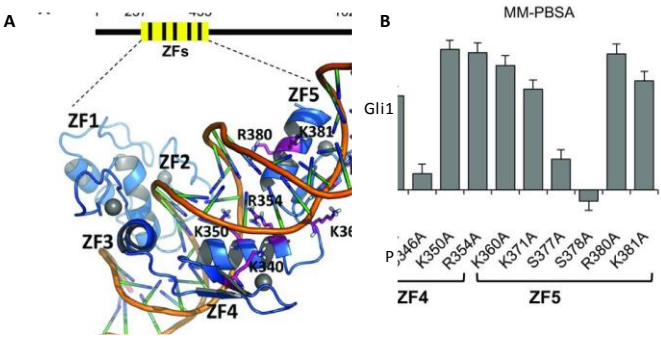

*Figure 10 Effect of Gli1ZF mutants on Gli1-dependent transcriptional activation. (**A**) Luciferase assay was performed in HEK293T cells transfected with GliBS-Luc, pRL-TK Renilla (normalization control), Flag- Gli1 WT or the indicated Flag-Gli1 mutants. Data show the mean ± SD of three independent experiments. *P< 0.05; **P< 0.01 vs Gli1 WT. (**B**) Gli1/DNA binding. Double-stranded oligonucleotide containing the canonical GliBS sequence or mutated GliBS sequence used as control was used as probe (P) in EMSA experiments. The assay was performed using recombinant GST-Gli1ZF-WT (Gli1 zinc-finger fragment: aa 242–424), GST-Gli1ZF-K350A, GST-Gli1ZF-K340A. Data are shown as a ratio of GST-Gli1ZF-WT or GST-Gli1ZF mutants bound to the labeled GliBS probe/GliBS free probe normalized to the amount of GST-Gli1ZF-WT/DNA binding ± SD *P< 0.05 vs Gli1 WT.*

To correlate computational with experimental studies, a mutation assay was performed on HEK293T cells; these samples transiently express ectopic Gli1 or different Gli1 mutants, and a Gli-dependent luciferase reporter. The results obtained from such mutagenesis assays highlighted the role played by those residues in ZF4 and ZF5 domains in the transcriptional activity of Gli1[37] (Figure 10).

A2.2 *In Silico* Screening: Gli1 Linkage to Natural Products

An *in house* library composed of about 1000 unique natural products is available in Prof. Bruno Botta's laboratory, and it was the starting point to elucidate how Gli1 binding to DNA might be modulated by small molecules[38]. Literature data and results from the mutagenesis assays were used as source for a docking studies[39]. According to the setting of the docking analysis, only small molecules able to interact with at least one of the basic residues (ZF4, ZF5 ones) were selected[34]. The *in silico* screening identified six molecules (three vismiones, GlaB, chalcone V94 and the opioid alkaloid narceine) as potential Gli1 inhibitors[37] (Figure 11).

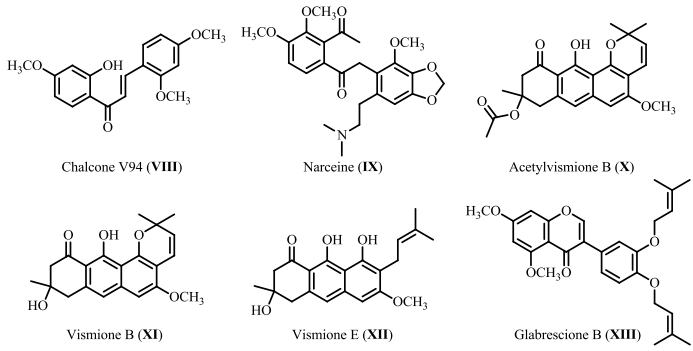

Figure 11 Structure of the six virtual hits.

To assess the functional activity of these products as specific modulators of Gli1, we performed the Gli-dependent luciferase reporter assay on HEK293T cells (Figure 12).

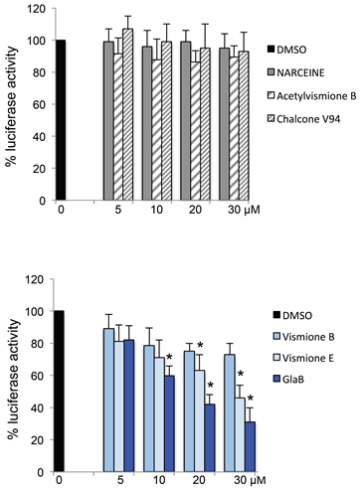

Figure 12 Gli1-induced transcription in HEK293T cells, treated with increasing concentrations of different compounds or DMSO as control[37] *(Reproduced with permission).*

The results of biological assays highlighted for GlaB and Vismione E an inhibitory luciferase activity comparable to the GANT61 one, for Vismione B a partial inhibitory activity and other compound resulted not active[37]. Since the chemical instability of the vismione scaffold in different conditions, our studies were focused on GlaB and on its synthetic derivatives.

Chapter A3

Total Synthesis, SAR and Biological Evaluation of Isoflavone Derivatives

A3.1 The Importance of the Isoflavone Scaffold

Isoflavones are a class of natural compounds mainly occurring in plants of the *Leguminosae* family, and possess natural roles in plants defense. In last decades, these compounds have received much attention due to their interesting biological activity and benefits to human health[40, 41]. Moreover, as highlighted by genistein and its derivatives, isoflavones have displayed noticeable pharmacophoric preference for Hh targets[30].

The isoflavone nucleus consists of two phenyl rings linked by a propane bridge to form an oxygenated heterocyclic ring, resulting in the typical 15 carbon atoms skeleton (C6-C3-C6) with three rings, labelled A, B and C (Figure 13). Isoflavonoids differ from flavonoid basic structure because B-ring attaches to C-3 instead of C-2.

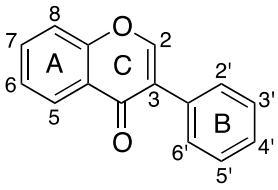

Figure 13 Isoflavones skeleton C6-C3-C6.

Most of the isoflavones have been isolated from natural sources, but extraction methods furnish only very few amounts of pure samples. However, their simple structure features can be approached by convenient synthetic method.

A3.2 Computational Design of Isoflavones Targeting Smo or Gli

By screening of a natural compounds library, GlaB, a prenylated isoflavone, was recentely identified by our research group as the first small molecule acting as direct inhibitor of Gli1/DNA interaction and endowed by a significant anticancer efficacy *in vivo* and *in vitro* against Hh-dependent MB and BCC. The mechanism of action of GlaB was largely studied at molecular leves, thus pointing to the druggability of Gli1/DNA interaction in the treatment of Hh-dependent cancers. GlaB was considered as *starting point* to develop numerous derivatives.

Previously, a number of GlaB synthetical derivatives possessing modifications on the ring B have been synthesized and tested as Hh inhibitors[37], displaying no effects (**DGB1-5**, Figure 14). This data focused preliminary structure-activity relationships of GlaB, and led us to identify relevant molecular key factors for the inhibition of Gli1 binding to DNA and related transcriptional activities.

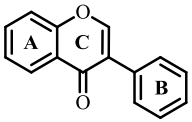

Isoflavone core

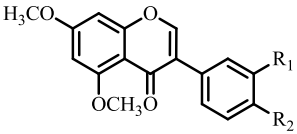

DGB$_1$: R_1 = H; R_2 = H
DGB$_2$: R_1 = R_2 = OH
DGB$_3$: R_1 = OCH_3; R_2 = OH
DGB$_4$: R_1 = OH; R_2 = OCH_3
DGB$_5$: R_1 = O*i*Pr; R_2 = OCH_3

Figure 14 DGB 1-5 derivatives.

These evidences highlighted the pharmacophoric importance of the substitutions at the isoflavone's ring B in binding to Gli1 and preventing its interaction to DNA.

Here we designed a small-sized library of isoflavones bearing different substituents in different position of the ring B.

These molecules (Table 1)[42] were tested *in silico* to investigate the interaction with the heptahelical bundle of Smo or the DNA binding site of Gli1. The computational protocols already validated in previous works[37, 43, 44, 45, 46], displayed that the *O*-substitutions at *para* position of ring B favoured the interaction with Smo, meanwhile the same substitutions at *meta* position preferred the Gli1 interaction.

We observed these results through the analysis of the shape of the binding sites of Smo or Gli1: Smo possesses a narrow and elongated

binding site in the linear heptahelical bundle of the receptor, Gli1 has a marginally bended binding site at the interface between ZF4 and ZF5.

Based on molecular modelling suggestions, we decided to design and synthesize the compounds reported in Table 1, to investigate their effects on the modulation of Hh signaling.

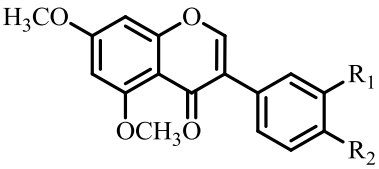

Table 1 Chemical structure of isoflavone derivatives investigated in this work as Hh inhibitors[42].

Cmpd	R_1	R_2	Cmpd	R_1	R_2
GlaB	-OPrenyl	-OPrenyl	**12**	-O*p*-BnCF_3	-OCH_3
4c	-OH	-H	**13**	-OCH_3	-O*p*-BnCF_3
5	-OPrenyl	-OCH_3	**14**	-O*p*-BnCF_3	-H
6	-OCH_3	-OPrenyl	**15**	-OBn	-OBn
7	-OPrenyl	-H	**16**	-O*p*-BnCN	-OCH_3
8	-OBn	-OCH_3	**17**	-O*p*-BnCO_2CH_3	-OCH_3
9	-OCH_3	-OBn	**18**	-O*p*-BnCO_2NH_3	-OCH_3
10	-OGeranyl	-OCH_3	**19**	-O*p*-BnNO_2	-OCH_3
11	-OCH_3	-OGeranyl			

A3.3 Synthetic Strategy to Isoflavone Derivatives

Since extraction methods developed allow us to get very limited amounts of pure isoflavone, several synthetic procedures used for the preparation of isoflavones have been developed[47].

Previously, we afforded a synthetic route for the total synthesis of isoflavones scaffold (and, in particular, of GlaB), featuring six-step with an overall yield of 7%[48]; that approach is based on a palladium catalyzed cross coupling reaction of 3-iodochromone with the corresponding boronic acid. This route affects with the impossibility to synthesize GlaB derivatives, due to the challenging mono-functionalization of the two hydroxyl groups on ring B. This inspired us to mature a mild and cost effective method, inspired to the "deoxybenzoin route"[49], which might enable the synthesis of isoflavones bearing different substituents on *meta* and *para* positions of ring B. This route foresees three simple steps.

The first step of the route consists in a Friedel-Crafts acylation, in which 3,5-dimethoxyphenol was treated with suitable phenyl acetic acids in presence of $BF_3 \cdot Et_2O$, used as Lewis acid; this step leads to the formation of the deoxybenzoin intermediate. Appropriate substituted phenyl acetic acids are necessary to achieve the synthesis of free *meta*- or *para*-hydroxyl groups on ring B. This step is followed by a Vilsmeier-Haak reaction, in presence of (chloromethylene)dimethyliminium chloride, that accomplishes the addition of one carbon atom and the cyclization of deoxybenzoin,

affording the formation of the isoflavone scaffoild (Scheme 1). The last step is represented by a reaction of functionalization of the isoflavone ring B, and was performed using an alkyl or aryl bromide and K_2CO_3 in refluxing acetone. This route (with an overall yield of around 15%), achieved the preparation of a small library of GlaB-ring B derivatives *meta*- or *para*- substituted, ready to be tested against the Hh pathway.

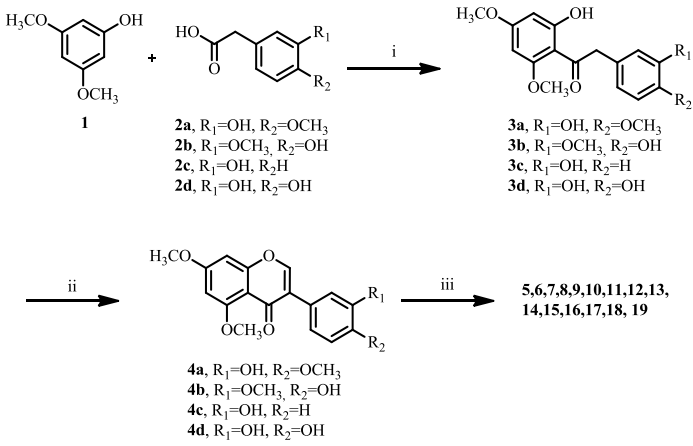

Scheme 1 Deoxybenzoin approach: i) $BF_3{\cdot}OEt_2$, 90 °C, 90 min 50-60%; ii) $BF_3{\cdot}OEt_2$, (chloromethylene)dimethyliminium chloride, DMF, rt, 2 h 28-32%; iii) alkyl- or benzyl- bromide, K_2CO_3, acetone, 45 °C, 17 h, 88-95%.

A3.4 Biological Evaluation of Isoflavones Derivatives

A3.4.1 Hh inhibition by Isoflavones Derivatives

Biological investigation of newly isoflavones were performed in a luciferase report assay using, the NIH3T3 Shh-Light II as sample cells (which incorporate Gli-responsive firefly luciferase reporter) and the pRL-TK *Renilla* as normalization control. The procedure adopted to investigate the ability of the new isoflavones to inhibit Hh signaling provided the treatment of the cells with a synthetic Smo antagonist (SAG) alone, or in combination with selected molecules[45].

We observed two different behaviors according to the *meta*- and the *para*-position substitutions on the B ring:

- *meta* substitutions: compounds **4c**, **14**, **16**, **17**, **18** and **19** exhibited mild activity at the concentration of 30 μM; **5**, **8**, **10** and **12** displayed high activity, with a range of IC_{50} between 2 and 4 μM; **7** was inactive (Figures 15 and 16a, Table 2);
- *para* substitutions: compounds **13** and **15** exhibited high activity as Hh inhibitors with an IC_{50} of 3.4 μM for the first and 0.29 μM for the latter; **6** and **9** showed mild activity and **11**, in the end, evidenced to be toxic[45] (Figure 16b and Table 2).

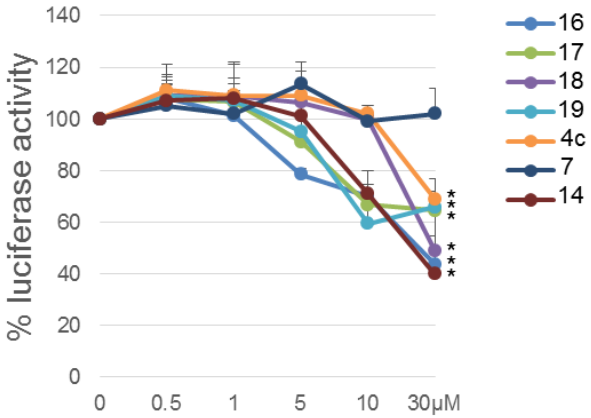

Figure 15 Hh inhibition by isoflavones ***4c***, ***7***, ***14***, ***16***, ***17***, ***18***, *and* ***19****. Dose-response curve of compounds with a substituent at* –meta *position of ring B in SAG-treated NIH3T3 Shh-Light II cells. Treatment time was 48 h, and normalization was against* Renilla *luciferase. Data show the mean ± SD of three independent experiments: (*) P < 0.05 vs SAG.*

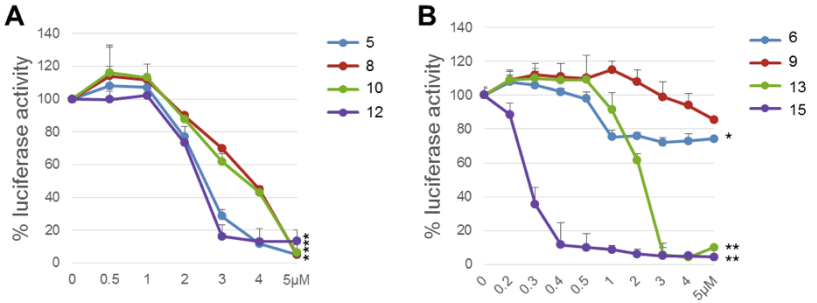

Figure 16 Hh inhibition by isoflavones ***5***, ***6***, ***8***, ***9***, ***10***, ***12***, ***13***, ***15****. Dose-response curve of compounds with a substituent at* meta *(A) or at* para *(B) position of ring B in SAG-treated NIH3T3 Shh-Light II cells. Treatment time was 48 h, and normalization was against* Renilla *luciferase. Data show the mean ± SD of three independent experiments: (*) P < 0.05 vs SAG; (**) P < 0.01 vs SAG.*

Table 2 IC_{50} values for new isoflavone derivatives selected in the Shh-Light II cells and in MEFs assay.

	Substitution at *meta* position	
	Shh-Light II IC_{50} (µM)	**MEFs IC_{50} (µM)**
5	2.87±0.33	5.695±0.84
8	3.719±0.88	17.12±0.87
10	3.61±0.31	21.22±1.21
12	2.58±0.12	11.50±0.85
16	16±1.1	/
17	> 30	/
18	> 30	/
19	> 30	/
4c	> 30	/
7	> 30	> 20
14	10.47±0.73	26.73±1.7
	Substitution at *para* position	
	Shh-Light II IC_{50} (µM)	**MEFs IC_{50} (µM)**
6	6.97±0.67	10.7±1.01
9	6.921±0.76	39.2±2.03
11	nd	nd
13	3.477±0.66	55.29±2.57
15	0.29±0.12	57.74±3.98

The structure of the most effective derivatives are summarized in figure 17.

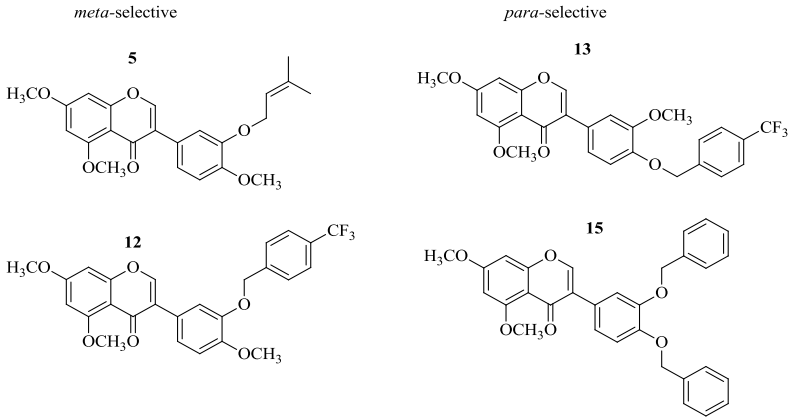

Figure 17 Structure of the most effective synthetic derivatives meta- (on the left) and para- substituted.

A3.5 Smo and Gli1 Antagonists

To explore the activity of the most powerful molecules as Gli1 or Smo modulators, we performed the Gli1-dependent luciferase reporter screening assay, in which increasing amount of selected molecules were incubated with mouse embryonic fibroblasts (MEFs) expressing ectopic Gli1. To validate the assay method, the FDA approved molecule Vismodegib (GDC-0449) was used as control (Figure 18). As showed in figure 17a, compounds **5** and **12** are the most promising Gli1 activity inhibitors, with IC_{50} values between 5 and 11 μM, while Vismodegib exhibited no effect on Gli1 transcriptional activity. These results are in agreement with computational and experimental studies.

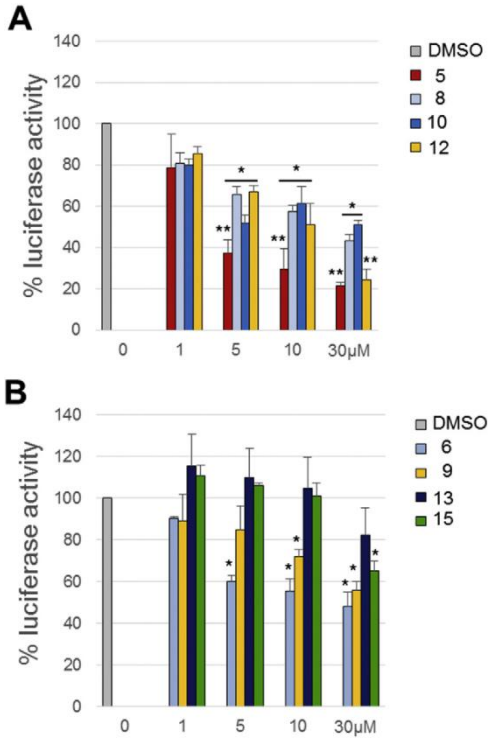

Figure 18 Specificity of Smo and Gli1 antagonists.

The preliminary results that emphasized the Gli1 inhibition efforded by **5** and **12** derivatives, were confirmed in $Smo^{-/-}$ MEFs transfected with ectopic Gli (Figure 19).

Compounds **5** and **12** inhibited the luciferase activity Gli-responsive elements (Figure 18a), while compound **13** and **15** did not showed activity (Figure 18b). Moreover, to demonstrate that **5** and **12** operate downstream of Smo, these molecules were tested in $SuFu^{-/-}$ MEFs cells, featured by constitutive activation of the Hh pathway due to the loss of the negative regulator SuFu. Compounds **5** and **12**

critically reduced the expression of Gli1 and Gli2, the final effectors of Hh pathway; on the other side, compounds **13** and **15** showed no activity.

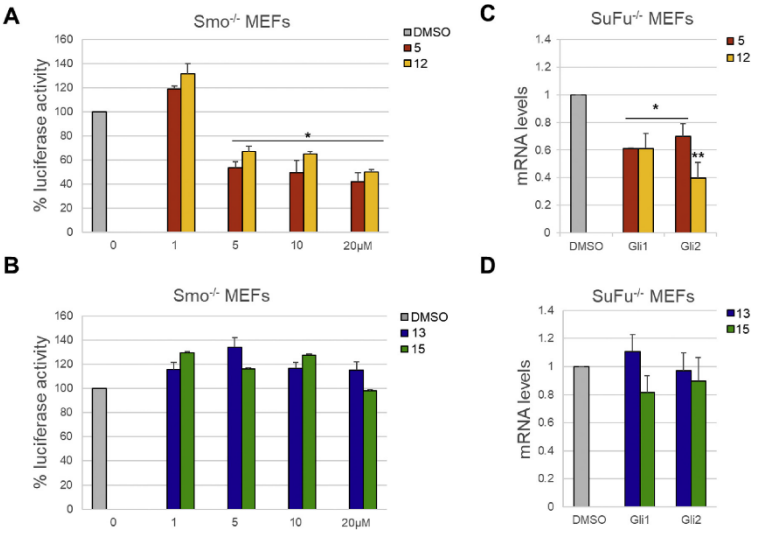

Figure 19 Specificity of Smo and Gli antagonists.

The results obtained from these biological assays confirm the computational modeling predictions, evidencing that isoflavones with a *para*-substituent on the B ring act on upstream receptor Smo, instead those presenting *meta*-substitutions target the downstream effectors Gli.

A3.6 Binding Sites of Smo and Gli1 Antagonists: Docking Analysis of the New Isoflavone Derivatives

The possible binding mode of the most promising Hh inhibitors towards Smo or Gli1 crystallographic structure was evaluated thanks to molecular modeling simulations. Noteworthy, our research group was able to predict the binding mode of Gli1[34] and Smo antagonists[49, 50] using established computational protocols, which were used to dock compounds **5** and **12** towards Gli1ZF domain, and molecules **13** and **15** whithin the heptahelical bundle of Smo.

- *Gli1 antagonists evaluation (**5** and **12** derivatives)*

Molecular docking of Gli1ZF/antagonists highlighted a comparable binding mode of the two molecules **5** and **12**, with the isoflavone core occupying a surface region at the interface between ZF4 and ZF5 (Figure 20). The interactions established are comparable to the ones already observed for GlaB[34], even if the isoflavone core is established in a different manner: the isoflavone core of the new synthetic molecules interacts with the K350 through H-bond, previously highlighted by mutagenesis studies as a crucial center for Gli1 transcriptional activity[34], and with T355, K360 and H351. The ring B of the isoflavone is docked in a model that hides the nuclear localization system (NLS) at level of the residue T374 to the solvent area. The isoprenyl group present in **5** is docked in a groove near S357 and N358 residues (figure 20a), while the aromatic portion of **12** is

oriented towards the ZF5, with which establishes π–π stacking interaction with the residue T373 (Figure 20b).

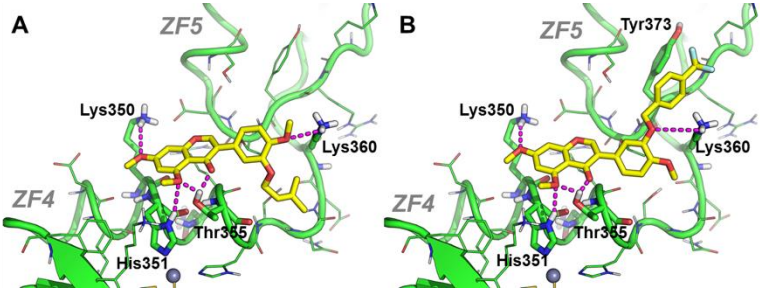

*Figure 20 Predicted binding mode of Gli1 antagonists. The docking pose of **5** (A) and **12** (B) is shown as yellow sticks. Gli1ZF is shown as green cartoon. Residues within 5 Å from the ligands are showed as lines. Residues H-bonded or stacked to the ligands are showed as sticks, and are labeled. Residues numbers correspond to the full length human Gli1. H-bonds are showed as magenta dashed lines, Zn(II) ions as grey spheres.*

➢ *Smo antagonists evaluation (**13** and **15**)*

Synthetic molecules **13** and **15** adapt in the lipophilic site present in the heptahelical bundle of the receptor. Indeed, the isoflavone core of the Smo antagonists binds in two conformations, which are most likely biased by compared to the single substitutions at *para* position on the ring B of **13**, and is in part due to the presence of two aryl substituents on the B ring of **15** (Figure 21). Isoflavone core of **13** binds a Smo region generally occupied by multiple antagonists, as confirmed by X-ray crystallography,[46, 50, 51, 52, 53] and establishes: H-bonds with R400, both H-bonds and π–π interactions with T394 and π–π stacking interactions with F484 (Figure 21a). The lipophilic

portions are docked in the intramembrane region of the receptor[52, 54], while the trifluoromethyl moiety is near the entrance of the binding site, corresponding to the extracellular portion of Smo. In the case of **15**, in which B ring is substituted by two hydrophobic benzyloxy groups, the isoflavone core binds the extracellular portion of Smo in an opposite site than to **13**; in fact, the two hydrophobic substituents are projected in the heptahelical bundle of Smo, near to non-polar residues F222, M230, W281, F391, H470, L515 and L522. Among all the aminoacids present in the heptahelical bundle of Smo, H470 established π–π interactions with the benzyl moieties present in the molecule **15** (Figure 21b).

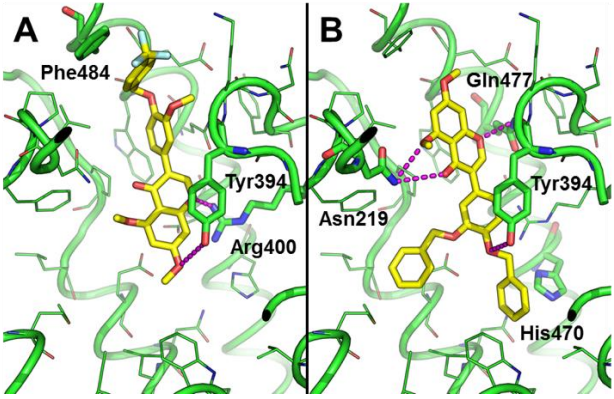

*Figure 21 Predicted binding mode of Smo antagonists. The docking pose of **13** (A) and **15** (B) is shown as yellow sticks. Smo is shown as green cartoon. Residues within 5 Å from the ligands are showed as lines. Residues H-bonded or stacked to the ligands are showed as sticks, and are labeled. Residues numbers correspond to the full length human Smo. H-bonds are showed as magenta dashed lines.*

A3.7 Smo and Gli Antagonists: a Smart Combination in Anticancer Treatment

Hh pathway aberrant activation is a crucial issue in tumorigenesis, and in the last decade the design of Hh inhibitors is giving rise to increasing interest in drug discovery. With the aim to overcome complications due to the resistance phenomena, we decided to combine two isoflavones targeting Smo or Gli1, respectively, and to investigate their potential synergistic affect.

We analyzed the ability to inhibit Hh-dependent tumor growth in primary MB cells freshly isolated form Ptch $^{\pm}$ mice tumors, and tested in short-term cultures to maintain Hh sensitivity *in vitro*. The new synthetic isoflavones exhibited an inhibitory cell growth with comparable efficiency to the GlaB, used as reference (Table 3 and Figure 22).

Table 3 Percentage of growth inhibition in primary MB cells freshly isolated from Ptch$^{+/-}$ mice, after 72 h of incubation with the Gli1 selected antagonists.

[μM]	**GlaB**	**5**	**12**	**13**	**15**
0.125	28.6±2.7	5.9±3	37.7±3.1	20.8±5.3	33.3±3.8
0.25	42.4±3.1	26.3±4	40.6±2.3	23.5±3.1	44.2±4.9
0.5	46.6±3.4	29.2±3.6	44.52±3.6	32.5±1.3	51.4±5.1
1	55.9±4	35.6±2.1	50.9±4.8	51.8±3.5	61.2±4.8
5	65.1±5.3	55.4±5	54±5	54.2±4.4	66.6±4.1

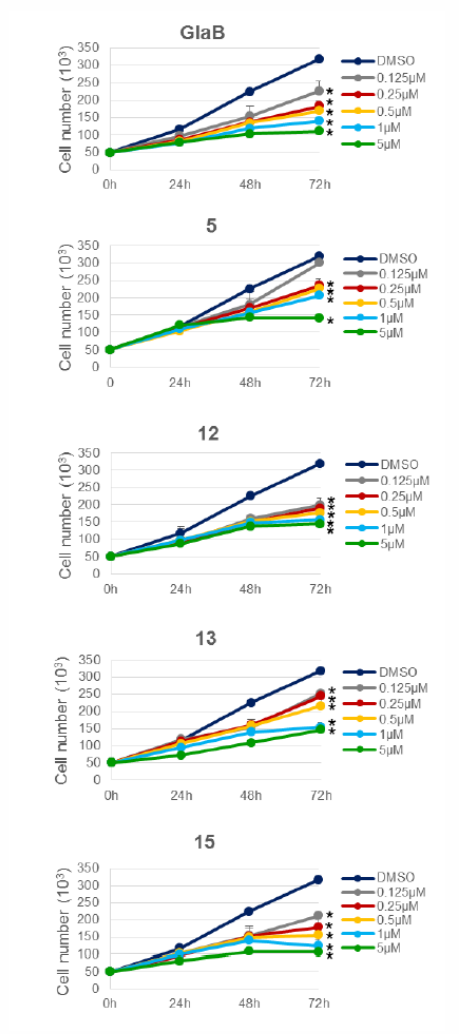

Figure 22 Inhibition of Hh-dependent tumor growth. Primary MB cells were freshly isolated from Ptch1$^{+/-}$ mice tumor and treated with a Smo- or a Gli1- antagonist, at the indicated concentration, or with DMSO only, as control. After the indicated times, a trypan blue count was performed to determine the growth rate of viable cells. In all experiments data show the mean ± SD of three independent experiments: (*) P < 0.01 vs CTR (DMSO).

Remarkably, the combination between a Gli1 (**5**, **12** and **GlaB**) and a Smo (**13** or **15**) antagonist reduced cells proliferation at striking lower concentrations (Table 4 and Figure 22). In fact, GlaB afforded a 46% growth inhibition (Table 3) at the concentration of 0.5 μM, meanwhile the combination of **12** and **13** afforded a comparable inhibition at the final concentration 0.125 μM (Table 4).

Table 4 Percentage of growth inhibition in primary MB cells freshly isolated from Ptch$^{+/-}$ mice, after 72 h of incubation with the binary combination between a Gli1- and a Smo- antagonist.

[μM]	12 + 13	12 + 15	5 + 13	5 + 15	GlaB + 13	GlaB + 15
0.125	44.2±2.7	35.5±5	31.8±2.7	32.0±4.6	33.5±1.1	38.3±4.7
0.25	50.1±2.9	50±3.7	33±2	34±2.1	53.1±2.5	63.4±3.1
0.5	53.5±3.9	55.2±4.6	35±3.3	40±3.6	60.1±1.6	70±4.2
1	61.9±3.4	67.9±3.8	45.7±3	51.9±2.7		
2	58.6±4	68.2±1.3	47.1±1.5	60.4±1.5		

The combination of GlaB with isoflavone **13** or derivative **15** bear 53% and 63.4% Hh-dependent tumor growth inhibition at the concentration of 0.25 μM, respectively. The best result was accomplished with the binary administration of GlaB and **15**: a 70% cell growth inhibition at the concentration of 0.5 μM (Table 4 and Figure 23).

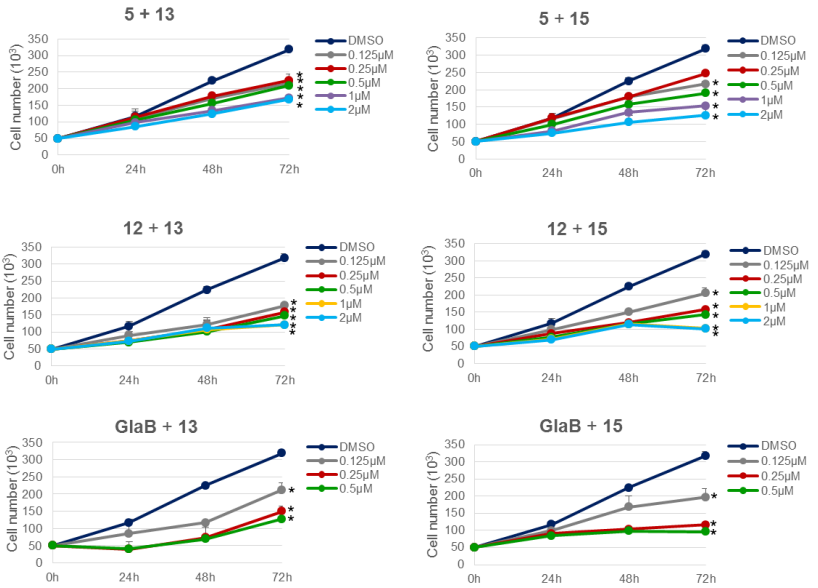

Figure 23 Synergistic combination of isoflavone Smo and Gli antagonists. Primary MB cells were freshly isolated from Ptch1$^{+/-}$ mice tumor and treated with the binary combination between a Smo- and a Gli1- antagonist, at the indicated concentration. DMSO was used as control. After the indicated times, a trypan blue count was performed to determine the growth rate of viable cells. In all experiments data show the mean ± SD of three independent experiments: (*) P < 0.01 vs CTR (DMSO).

A3.8 Conclusions

A new synthetic route leads us to obtain new isoflavone derivatives, and these were tested *in vitro*. Here, we reported a number of isoflavones able to interact especially with Smo receptor or the Gli protein; experimental results displayed that isoflavones with *meta* substitutions on B ring binds preferrentially Gli1ZF domain,

meanwhile the *para* substituted derivates bind the Smo receptor. These results are in agreement with molecular modeling studies.

Furthermore, we observed that the co-admistration of a Smo and a Gli antagonist afforded similar Hh inhibition effects with individual doses of compounds **12** and **13** decreased by four time at sub-molar concentrations; the most powerful effect was obtained when GlaB was combined with compound **15**.

In conclusions, our results highlighted that targeting Hh pathway at both upstream and downstream levels, using a Smo inhibitor and a Gli1 antagonist, efficiently improve Hh inhibition at lower individual molecules doses.

We expect that our study could trigger more investigations on clinically highlighting Hh inhibitors, and support the treatment of Hh-dependent tumors with a combination therapy.

A3.9 General Methods for Sapienza project

All non-aqueous reactions were performed under an argon atmosphere using flame-dried glassware and standard syringe/septa techniques.

All absolute solvents were purchased as anhydrous grade from Sigma Aldrich and used without further purification unless otherwise stated. Solvents for extractions, flash column chromatography (FC) and thin layer chromatography (TLC) were purchased as commercial grade from Sigma Aldrich and used without further purification unless otherwise stated. Reactions were magnetically stirred and monitored by TLC performed on Merck TLC aluminum sheets (silica gel 60 F254). Spots were visualized with UV light (λ = 254 nm). Chromatographic purification of products (FC) was performed using Sigma Aldrich silica gel 60 for preparative column chromatography (particle size 40-63 μm).

Melting points (**Mp**) were obtained in open capillary tubes using a Büchi melting point apparatus B-545 and are uncorrected.

^{1}H- and ^{13}C-NMR spectra were recorded in $CDCl_3$, acetone-d_6, DMSO-d_6 or methanol-d_4 on a Bruker AV-400 400 MHz spectrometer (operating at 400 MHz for ^{1}H and 100 MHz for ^{13}C) at room temperature and tetramethylsilane (TMS) as internal standard. Chemical shifts (δ) are reported in parts per million (ppm) and are

referenced to $CDCl_3$ (δ = 7.26 ppm for ^1H, δ = 77.16 ppm for ^{13}C), acetone-d_6 (δ = 2.05 ppm for ^1H, δ = 29.84 ppm for ^{13}C) DMSO-d_6 (δ = 2.50 ppm for ^1H, δ 39.52 ppm for ^{13}C), or MeOH-d_4 (δ = 3.31 ppm for ^1H, δ 49.00 ppm for ^{13}C). All ^{13}C-NMR spectra were measured with complete proton decoupling. Data for NMR spectra are reported as follows: s = singlet, d = doublet, t = triplet, q = quartet, m = multiplet, br = broad signal, *J* = coupling constant in Hz.

High-resolution mass spectra (HRMS) were recorded on Bruker BioApex Fourier transform ion cyclotron resonance (FT-ICR) mass spectrometer.

HPLC analysis were performed on a Waters 2690 Separation Module, equipped with a Rheodyne Model 8125 20-µL injector and a Model M486 programmable multi-wavelength detector (PDA). Chromatographic data were collected and processed using the Empower Chromatography Manager software. Column: Phenomenex Luna C18, 5 µm (250 × 4.6 mm); eluent A) H_2O/CH_3CN, 95:5 v/v, eluent B) H_2O/CH_3CN, 5:95 v/v; gradient elution: for 0-5 min A:B = 50:50; 5-20 min up to 100% B; 20-25 min to 100% B; Flow rate: 1.0 ml/min; UV detection at 295 nm. The purity of the compounds was always higher than 95 %.

The compounds are referred to by increasing numbers **X**, following the sequential references in the main text.

A3.10 Total Synthesis of GlaB and GlaB Ring-B Derivatives

A3.10.1 General procedure for the preparation of deoxybenzoines

In a two-neck round-bottom flask a mixture of 3,5-dimethoxyphenol (6 mmol, 1.00 equiv.), 3,4-disubstituted-phenylacetic acid (6 mmol, 1.00 equiv.) and $BF_3 \cdot Et_2O$ (48 mmol, 8.00 equiv.) was stirred at 90 °C for 90 min under argon. The reaction mixture was poured into 10% aqueous NaOAc (100 mL) and allowed to stir at room temperature for 24 h, forming a brown precipitate. The precipitate was filtered and washed with H_2O (2 x 20 mL). The precipitate was resuspended with EtOAc, dried over Na_2SO_4 and finally concentrated *in vacuo*. The residue was purified by FC using a mixture of Petroleum Ether/EtOAc as eluent, to obtain the corresponding deoxybenzoin.

1-(2-hydroxy-4,6-dimethoxyphenyl)-2-(3-hydroxy-4-methoxyphenyl)ethanone (3a)

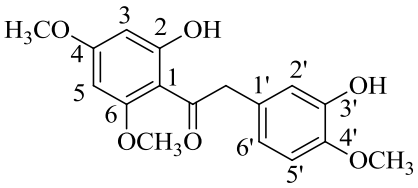

3a

Pale Yellow solid (Yield 55%); mp: 114.2-115.3 °C; TLC (Petroleum Ether/EtOAc, 7:3 v/v): R_f= 0.33.

^{1}H NMR (400 MHz, $(CD_3)_2CO$): δ_H 13.88 (s, 1H, C2-OH), 7.51 (brs, 1H, OH), 6.84 (d, *J* = 8.4 Hz, 1H, H-5'), 6.76 (d, *J* = 2.4Hz, 1H, H-2'), 6.67 (dd, *J* = 8.0 Hz, *J* = 2.0 Hz, 1H, H-6'), 6.06 (d, *J* = 2.0 Hz, 1H, H-5), 6.04 (d, *J* = 2.4 Hz, 1H, H-3), 4.20 (s, 2H, CH_2), 3.93 (s, 3H, OCH_3), 3.84 (s, 3H, OCH_3), 3.80 (s, 3H, OCH_3); **^{13}C NMR** (100 MHz, $(CD_3)_2CO$): δ_C 204.18, 168.70, 167.40, 163.76, 147.22, 147.10, 129.51, 121.34, 117.29, 112.25, 106.10, 94.56, 91.47, 56.23, 56.19, 56.04, 50.00; **HRMS (*m/z*)**: $[M+H]^+$ calcd. for $C_{17}H_{19}O_6$, 319.11761; found, 319.11767.

2-(4-hydroxy-3-methoxyphenyl)-1-(2-hydroxy-4,6-dimethoxyphenyl)ethanone (3b)

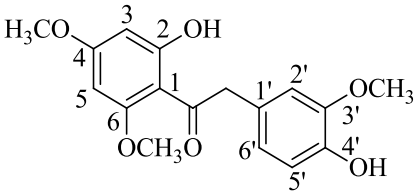

3b

Pale Yellow solid (Yield 55%); mp: 133-135 °C; TLC (Petroleum Ether/EtOAc, 7:3 v/v): R_f = 0.33.

^{1}H NMR (400 MHz, $(CD_3)_2CO$): δ_H 13.87 (s, 1H, C2-OH), 7.42 (brs, 1H, OH), 6.86 (d, *J* = 1.6 Hz, 1H, H-2'), 6.74 (d, *J* = 8.0 Hz, 1H, H-5'), 6.69 (dd, *J* = 8.0 Hz , *J* = 1.6 Hz, 1H, H-6'), 6.07 (d, *J* = 2,4 Hz, 1H, H-5), 6.05 (d *J* = 2,4 Hz, 1H, H-3), 4.23 (s, 2H, CH_2), 3.95 (s, 3H, OCH_3), 3.84 (s, 3H, OCH_3), 3.81 (s, 3H, OCH_3); **^{13}C NMR** (100 MHz, $(CD_3)_2CO$): δ_C 203.38, 167.79, 166.50, 162.89, 147.21, 145.29, 126.95, 122.07, 114.65, 113.18, 105.25, 93.70, 90.59, 55.32, 55.16, 49.32; **HRMS** (*m/z*): $[M+H]^+$ calcd. for $C_{17}H_{19}O_6$, 319.11761; found, 319.11794.

1-(2-hydroxy-4,6-dimethoxyphenyl)-2-(3-hydroxyphenyl) ethanone (3c)

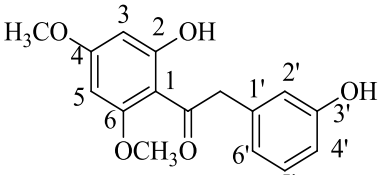

3c

Pale Orange solid (Yield 60%). **Mp**: 103.5-105 °C. **TLC** R*f* = 0.30 (EtOAc/PE 2:3, UV).

^{1}H-NMR (400 MHz, acetone-d_6): δ_H 13.85 (s, 1H, OH), 8.22 (brs, 1H, OH), 7.12 (t, *J*= 8.0 Hz, 1H, H-5'), 6.75-6.73 (m, *J*= 1.6 Hz, 1H, H-2'), 6.71-6.70 (m, 1H, H-4'), 6.68 (dd, *J*= 8.0, *J*= 2.4 Hz, 1H, H-6'), 6.06 (d, *J* = 2.0 Hz, 1H, H-5), 6.05 (d, *J* = 2.0 Hz, 1H, H-3), 4.25 (s, 2H, CH_2), 3.92 (s, 3H, OCH_3), 3.85 (s, 3H, OCH_3). **^{13}C-NMR** (100 MHz, acetone-d_6): δ_C 203.82, 168.72, 167.51, 163.81, 138.24, 129.99, 121.54, 117.20, 114,23, 94.61, 91.52, 56.19, 56.07, 50.64. **HRMS** (ESI): calcd. for $C_{16}H_{17}O_5$ [$(M+H)^+$]: 289.10705; found, 289.10683.

2-(3,4-dihydroxyphenyl)-1-(2-hydroxy-4,6-dimethoxyphenyl)ethanone (3d)

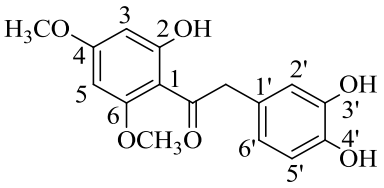

3d

Pale Brown solid (Yield 50%); mp: 130-132 °C; TLC (Petroleum Ether/EtOAc, 7:3 v/v): R_f = 0.30.

^{1}H NMR (400 MHz, $(CD_3)_2CO$): δ_H 13.90 (s, 1H, C2-OH), 7.76 (brs, 2H, OH), 6.75-6.73 (m, 2H, H-2' and H-5'), 6.58 (dd, *J* = 8.0 Hz, *J* = 1.2 Hz, 1H, H-6'), 6.06 (d, *J* = 2.0 Hz, 1H, H-5), 6.04 (d, *J* = 2.8 Hz, 1H, H-3), 4.16 (s, 2H, CH_2), 3.93 (s, 3H, OCH_3), 3.84 (s, 3H, OCH_3). **^{13}C NMR** (100 MHz, $(CD_3)_2CO$): δ_C 204.34, 168.71, 167.37, 163.74, 145.64, 144.58, 128.15, 121.77, 117.38, 115.84, 106.08, 94.55, 91.45, 56.17, 56.03, 49.99; **HRMS** (*m/z*): $[M+H]^+$ calcd. for $C_{16}H_{17}O_6$, 305.10196; found, 305.10178.

A3.10.2 General Procedure for the Vilsmeier-Haack Reaction for the Preparation of Isoflavones

In a two-neck round-bottom flask a solution of deoxybenzoin (3 mmol, 1.00 equiv.) in DMF (5 mL) was cooled to 0 °C and $BF_3 \cdot Et_2O$ (9 mmol, 3.00 equiv.) was added drop wise under argon. In another flask, DMF (8 mL) was cooled to 0 °C and PCl_5 (4.5 mmol, 1.50 equiv.) was added. The mixture was then allowed to stir at 55 °C for 20 min. The light yellow colored solution containing *N,N'*-dimethyl(chloromethylene)ammonium chloride was then added to the above reaction mixture at 0 °C. The mixture was stirred at room temperature for 2 h under argon and then poured into 0.1 N methanolic HCl (70 mL) and allowed to stir at 70 °C for 2 h. After removing the solvents *in vacuo*, H_2O (50 mL) and EtOAc (50 mL) were added and the aqueous phase was extracted with EtOAc (3 x 100 mL). The combined organic layers were washed once with brine (100 mL), dried over Na_2SO_4, and finally concentrated under reduced pressure. The residue was purified by FC using Petroleum Ether/EtOAc as eluent, to give the corresponding isoflavone.

3-(3-hydroxy-4-methoxyphenyl)-5,7-dimethoxy-4H-chromen-4-one (4a)

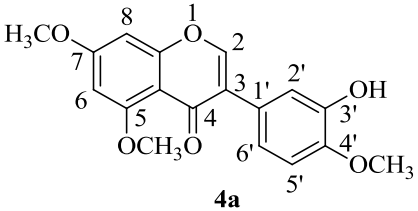

4a

Brown solid (Yield 32%); mp: 175-177 °C; TLC (Petroleum Ether/EtOAc, 3:7 v/v): R_f = 0.35.

^{1}H NMR (400 MHz, $(CD_3)_2SO$): δ_H 8.97 (s, 1H, OH), 8.14 (s, 1H, H-2), 6.98 (d, *J* = 2.0 Hz, 1H, H-2'), 6.93 (d, *J* = 8.0 Hz, 1H, H-5'), 6.87 (dd, *J* = 8.0 Hz, *J* = 2 Hz, 1H, H-6'), 6.65 (d, *J* = 2.0 Hz, 1H, H-6), 6.50 (d, *J* = 2.4 Hz, 1H, H-8), 3.88 (s, 3H, OCH_3), 3.82 (s, 3H, OCH_3), 3.78 (s, 3H, OCH_3); **^{13}C NMR** (100 MHz, $(CD_3)_2SO$): δ_C 173.69, 163.56, 160.80, 159.15, 150.89, 147.40, 145.92, 145.78, 124.79, 119.78, 116.63, 116.54, 111.81, 108.97, 96.17, 92.91, 56.12, 55.94, 55.63; **HRMS** (*m/z*): $[M+H]^+$ calcd. for $C_{18}H_{17}O_6$, 329.10196; found, 329.10203.

3-(4-hydroxy-3-methoxyphenyl)-5,7-dimethoxy-4H-chromen-4-one (4b)

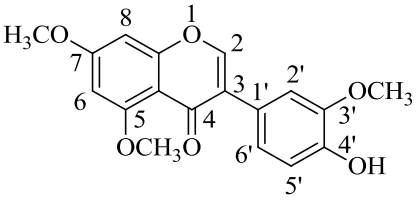

4b

Brown Solid (Yield 31%); mp: 223-224 °C; TLC (Petroleum Ether/EtOAc, 3:7 v/v): R_f = 0.29.

^{1}H NMR (400 MHz, $CDCl_3$): δ_H 7.77 (s, 1H, H-2), 7.28 (s, 1H, H-2'), 6.91 (d, *J* = 8.0 Hz,1H, H-5'), 6.87 (d, *J* = 8.0 Hz, 1H, H-6'), 6.44 (brd, 1H, H-6), 6.37 (brd, 1H, H-8), 5.80 (s, 1H, OH), 3.93 (s, 3H, OCH_3), 3.90 (s, 3H, OCH_3), 3.88 (s, 3H, OCH_3); **^{13}C NMR** (100 MHz, $CDCl_3$): δ_C 175,58, 164.00, 161.58, ,160.00, 150.32, 146.29, 145.81, 126.13, 124.26, 121.68, 114.23, 112.65, 110.02, 96.30, 92.65, 56.51, 56.19, 55.85; **HRMS** (*m/z*): $[M+H]^+$ calcd. for $C_{16}H_{17}O_6$, 329.10196; found, 329.10171.

3-(3-hydroxyphenyl)-5,7-dimethoxy-4H-chromen-4-one (4c)

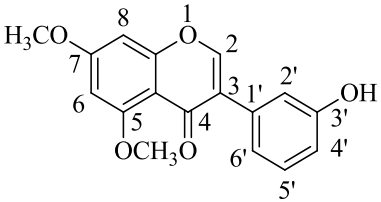

4c

Brown Solid (Yield 28%); mp: 194.8-196.7 °C; TLC (Petroleum Ether/EtOAc, 3:7 v/v): R_f = 0.30.

^{1}H NMR (400 MHz, $(CD_3)_2SO$): δ_H 9.43 (s, 1H, OH), 8.20 (s, 1H, H-2), 7.18 (t, *J* = 8.0 Hz, 1H, H-5'), 6.92 (s, 1H, H-2'), 6.88 (d, *J* = 8.0 Hz, 1H, H-4'), 6.75 (dd, *J* = 8.0 Hz, *J* = 2.0 Hz, 1H, H-6'), 6.67 (d, *J* = 2.0 Hz, 1H, H-6), 6.52 (d, *J* = 2.0 Hz, 1H, H-8), 3.88 (s, 3H, OCH_3), 3.83 (s, 3H, OCH_3); **^{13}C NMR** (100 MHz, $(CD_3)_2SO$): δ_C 173.50, 163.66, 160.83, 159.17, 156.96, 151.50, 133.39, 128.96, 125.08, 119.64, 116.22, 114.62, 108.98, 96.27, 92.99, 56.16, 55.99; **HRMS** (*m/z*): $[M+Na]^+$ calcd. for $C_{17}H_{14}O_5Na$, 321.07334; found, 321.07312.

3-(3,4-dihydroxyphenyl)-5,7-dimethoxy-4H-chromen-4-one (4d)

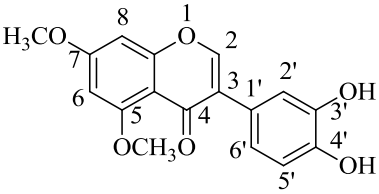

4d

White solid (Yield 30%), Mp: 127–129°C.

^{1}H-NMR (400 MHz, methanol-d_4): δ = 7.86 (s, 1H, H-2), 6.88 (brs, 1H, H-2′), 6.70 (brs, 2H, H-5′ and H-6′), 6.50 (d, *J* = 2.0 Hz, 1H, H-6), 6.40 (d, *J* = 2.0 Hz, 1H, H-8), 3.80 (s, 3H, OCH_3), 3.79 (s, 3H, OCH_3). **^{13}C-NMR** (100 MHz, methanol-d_4): 175.0, 165.1, 161.1, 159.9, 151.3, 145.1, 145.0, 126.5, 123.1, 120.5, 117.0, 110.0, 114.5, 95.9, 92.8, 55.1. **HRMS** (ESI): calcd. for $C_{17}H_{15}O_6$ [$(M+H)^+$]: 315.086300; found, 315.086363.

A3.10.3 General Procedure for the Alkylation/Benzylation Reaction

To a solution of the isoflavone (0.18 mmol, 1.00 equiv.) in acetone (5 mL), K_2CO_3 (1.8 mmol, 10.00 equiv.) was added. After stirring for 15 min the corresponding alky/benzyl bromide (0.9 mmol, 5.00 equiv.) was added dropwise to the mixture and stirred at 45 °C overnight. After removing the acetone *in vacuo*, H_2O (10 mL) and EtOAc (20 mL) were added and the aqueous phase was extracted with EtOAc (3 x 20 mL). The combined organic layers were dried over Na_2SO_4, and finally concentrated under reduced pressure. The residue was purified by FC using Petroleum Ether/EtOAc as eluent to give the corresponding substituted-isoflavone**.**

Glabrescione B (XIII)

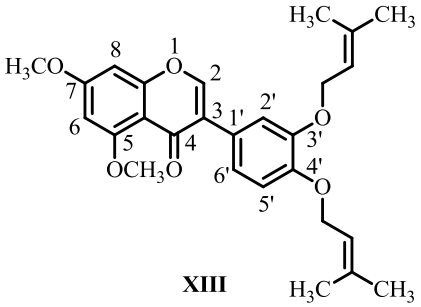

XIII

White solid (Yield 90%). Mp: 102–104°C.

^{1}H-NMR (400 MHz, acetone-d_6): δ = 7.94 (s, 1H, H-8), 7.16 (d, *J* = 1.6 Hz, 1H, H-15), 6.99 (dd, *J* = 8.0 Hz and 1.6 Hz, 1H, H-11), 6.89 (d, *J* = 8.0 Hz, 1H, H-12), 6.50 (d, *J* = 2.0 Hz, 1H, H-1), 6.42 (d, *J* = 2.0 Hz, 1H, H-3), 5.43 (m, 2H, 2 x =CH), 4.51 (d, *J* = 6.8 Hz, 4H, OCH_2), 3.86 (s, 3H, OCH_3), 3.81 (s, 3H, OCH_3), 1.70 (s, 6H, 2 CH_3), 1.67 (s, 6H, 2 CH_3). **^{13}C-NMR** (400 MHz, $CDCl_3$): δ = 175.6, 164.0, 161.2, 159.7, 150.2, 148.9, 148.5, 136.9, 126.5, 125.0, 121.4, 120.7, 115.5, 110.0, 114.0, 96.5, 92.6, 66.0, 56.4, 55.9, 25.6, 18.1. **HRMS** (ESI): calcd. for $C_{27}H_{31}O_6$ [$(M+H)^+$]: 451.211500; found, 451.211495.

5,7-dimethoxy-3-(4-methoxy-3-((3-methylbut-2-en-1-yl)oxy)phenyl)-4H-chromen-4-one (5)

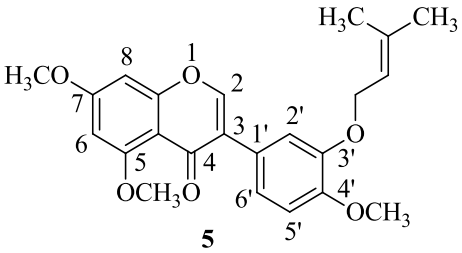

5

White Solid (Yield 95%); Mp: 113-113.2 °C; TLC (Petroleum Ether/EtOAc, 3:7 v/v): R_f = 0.33.

^{1}H NMR (400 MHz, $CDCl_3$): δ_H 7.76 (s, 1H, H-2), 7.22 (d, *J* = 2.0 Hz, 1H, H-2'), 7.01 (dd, *J* = 8.0 Hz, *J* = 1.6 Hz, 1H, H-6'), 6.88 (d, *J* = 8.0 Hz, 1H, H-5'), 6.44 (d, *J* = 1.2 Hz, 1H, H-6), 6.37 (d, *J* = 2.4 Hz, 1H, H-8), 5.55 (t, *J* = 6.8 Hz, 1H, CH), 4.59 (d, *J* = 8.0 Hz, 2H, CH_2), 3.94 (s, 3H, OCH_3), 3.88 (s, 3H, OCH_3), 3.87 (s, 3H, OCH_3), 1.76 (s, 3H, CH_3), 1.71 (s, 3H, CH_3); **^{13}C NMR** (100 MHz, $CDCl_3$): δ_C 175.49, 163.97, 161.59, 159.98, 150.28, 149.49, 148.03, 137.80, 126.14, 124.78, 121.45, 120.00, 114.61, 111.20, 110.07, 96.29, 92.64, 65.93, 56.51, 56.02, 55.84, 25.99, 18.38; **HRMS** (*m/z*): $[M+H]^+$ calcd. for $C_{23}H_{25}O_6$, 397.16456; found, 397.16441.

5,7-dimethoxy-3-(3-methoxy-4-((3-methylbut-2-en-1-yl)oxy)phenyl)-4H-chromen-4-one (6)

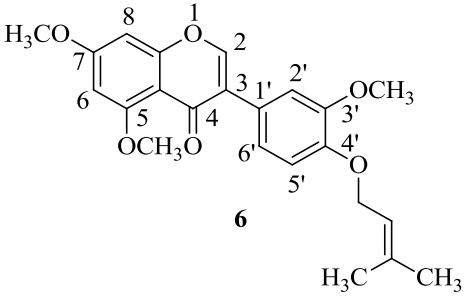

6

White Solid (Yield 95%); mp: 130.9-132.6 °C; TLC (Petroleum Ether/EtOAc, 3:7 v/v): R_f = 0.36.

^{1}H NMR (400 MHz, $CDCl_3$): δ_H 7.77 (s, 1H, H-2), 7.23 (s, 1H, H-2'), 6.95 (dd, *J* = 8.0 Hz, *J* = 2.0 Hz, 1H, H-6'), 6.87 (d, *J* = 8.0 Hz, 1H, H-5'), 6.43 (d, *J* = 1.6 Hz, 1H, H-6), 6.36 (d, *J* = 1.6 Hz, 1H, H-8), 5.52 (t, *J* = 6.4 Hz, 1H, CH), 4.59 (d, *J* = 7.8 Hz, 1H, CH_2), 3.93 (s, 3H, OCH_3), 3.89 (s, 3H, OCH_3), 3.88 (s, 3H, OCH_3), 1.76 (s, 3H, CH_3), 1.72 (s, 3H, CH_3); **^{13}C NMR** (100 MHz, $CDCl_3$): δ_C 175.64, 163.96, 161.59, 159.96, 150.30, 149.12, 148.29, 137.63, 126.11, 124.94, 121.12, 120.14, 113.18, 112.84, 110.06, 96.28, 92.64, 65.86, 56.50, 56.11, 55.83, 25.93, 18.34; **HRMS** (*m/z*): $[M+H]^+$ calcd. for $C_{25}H_{20}F_3O_5$, 457.12573; found, 457.12543.

5,7-dimethoxy-3-(3-((3-methylbut-2-en-1-yl)oxy)phenyl)-4H-chromen-4-one (7)

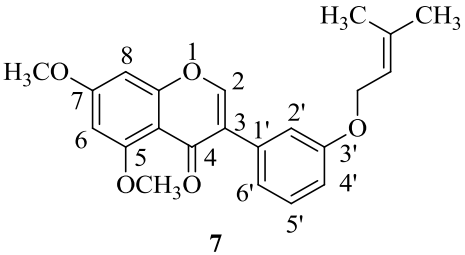

7

Yellow Oil (Yield 95%); TLC (Petroleum Ether/EtOAc, 2:3 v/v): R_f = 0.31.

^{1}H NMR (400 MHz, $CDCl_3$): δ_H 7.79 (s, 1H, H-2), 7.29 (t, *J* = 7.6 Hz, 1H, H-5'), 7.16 (d, *J* = 2.0 Hz, 1H, H-2'), 7.08 (d, *J* = 8.0 Hz, 1H, H-4'), 6.92 (dd, *J* = 8.0 Hz, *J* = 1.2 Hz, 1H, H-6'), 6.45 (d, *J* = 2.0 Hz, 1H, H-6), 6.37 (d, *J* = 2.0 Hz, 1H, H-8), 5.51 (t, *J* = 6.8 Hz, 1H, CH), 4.53 (d, *J* = 6.8 Hz, 1H, CH_2), 3.94 (s, 3H, OCH_3), 3.89 (s, 3H, OCH_3), 1.79 (s, 3H, CH_3), 1.74 (s, 3H, CH_3); **^{13}C NMR** (100 MHz, $CDCl_3$): δ_C 175.21, 164.05, 161.64, 159.99, 158.85, 150.78, 138.27, 133.51, 129.23, 126.41, 121.61, 119.85, 115.38, 114.92, 110.14, 96.38, 92.68, 64.95, 56.51, 55.87, 29.84, 25.99, 18.35; **HRMS** (*m/z*): $[M+H]^+$ calcd. for $C_{22}H_{23}O_5$, 367.15400; found, 367.15362.

3-(3-(benzyloxy)-4-methoxyphenyl)-5,7-dimethoxy-4H-chromen-4-one (8)

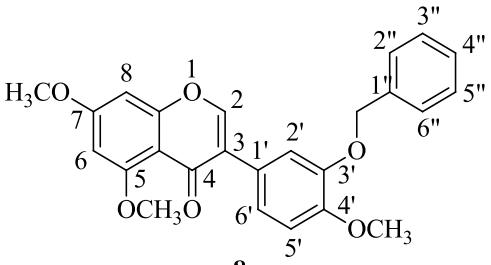

8

Light Brown Solid (Yield 95%); mp: 128-129 °C TLC (Petroleum Ether/EtOAc, 3:7 v/v): R_f = 0.36.

^{1}H NMR (400 MHz, $CDCl_3$): δ_H 7.45 (s, 1H, H-2), 7.37-7.26 (m, 3H, H-3",H-4" and H-5"), 7.06 (d, *J* = 8.0 Hz, 1H, H-6"), 6.91 (d, *J* = 8.0 Hz, 1H, H-2"), 6.44 (brd, 1H, H-6), 6.37 (brd, 1H, H-8), 5.17 (s, 2H, CH_2), 3.95 (s, 3H, OCH_3), 3.90 (s, 3H, OCH_3), 3.89 (s, 3H, OCH_3); **^{13}C NMR** (100 MHz, $CDCl_3$): δ_C 175.59, 164.01, 159.99, 150.35, 148.01, 137.32, 128.60, 127.90, 127.68, 124.87, 122.14, 115.58, 111.75, 96.35, 92.69, 71.27, 56.61, 56.21, 55.90; **HRMS** (*m/z*): $[M+H]^+$ calcd. for $C_{25}H_{23}O_6$, 419.15891; found, 419.14871.

3-(4-(benzyloxy)-3-methoxyphenyl)-5,7-dimethoxy-4H-chromen-4-one (9)

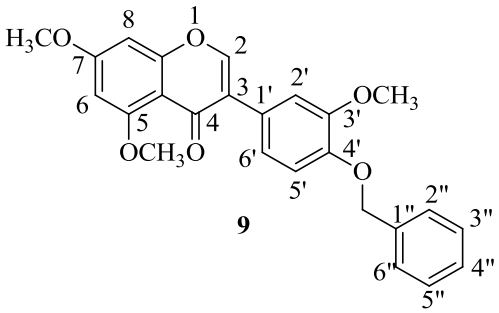

9

Pale White solid (Yeld 95%); mp: 148.5-149 °C; TLC (Petroleum Ether/EtOAc, 3:7 v/v): R_f = 0.28.

^{1}H NMR (400 MHz, $CDCl_3$): δ_H 7.75 (s, 1H, H-2), 7.43 (d, *J* = 8.0 Hz, 2H, H-2", H-6"), 7.35 (t, *J* = 8.0 Hz, 1H, H-3", H-5"), 7.29 (d, *J* = 7.2 Hz, 1H, H-4"), 7.25 (s, 1H, H-2'), 6.89 (d, *J* = 8.0 Hz, 1H, H-6), 6.86 (d, *J* = 8.0 Hz, 1H, H-8), 6.42 (brd, 1H, H-6), 6.36 (brd, 1H, H-8), 5.17 (s, 2H, CH_2), 3.93 (s, 3H, OCH_3), 3.91 (s, 3H, OCH_3), 3.87 (s, 3H, OCH_3); **^{13}C NMR** (100 MHz, $CDCl_3$): δ_C 175.48, 164.00, 161.61, 159.98, 150.37, 149.36, 148.20, 137.31, 128.65, 127.90, 127.36, 125.52, 121.16, 113.83, 113.61, 110.07, 96.32, 92.66, 71.12, 56.52, 56.25, 55.85; **HRMS** (*m/z*): $[M+H]^+$ calcd. for $C_{25}H_{23}O_6$, 419.14891; found, 419.14962.

(E)-3-(3-((3,7-dimethylocta-2,6-dien-1-yl)oxy)-4-methoxyphenyl)-5,7-dimethoxy-4H-chromen-4-one (10)

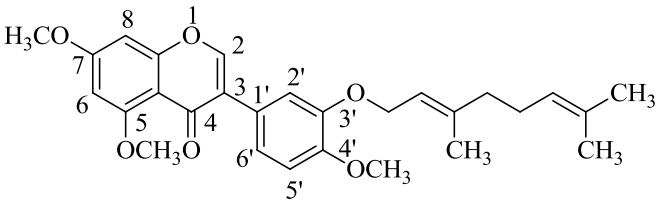

10

Pale White Solid (Yield 88%); mp: 92-93.3 °C; TLC (Petroleum Ether/EtOAc, 3:7 v/v): R_f = 0.28.

^{1}H NMR (400 MHz, $CDCl_3$): δ_H 7.76 (s, 1H, H-2), 7.22 (d, *J* = 2.0 Hz, 1H, H-2'), 7.02 (dd, *J* = 8.0 Hz, *J* = 2.0 Hz, 1H, H-6'), 6.88 (d, *J* = 8.0 Hz, 1H, H-5'), 6.43 (d, *J* = 2.0 Hz, 1H, H-6), 6.36 (d, *J* = 2.0 Hz, 1H, H-8), 5.55 (t, *J* = 6.0 Hz, 1H, CH), 5.09 (t, *J* = 6.0 Hz, 1H, CH), 4.62 (d, *J* = 6.0 Hz, 2H, CH_2), 3.94 (s, 3H, OCH_3), 3.88 (s, 6H, OCH_3), 2.10-2.04 (m, 4H, CH_2), 1.71 (s, 3H, CH_3), 1.66 (s, 3H, CH_3), 1.59 (s, 3H, CH_3); **^{13}C NMR** (100 MHz, $CDCl_3$): δ_C 175.47, 163.96, 161.59, 159.97, 150.27, 149.50, 148.04, 140.80, 131.78, 126.14, 124.79, 124.09, 121.51, 119.78, 114.70, 111.24, 110.07, 96.28, 92.64, 66.08, 56.50, 56.03, 55.84, 39.72, 26.44, 25.78, 17.79, 16.85; **HRMS** (*m/z*): $[M + H]^+$ calcd. for $C_{23}H_{25}O_6$, 465.22717; found, 465.22743.

(*E*)-3-(4-((3,7-dimethylocta-2,6-dien-1-yl)oxy)-3-methoxyphenyl)-5,7-dimethoxy-4H-chromen-4-one (11)

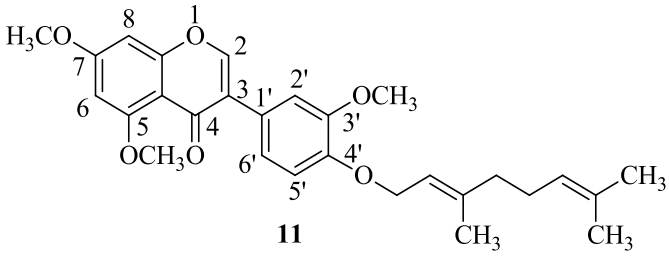

11

Pale White Solid (Yield 89%); mp: 93.5-95.3 °C; TLC (Petroleum Ether/EtOAc, 3:7 v/v): R_f = 0.34.

^{1}H NMR (400 MHz, $CDCl_3$): δ_H 7.79 (s, 1H, H-2), 7.23 (s, 1H, H-2'), 6.95 (d, *J* = 8.0 Hz, 1H, H-6'), 6.88 (d, *J* = 8.0 Hz, 1H, H-5'), 6.43 (d, *J* = 2.0 Hz, 1H, H-6), 6.37 (d, *J* = 2.0 Hz, 1H, H-8), 5.52 (t, *J* = 6.0 Hz, 1H, CH), 5.07 (t, *J* = 6.0 Hz, 1H, CH), 4.63 (d, *J* = 8.0 Hz, 2H, CH_2), 3.93 (s, 3H, OCH_3), 3.89 (s, 3H, OCH_3), 3.88 (s, 3H, OCH_3), 2.09 (d, *J* = 6.0 Hz, 2H, CH_2), 2.06 (d, *J* = 5.6 Hz, 2H, CH_2), 1.72 (s, 3H, CH_3), 1.67 (s, 3H, CH_3), 1.59 (s, 3H, CH_3); **^{13}C NMR** (100 MHz, $CDCl_3$): δ_C 175.49, 163.97, 161.58, 159.96, 150.29, 149.11, 148.30, 140.61, 131.82, 126.10, 124.95, 124.01, 121.12, 119.96, 113.19, 112.92, 110.04, 96.28, 92.64, 66.00, 56.49, 56.11, 55.83, 39.66, 26.39, 25.79, 17.80, 16.80; **HRMS** (*m/z*): $[M+H]^+$ calcd. for $C_{25}H_{20}F_3O_5$, 465.22717; found, 465.22715.

5,7-dimethoxy-3-(4-methoxy-3-((4-(trifluoromethyl)benzyl)oxy)phenyl)-4H-chromen-4-one (12)

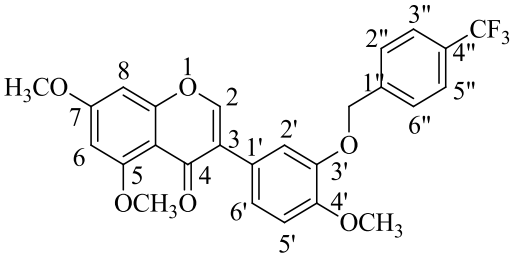

12

Pale White Solid (Yield 92%); mp: 131-134 °C; TLC (Petroleum Ether/EtOAc, 3:7 v/v): R_f = 0.32.

^{1}H NMR (400 MHz, $CDCl_3$): δ_H 7.73 (s, 1H, H-2), 7.63-7.57 (m, 4H, H-2", H-3", H-5" and H-6"), 7.29 (d, *J* = 1.6 Hz, 1H, H-2'), 7.05 (dd, *J* = 8.0 Hz, *J* =2 Hz, 1H, H-6'), 6.92 (d, *J* = 8.0 Hz,1H, H-5'), 6.43 (d, *J* = 2.0 Hz, 1H, H-6), 6.37 (d, *J* = 1.6 Hz, 1H, H-8), 5.22 (s, 2H, CH_2) 3.94 (s, 3H, OCH_3), 3.90 (s, 3H, OCH_3), 3.88 (s, 3H, OCH_3); **^{13}C NMR** (100 MHz, $CDCl_3$): δ_C 175.47, 164.06, 161.60, 159.99, 150.33, 149.78, 147.58, 141.43, 127.58, 125.82, 125.59, 125.55, 124.98, 122.31, 115.70, 111.75, 110.03, 96.36, 92.68, 70.42, 56.53, 56.15, 55.86; **HRMS** (*m/z*): $[M+H]^+$ calcd. for $C_{26}H_{22}F_3O_6$, 487.13630; found, 487.13656.

5,7-dimethoxy-3-(3-methoxy-4-((4-(trifluoromethyl)benzyl)oxy)phenyl)-4H-chromen-4-one (13)

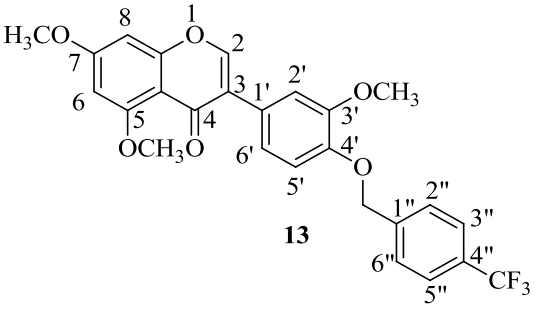

13

White Solid (Yield 94%); mp: 136.8-137.9 °C; TLC (Petroleum Ether/EtOAc, 3:7 v/v): R_f = 0.32.

^{1}H NMR (400 MHz, $CDCl_3$): δ_H 8.02 (d, *J* = 8.0 Hz, 2H, H-5" and H-3"), 7.71 (s, 1H, H-2), 7.52 (d, *J* = 8.0 Hz, 2H, H-2" and H-6"), 7.06 (s, 1H, H-2'), 7.04 (dd, *J* = 8.0 Hz, *J* = 1.6 Hz, 1H, H-6'), 6.92 (d, *J* = 1.6 Hz, 1H, H-5'), 6.43 (d, *J* = 2.0 Hz, 1H, H-6), 6.37 (d, *J* = 1.6 Hz, 1H, H-8), 5.22 (s, 2H, CH_2), 3.93 (s, 3H, OCH_3), 3.90 (s, 3H, OCH_3), 3.88 (s, 3H, OCH_3); **^{13}C NMR** (100 MHz, $CDCl_3$): δ_C 175.44, 167.07, 164.02, 161.58, 159.97, 150.31, 149.76, 147.64, 142.59, 129.93, 129.61, 127.14, 125.85, 124.93, 122.30, 115.66, 111.73, 110.02, 96.33, 92.66, 70.61, 56.52, 56.16, 55.85, 52.20, 29.82; **HRMS** (*m/z*): $[M+H]^+$ calcd. for $C_{26}H_{22}F_3O_6$, 487.13630; found, 487.13647.

5,7-dimethoxy-3-(3-((4-(trifluoromethyl)benzyl)oxy)phenyl)-4H-chromen-4-one (14)

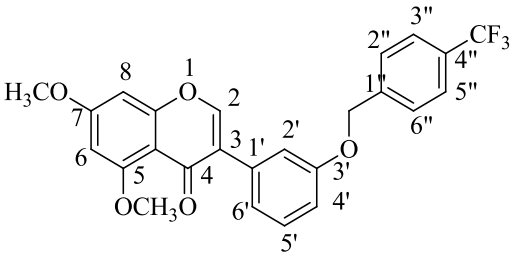

14

White Solid (Yield 91%); mp: 136.5-137 °C; TLC (Petroleum Ether/EtOAc, 3:7 v/v): R_f = 0.31.

^{1}H NMR (400 MHz, $CDCl_3$): δ_H 7.80 (s, 1H, H-2), 7.64 (d, *J* = 8.0 Hz, 2H, H-5" and H-6"), 7.56 (d, *J* = 8.0 Hz, 2H, H-2" and H-3"), 7.33-7.29 (m, 2H, H-2' and H-5'), 7.09 (d, *J* = 8.0 Hz, 1H, H-6'), 6.96 (dd, *J* = 8.0 Hz, *J* = 2.4 Hz, 1H, H-4'), 6.45 (d, *J* = 2.4 Hz, 1H, H-6), 6.39 (d, *J* = 2.4 Hz, 1H, H-8), 5.16 (s, 2H, CH_2), 3.95 (s, 3H, OCH_3), 3.98 (s, 3H, OCH_3); **^{13}C NMR** (100 MHz, $CDCl_3$): δ_C 175.19, 164.13, 161.65, 159.99, 158.35, 150.86, 141.32, 133.75, 130.29, 129.97, 129.44, 127.52, 126.10, 125.63, 125.60, 122.01, 115.80, 114.98, 110.08, 96.43, 92.72, 69.27, 56.52, 55.88; **HRMS** (*m/z*): $[M+H]^+$ calcd. for $C_{23}H_{25}O_6$, 457.12573; found, 457.12543.

3-(3,4-bis(benzyloxy)phenyl)-5,7-dimethoxy-4H-chromen-4-one (15)

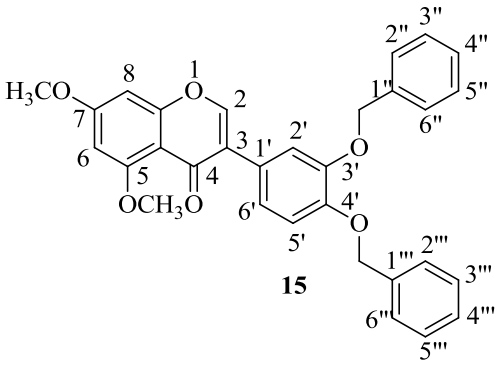

15

Pale Yellow Solid (Yield 90%); mp: 144.7-146.1 °C; TLC (Petroleum Ether:EtOAc, 3:2 v/v): R_f = 0.34.

^{1}H NMR (400 MHz, $CDCl_3$): δ_H 7.61 (s, 1H, H-2), 7.36 (t, *J* = 8.0 Hz, 1H, H-2'), 7.16-7.28 (m, 10H, H-2", H-2"', H-3", H-3"', H-4", H-4"', H-5", H-5"', H-6" and H-6"'), 6.91 (dd, *J* = 8.0 Hz, *J* = 1.2 Hz, 1H, H-6'), 6.85 (d, *J* = 8.0 Hz, 1H, H-5'), 6.33 (d, *J* = 2.0 Hz, 1H, H-6), 6.27 (d, *J* = 2.0 Hz, 1H, H-8), 5.09 (s, 2H, CH_2), 5.08 (s, 2H, CH_2), 3.84 (s, 3H, OCH_3), 3.78 (s, 3H, OCH_3); **^{13}C NMR** (100 MHz, $CDCl_3$): δ_C 175.41, 163.99, 161.58, 159.95, 150.37, 149.01, 148.79, 137.46, 128.56, 128.52, 127.84, 127.82, 127.59, 127.39, 125.69, 122.19, 116.50, 114.95, 110.03, 96.31, 92.65, 71.47, 71.41, 56.50,

55.83; **HRMS** (*m/z*): $[M+H]^+$ calcd. for $C_{31}H_{27}O_6$, 495.18022; found, 495.17997.

4-((5-(5,7-dimethoxy-4-oxo-4H-chromen-3-yl)-2-methoxyphenoxy)methyl)benzonitrile **(16)**

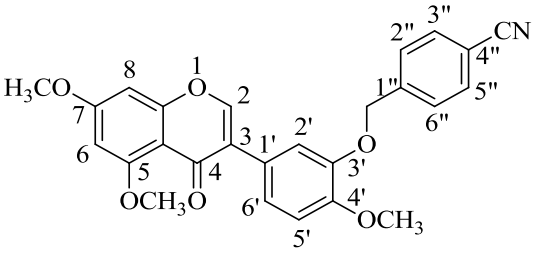

16

Pale Yellow Solid, (Yield 93%); mp: 178.5-180.1 °C; TLC (Petroleum Ether/EtOAc, 3:7 v/v): R_f = 0.36.

^{1}H NMR (400 MHz, $CDCl_3$): δ_H 7.73 (s, 1H, H-2), 7.65 (d, *J* = 8.0 Hz, 2H, H-3",H-5"), 7.56 (d, *J* = 8.0 Hz, 2H, H-2",H-6"), 7.29 (s, 1H, H-2'), 7.03 (d; *J* = 2.0 Hz, 1H, H-6'), 6.92 (d, *J* = 8.0 Hz, 1H, H-5'), 6.43 (d, *J* = 2.0 Hz, 1H, H-6), 6.37 (d, *J* = 2.0 Hz, 1H, H-8), 5.21 (s, 2H, CH_2), 3.94 (s, 3H, OCH_3), 3.90 (s, 3H, OCH_3), 3.88 (s, 3H, OCH_3); **^{13}C NMR** (100 MHz, $CDCl_3$): δ_C 175.46, 164.06, 161.55, 159.96, 150.34, 149.73, 147.30, 142.86, 132.45, 127.74, 124.97, 122.38, 115.80, 111.71, 111.59, 109.96, 96.36, 92.67, 77.48, 77.16, 76.84, 70.23, 56.53, 56.10, 55.87; **HRMS** (*m/z*): $[M+H]^+$ calcd. for $C_{26}H_{22}NO_6$, 444.14416; found, 444.14302.

Methyl-4-((5-(5,7-dimethoxy-4-oxo-4H-chromen-3-yl)-2-methoxyphenoxy)methyl)benzoate **(17)**

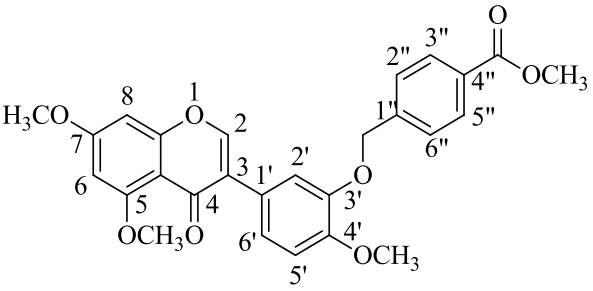

17

Pale White Solid (Yield 91%); mp: 182.4-183.3 °C; TLC (Petroleum Ether/EtOAc, 2:3 v/v): R_f = 0.33.

^{1}H NMR (400 MHz, $CDCl_3$): δ_H 8.03 (d, *J* = 8.0 Hz, 2H, H-3" and H-5"), 7.71 (s, 1H, H-2), 7.53 (d, *J* = 8.0 Hz, 2H, H-2" and H-6"), 7.06 (dd, *J* = 8.0 Hz, *J* = 2.0 Hz, 1H, H-6'), 6.92 (d, *J* = 8.0 Hz, 1H, H-5'), 6.43 (d, *J* = 2.0 Hz, 1H, H-6), 6.37 (d, *J* = 2.0 Hz, 1H, H-8), 5.23 (s, 2H, CH_2), 3.94 (s, 3H, OCH_3), 3.91 (s, 3H, OCH_3), 3.88 (s, 3H, OCH_3); **^{13}C NMR** (100 MHz, $CDCl_3$): δ_C 175.44, 164.06, 161.61, 159.99, 150.42, 149.39, 147.75, 141.43, 130.26, 127.36, 126.05, 125.66, 125.62, 121.17, 113.91, 113.69, 110.02, 104.61, 96.36, 92.68, 70.37, 56.53, 56.23, 55.86; **HRMS** (*m/z*): $[M+H]^+$ calcd. for $C_{27}H_{25}O_8$, 477.15439; found, 477.15582.

4-((5-(5,7-dimethoxy-4-oxo-4H-chromen-3-yl)-2-methoxyphenoxy)methyl)benzamide **(18)**

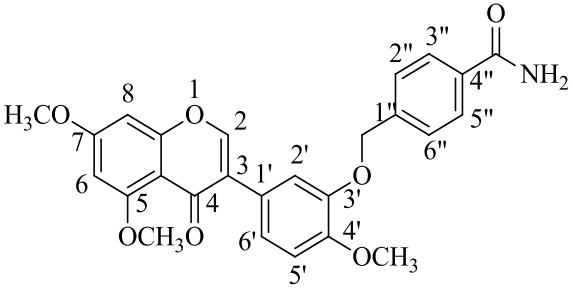

18

Pale White Solid (Yield 93%); mp: 219-221 °C; TLC ($CHCl_3$/CH_3OH, 97:3 v/v): R_f = 0.32.

^{1}H NMR (400 MHz, $CDCl_3$): δ_H 8.32 (s, 1H, NH), 8.21 (s, 1H, H-2), 7.99 (s, 1H, NH), 7.89 (d, *J* = 8.0 Hz, 2H, H-3" and H-5"), 7.53 (d, *J* = 8.0 Hz, 2H, H-2" and H-6"), 7.39 (s, 1H, H-2'), 7.09 (d, *J* = 8.0 Hz, 1H, H-6'), 7.02 (d, *J* = 8.0 Hz, 1H, H-5'), 6.67 (brd, 1H, H-6), 6.52 (brd, 1H, H-8), 5.15 (s, 2H, CH_2), 3.88 (s, 3H, OCH_3), 3.83 (s, 3H, OCH_3), 3.80 (s, 3H, OCH_3); **^{13}C NMR** (100 MHz, $(CD_3)_2SO$): δ_C 196.49, 173.67, 167.66, 163.64, 160.83, 159.18, 151.25, 148.95, 147.12, 140.41, 133.75, 127.62, 127.34, 124.65, 124.54, 122.00, 114.83, 111.79, 108.93, 96.22, 92.96, 79.20, 69.62, 56.13, 55.99, 55.67; **HRMS** (*m/z*): $[M+H]^+$ calcd. for $C_{25}H_{20}F_3O_5$, 457.12573; found, 457.12543.

5,7-dimethoxy-3-(4-methoxy-3-((4-nitrobenzyl)oxy)phenyl)-4H-chromen-4-one **(19)**

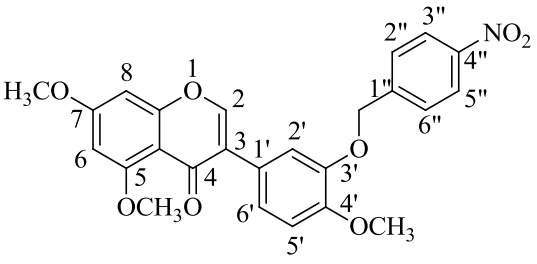

19

Pale White Solid (Yeld 95%); mp: 170.5-171.5 °C; TLC (Petroleum Ether/EtOAc, 2:3 v/v): R_f = 0.29.

^{1}H NMR (400 MHz, $CDCl_3$): δ_H 8.22 (d, *J* = 8.0 Hz, 2H, H-3" and H-5"), 7.74 (s, 1H, H-2), 7.64 (d, *J* = 8.0 Hz, 2H, H-2" and H-6"), 7.32 (s, 1H, H-2'), 7.04 (dd, *J* = 8.0 Hz, *J* = 2.0 Hz, 1H, H-6'), 6.93 (d, *J* = 8.0 Hz, 1H, H-5'), 6.44 (d, *J* = 2.0 Hz, 1H, H-6), 6.37 (d, *J* = 2.0 Hz, 1H, H-8), 5.27 (s, 2H, CH_2), 3.95 (s, 3H, OCH_3), 3.92 (s, 3H, OCH_3), 3.89 (s, 3H, OCH_3); **^{13}C NMR** (100 MHz, $CDCl_3$): δ_C 175.48, 164.10, 161.57, 159.99, 150.37, 149.78, 147.61, 147.27, 144.92, 127.79, 125.68, 125.02, 123.88, 122.48, 115.93, 111.77, 109.97, 96.38, 92.69, 70.05, 56.53, 56.13, 55.88; **HRMS** (*m/z*): $[M+H]^+$ calcd. for $C_{25}H_{22}NO_8$, 464.13399; found, 464.13435.

Chapter A4

Bibliography

1. J. Mann, *Nat. Rev. Cancer* 2002, **2**, 143.
2. D. G. I. Kingston, D. J. Newman, *Nat. Prod. Chem. Biol. First Ed. Ed. by Natanya Civjan,* 2012, 325–349.
3. M. E. Maier, *Nat. Prod. Rep.* , 2009, **26**, 1105–1124.
4. M. F. Clarke, J. E. Dick, P. B. Dirks, C. J. Eaves, C. H. M. Jamieson, D. L. Jones, J. Visvader, I. L. Weissman, G. M. Wahl, *Cancer Res.*, 2006, **66**, 9339–9344.
5. H. Clevers, *Nat. Med.*, 2011, **17**, 313–319.
6. T. Reya, S. J. Morrison, M. F. Clarke, I. L. Weissman, *Nature*, 2001, **414**, 105–111.
7. M. B. Insan, V. Jaitak, *Mini Rev. Med. Chem.*, 2014, **14**, 20–34.
8. R. Pardal, M. F. Clarke, S. J. Morrison, *Nat. Rev. Cancer*, 2003, **3**, 895–902.
9. L. Han, S. Shi, T. Gong, Z. Zhang, X. Sun, *Acta Pharm. Sin. B* 2013, **3**, 65–75.
10. R. Tannishtha, S. J. Morrison, M. F. Clarke, I. L. Weissman, *Nature*, 2001, **414**, 105–111.
11. Wang Z., Li Y., Long D., Sarkar F.H.; *Curr. Drug Targets*, 2010, **11**, 745.

12. Reya T., Duncan A.W., Ailles L., Domen J., Scherer D.C., Willert K., Hintz L., Nusse R., Weissman I.L., *Nature*, 2003, **423**, 409.
13. S. J. Scales, F. J. de Sauvage, *Trends Pharmacol. Sci.*, 2009, **30**, 303–312.
14. M. Varjosalo, J. Taipale, *Genes Dev.*, 2008, **22**, 2454–2472.
15. P. W. Ingham, A. P. McMahon, *Genes Dev.*, 2001, **15**, 3059–3087.
16. P. Kogerman, T. Grimm, L. Kogerman, D. Krause, A. B. Unden, B. Sandstedt, R. Toftgard, P. G. Zaphiropoulos, *Nat. Cell. Biol.*, 1999, **1**, 312–319.
17. D. M. Stone, M. Murone, S. Luoh, W. Ye, M. P. Armanini, A. Gurney, H. Phillips, J. Brush, A. Goddard, F. J. de Sauvage, *et al.*, *J. Cell Sci.* 1999, **112**, Pt 2, 4437–4448.
18. D. Amakye, Z. Jagani, M. Dorsch, *Nat. Med.* 2013, **19**, 1410–1422.
19. A. Ruiz i Altaba, P. Sanchez, N. Dahmane, *Nat. Rev. Cancer*, 2002, **2**, 361-372.
20. Y.-H. Bian, S.-H. Huang, L. Yang, X.-L. Ma, J.-W. Xie, H.-W. Zhang, *World J. Gastroenterol.*, 2007, **13**, 1659–1665.

21. A. N. Gerber, C. W. Wilson, Y.-J. Li, P.-T. Chuang,, *Oncogene*, 2006, **26**, 1122–1136.
22. P. Sanchez, A. M. Hernández, B. Stecca, A. J. Kahler, A. M. DeGueme, A. Barrett, M. Beyna, M. W. Datta, S. Datta, A. Ruiz i Altaba, *Proc. Natl. Acad. Sci. United States Am.*, 2004, **101**, 12561–12566.
23. L. L. Rubin, F. J. de Sauvage, Nat. Rev. Drug Discov. 2006, **5**, 1026–1033.
24. J. Xie, M. Murone, S. M. Luoh, a Ryan, Q. Gu, C. Zhang, J. M. Bonifas, C. W. Lam, M. Hynes, a Goddard, *et al.*, *Nature*, 1998, **391**, 90–92.
25. U. Tostar, C. J. Malm, J. M. Meis-Kindblom, L. G. Kindblom, R. Toftgård, A. B. Undén, *J. Pathol.*, 2006, **208**, 17–25.
26. M. D. Taylor, L. Liu, C. Raffel, C. Hui, T. G. Mainprize, X. Zhang, R. Agatep, S. Chiappa, L. Gao, A. Lowrance, *et al.*, *Nat. Genet.*, 2002, **31**, 306–310.
27. N. Takebe, P. J. Harris, R. Q. Warren, S. P. Ivy, *Nat Rev Clin Oncol.*, 2011, **8**, 97–106.
28. L. Fan, C. V. Pepicelli, C. C. Dibble, W. Catbagan, J. L. Zarycki, R. Laciak, J. Gipp, A. Shaw, M. L. G. Lamm, A. Munoz, *et al.*, *Endocrinology*, 2004, **145**, 3961–3970.
29. S. Coni, P. Infante, A. Gulino, *Biochem. Pharmacol.*, 2013, **85**, 623–628.

30. P. Infante, R. Alfonsi, B. Botta, M. Mori, L. Di Marcotullio, *Trends Pharmacol. Sci.*, 2015, **36**, 547–558.
31. Zhao. *et al.*, *Nature*, 2007, **450**, 252.
32. Heretsch *et al*., *Bioorg. Med. Chem*., 2010, **18**, 6613-6624.
33. R. L. Yauch, G. J. P. Dijkgraaf, B. Alicke, T. Januario, C. P. Ahn, T. Holcomb, K. Pujara, J. Stinson, C. A. Callahan, T. Tang, *et al*., *Science*, 2009, **80**, 572–574.
34. M. Lauth, Å. Bergström, *Proc.*, 2007, **104**, 8455–8460.
35. J. M. Hyman, A. J. Firestone, V. M. Heine, Y. Zhao, C. a Ocasio, K. Han, M. Sun, P. G. Rack, S. Sinha, J. J. Wu, *et al*., *Proc. Natl. Acad. Sci.*, 2009, **106**, 14132–14137.
36. J. Kim, J. J. Lee, J. Kim, D. Gardner, P. a Beachy, *Proc. Natl. Acad. Sci. U. S. A.*, 2010, **107**, 13432–13437.
37. P. Infante, M. Mori, R. Alfonsi, F. Ghirga, F. Aiello, S. Toscano, C. Ingallina, M. Siler, D. Cucchi, A. Po, *et al*., *EMBO J.*, 2015, **34**, 200–217.
38. N. P. Pavletich, C. O. Pabo, *Science*, 1993, **261**, 1701–1707.
39. M. L. Verdonk, J. C. Cole, M. J. Hartshorn, C. W. Murray, R. D. Taylor, *Proteins Struct. Funct. Bioinforma.*, 2003, **623**, 609–623.
40. K. P. Ko, *Asian Pacific J. Cancer Prev.*, 2014, **15**, 7001–7010.

41. H. Hussain, I. R. Green, *Expert Opin. Ther. Pat.* 2017, 1–12.
42. S. Berardozzi, F. Bernardi, P. Infante, C. Ingallina, S. Toscano, E. De Paolis, R. Alfonsi, M. Caimano, B. Botta, M. Mori, L. Di Marcotullio, F. Ghirga, *Eu. J. Med. Chem*, 2018, **156**, 554-562.
43. P. Infante, R. Alfonsi, C. Ingallina, D. Quaglio, F. Ghirga, I. D'Acquarica, F. Bernardi, L. Di Magno, G. Canettieri, I. Screpanti, A. Gulino, B. Botta, M. Mori, L. Di Marcotullio, *Cell Death Dis*., 2016, **7**, e2376.
44. R. Alfonsi, B. Botta, S. Cacchi, L. Di Marcotullio, G. Fabrizi, R. Faedda, A. Goggiamani, A. Iazzetti, M. Mori, *J. Med. Chem*., 2017, **60**, 1469-1477.
45. A. Calcaterra, V. Iovine, B. Botta, D. Quaglio, I. D'Acquarica, A. Ciogli, A. Iazzetti, R. Alfonsi, L. Lospinoso Severini, P. Infante, L. Di Marcotullio, M. Mori, F. Ghirga, *J. Enzyme Inhib. Med. Chem*., 2018, **33**, 349-358.
46. M.S. Christodoulou, M. Mori, R. Pantano, R. Alfonsi, P. Infante, M. Botta, G. Damia, F. Ricci, P.A. Sotiropoulou, S. Liekens, B. Botta, D. Passarella, *Chempluschem*, 2015, **80**, 938-943.
47. A. Lévai, *J. Heterocycl. Chem.*, 2004, **41**, 449–460.

48. M. Lauth, V. Rohnalter, A. Bergstrom, M. Kooshesh, P. Svenningsson, R. Toftgard, *Mol. Pharmacol*., 2010, **78**, 486-496.
49. K. Wahala, T. A. Hase, *J. Chem. Soc. Perkin Trans.*, 1991, **1**, 3005–3008.
50. E.F.X. Byrne, R. Sircar, P.S. Miller, G. Hedger, G. Luchetti, S. Nachtergaele, M.D. Tully, L. Mydock-McGrane, D.F. Covey, R.P. Rambo, M.S.P. Sansom, S. Newstead, R. Rohatgi, C. Siebold, *Nature*, 2016, **535**, 517-522.
51. C. Wang, H. Wu, T. Evron, E. Vardy, G.W. Han, X.P. Huang, S.J. Hufeisen, T.J. Mangano, D.J. Urban, V. Katritch, V. Cherezov, M.G. Caron, B.L. Roth, R.C. Stevens, *Nat. Commun.*, 2014, **5**, 4355.
52. C. Wang, H. Wu, V. Katritch, G.W. Han, X.P. Huang, W. Liu, F.Y. Siu, B.L. Roth, V. Cherezov, R.C. Stevens, *Nature*, 2013, **497**, 338-343.
53. U. Weierstall, D. James, C. Wang, T.A. White, D. Wang, W. Liu, J.C. Spence, R. Bruce Doak, G. Nelson, P. Fromme, R. Fromme, I. Grotjohann, C. Kupitz, N.A. Zatsepin, H. Liu, S. Basu, D. Wacker, G.W. Han, V. Katritch, S. Boutet, M. Messerschmidt, G.J. Williams, J.E. Koglin, M. Marvin Seibert, M. Klinker, C. Gati, R.L. Shoeman, A. Barty, H.N. Chapman, R.A. Kirian, K.R.

Beyerlein, R.C. Stevens, D. Li, S.T. Shah, N. Howe, M. Caffrey, V. Cherezov, *Nat. Commun*.,2014, **5**, 3309.

54. X. Zhang, F. Zhao, Y. Wu, J. Yang, G.W. Han, S. Zhao, A. Ishchenko, L. Ye, X. Lin, K. Ding, V. Dharmarajan, P.R. Griffin, C. Gati, G. Nelson, M.S. Hunter, M.A. Hanson, V. Cherezov, R.C. Stevens, W. Tan, H. Tao, F. Xu, *Nat. Commun*., 2017, **8**, 15383.

Part B

Towards the Total Synthesis of Madangamine B

This work of my PhD research was carried out in the laboratory of Prof. Mercedes Amat, at Universidad De Barcelona (Spain).

Chapter B1

General Introduction

B1.1 Marine alkaloids

B1.1.1 Alkaloids Isolated from Marine Sponges of the Genus *Haposclerida*

Sponges (*Phylum Porifera*) are usually described as the most primitive of all the multicellular organisms found in all the oceans of the world, at depths ranging from the shoreline to the deep abyssal plane. Sponges are typically betonic animals and, with the exception of about 150 species of freshwater, almost exclusively marine[1-4].

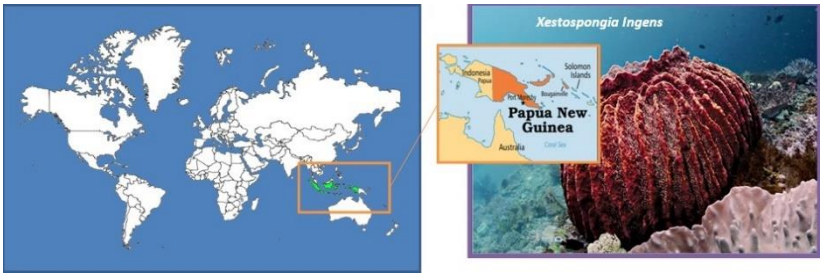

Figure 24 Papua New Guinea and Xestospongia Ingens sponge.

About a third of all marine products and more than half of all alkaloids, have been isolated from sponges (*Phylum Porifera*). A group of these alkaloids contains compounds, that although structurally different, are characterized by the presence of a 3-alkylpiperidine motif in their structure.

The alkyl component of this common structural motif is often a linear, saturated or unsaturated chain, which ranges from eight to

sixteen carbon atoms. The heterocyclic component can instead be found in different oxidation states, pyridine, tetrahydropyridine or piperidine. About one third of the known members of this group, which are either simple monomers or oligomers or high molecular weight polymers, contain pyridine. The remaining two-thirds, which have more complex cyclic structures and appear to be biogenetically derived from macrocyclic dimers, instead present piperidine and tetrahydropyridine heterocycles (figure 25).

The assumption of a common biogenetic origin is based on more evidence: perhaps the most important of these is the little diffusion in nature of a 3-alkylpiperidinic nucleus, so its presence in a group of metabolites isolated from members of a particular *phylum* represents a significant indication of the biogenetic correlation. Instead, the observation that the sponges, whose metabolites have the 3-alkylpiperidinic nucleus, all belong to the order *Haplosclerida*, provides a taxonomic support about the common biogenetic origin.

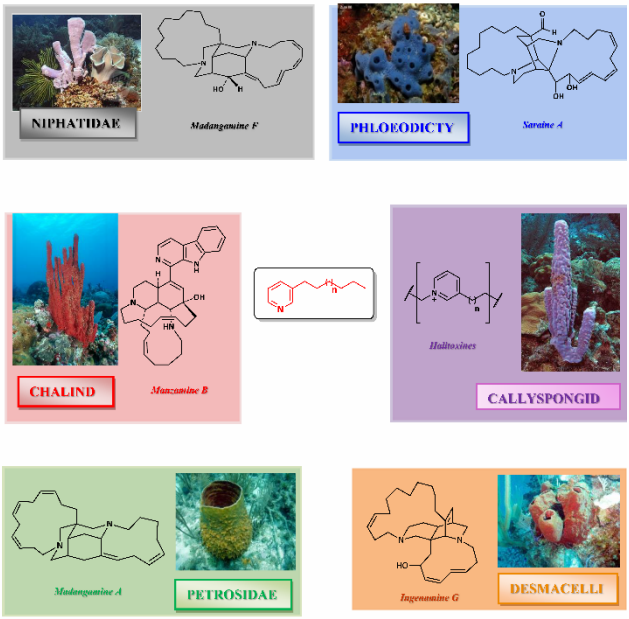

Figure 25 Alkaloids from the marine sponges of the order Haplosclerida.

B1.2 Structures of the Madangamines Alkaloids

Madangamines are a small group of pentacyclic alkaloids isolated from marine sponges of the genus *Haposclerida*.

Structurally are characterized by a perhydro-6,4-(iminomethano)isoquinoline core (ABC)[6, 7, 8] and by two linear carbon chains connecting N-7 to C-9 (D ring) and N-1 to C-3 (E ring). The western ring (D) differs in each madangamine in:

- Dimension (13- to 15-membered ring);

- Degree of unsaturations (one and three double bonds all in *cis* conformation);

The same eastern ring (E) is shared among madangamines A-E (two unsaturations for 11-membered ring), meanwhile the madangamine F presents 4 unsaturations for 13-membered chain, and an hydroxyl group in C-4 position of the C ring (figure 26).

The diazatricyclic core of these alkaloids shows a *diamond-lattice structure*, in which A, B and C rings possess a *chair* conformation. In particular, one of these rings displays a *flattened chair* conformation, due to the sp^2 hybridization of the C-3.

Madangamines A-E exhibit four stereocentres, C-2, C-5, the quaternary C-9, and C-12, and a conformationally locked N-7[2, 3, 11] (figure 25). The inability of that nitrogen to face the phenomenon of pyramidal inversion makes the lone pair locked within the core of the tricyclic system, and inaccessible to both protonation and formation of H-bond. As a consequence, the basicity of the N-7 decreases, as the polarity of the whole system.

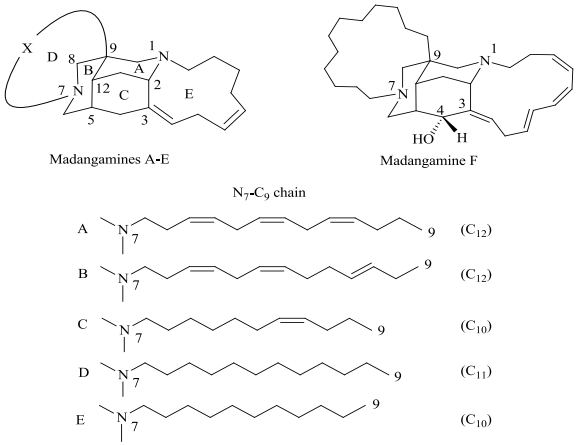

Figure 26 Structures of madangamines.

B1.3 Biological Activity

As cited before, madangamines showed significant *in vitro* cytotoxic activity[5] (figure26). In particular, madangamine A is endowed by *in vitro* cytotoxic activity against murine leukemia P388 (ED_{50} 0.93 μg/mL) and human lung A549 (ED_{50} 14 μg/mL), brain U373 (ED_{50} 5.1 μg/mL), and breast MCF-7 (ED_{50} 5.7 μg/mL) cancer cell lines[5]. Madangamine F shows weak cytotoxicity against human CNS SF-295 (ED_{50} 19.8 μg/mL), human breast MDA-MB-435 (ED_{50} 16.2 μg/mL), colon HCT-8 (ED_{50} > 25 μg/mL) and leukemia HL-60 (ED_{50} 16.7 μg/mL) cancer cell lines[5]. All tests were performed on MTT cell proliferation assay. Synthetic madangamine D also displays *in vitro* cytotoxicity against human colon HT29 (GI_{50} 4.4 μg/mL) and pancreas PSN1 (GI_{50} 7.4 μg/mL) cancer cell lines, but it is inactive

against lung NSCLC A549 and breast MDA-MB-231 cancer cell lines at the highest assayed concentration (10 μg/mL). No bioactivity data have been reported for natural madangamines B-E[5].

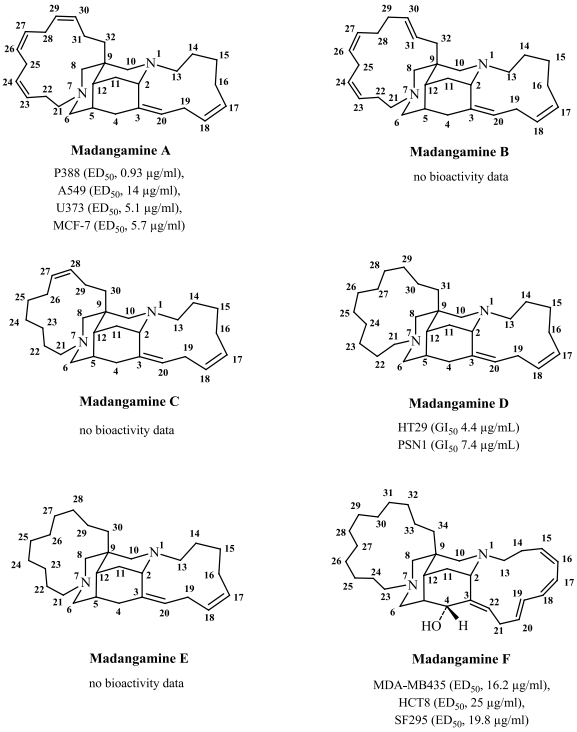

Figure 27 Biological activities of madangamines.

The continuous evaluation of the antitumor potential of new cytotoxic natural products is essential to overcome problems connected to the drug resistance. Natural madangamines A and F, and synthetic madangamine D showed promising EC_{50} values against several cancer cell lines. At the outset of this PhD thesis no further

biological data were available. At the same time, not even synthetic madangamine B was obtained and neither tested. The goal of Amat's group was to totally synthesize (+)-madangamine B (figure 28), also in order to investigate how this complex macrocycle should affect cancer growth.

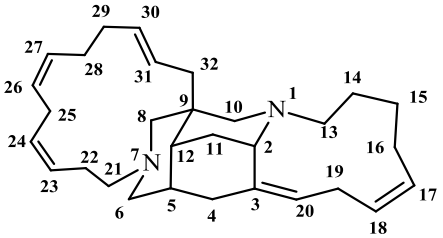

Madangamine B

Figure 28 Madangamine B.

Chapter B2

Towards the Total Synthesis of Mafangamine B

Here, in this complex project, we describe the preparation of the ABC diazatricyclic core, in the synthesis of the fragments C-13/C-20 (fundamental for E ring construction) and C-21/C-32 (necessary for D ring) and of the 8-oxomorphane, used as model to study the closure of E ring.

B2.1 Synthetic Strategy

The strategy to be followed for the synthesis of madangamine B was analogous to the one previously developed by Prof. Mercedes Amat and co-workers for the preparation of madangamine D[11]; this strategy entails the initial construction of the ABC diazatricyclic core, shared by madangamines A to E, and subsequent annulation of the macrocyclic D and E rings.

The stereoselective construction of the fully functionalized diazatricyclic core in enantiopure form was carried out starting from lactam derivative **27a**, the enantiomeric scaffold achieved through strereoselective cyclocondensation between (*R*)-phenylglycinol, a chiral inductor, and the oxoester 4-formyl-6-heptanoate (A route, scheme 2).

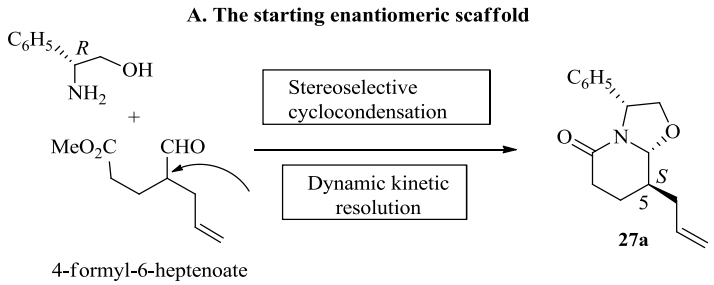

Scheme 2 Synthesis of the starting enantiomeric scaffold.

A stereoselective conjugate addition on the corresponding unsaturated derivative, in which the double bond is activate by a carbonyl alkoxy group, leads to the introduction of an allyl substituent at C-12, leading to a *cis*-diallyl-substituted lactam (C-12, C-5). A RCM of the diallylic derivative was performed for the closure of the carbocyclic C ring, common in all madangamines. The generation of the quaternary stereocenter at the C-9 position, by alkylation of the enolate, takes advantage of the acidity of the hydrogen next to the carbonyl of the ester and of the amide-lactam. The shape of the *cis*-octahydroisoquinoline allowed the selective approach of the alkylating reagent from the less hindered zone. In this way the introduction of the carbon chain with the opportune functionalization at the terminal position for the construction of the D ring was allowed. The subsequent removal of the phenylethanol moiety of the chiral inductor and the closure of the piperidine A ring by an intramolecular aminohydroxylation represented the final strategic steps necessary to

complete the synthesis of the diazatricyclic core of madangamines[10] (B route, scheme 3).

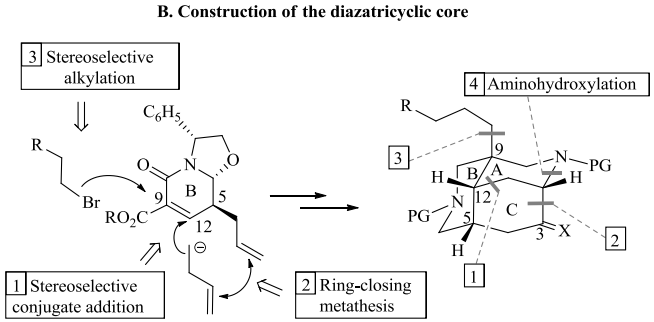

Scheme 3 Construction of the diazatricyclilc core.

For the closure of the macrocyclic D ring, not treated herein, the synthetic strategies depend on the synthesis of a 12-membered chain containing three unsaturations; meanwhile, for the closure of the unsaturated macrocycle E the introduction in C-3 position of an 8-membered chain, containing two unsaturation in *Z* configuration, and a following macrolactamization will be necessary[11]**.** The first step involves a Wittig type olefination in which carbon-carbon double bond with the *Z*-configuration has to be stereoselectively generated (C route, scheme 4).

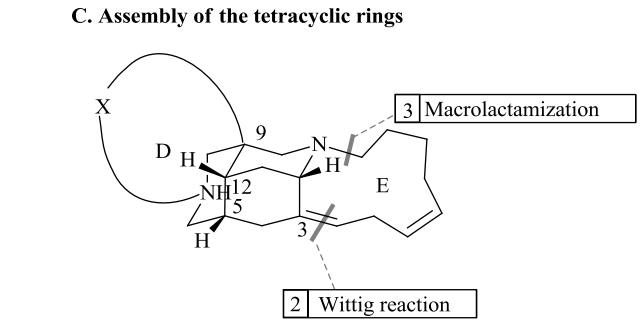

Scheme 4 Synthetic strategy in madangamines construction.

B2.2 Synthesis of the Diazatricyclic Core

In this chapter it is described in details the synthetic steps adopted for the construction of the diazatryciclic core, starting from the lactam **27a** featuring the piperidine ring B and the C-5 stereocenter of these natural compounds.

The general tranformations to obtain the desired ABC core is described in scheme 5.

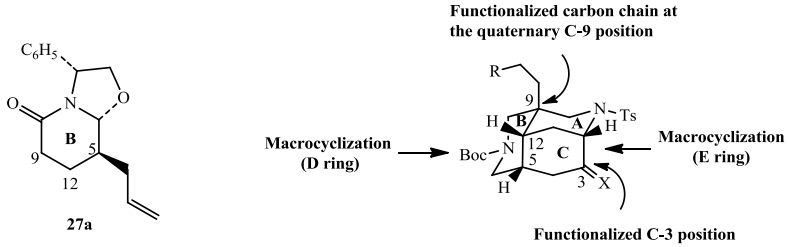

Scheme 5 Desired structure of the ABC core.

The first step of the synthesis is oriented to the building of the quinoline, presenting an hydroxymethyl group at the chiral C-9 position, and a functionalized chain useful for the D ring closure in further steps.

The key steps in the synthesis of *cis*-octahydroisoquinoline (**37**) are (scheme 6):

1. Stereoselective conjugate addition (on C-12 position) of the allyl group to the unsaturated lactam derived from **27a**;
2. Olefin metathesis for closure of the ring C;
3. Stereoselective alkylation in C-9;
4. Removal of the phenylethanolic portion of the chiral inducer;
5. Reduction of the carbonyl group of ester in C-9.

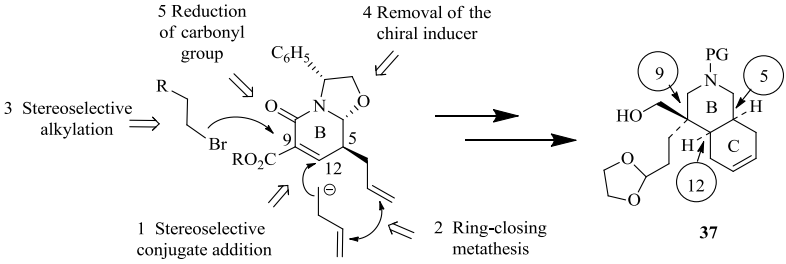

*Scheme 6 Key steps in synthesis of **37**.*

In the *cis*-octahydroisoquinoline intermediate, the key stereocenters C-5, C-9 and C-12 were already present and, specifically, two of these were generated by stereoselective

conjugated addition (C-12) and alkylation of the enolate (C-9). Starting from compound **37**, the key step to the final assembly of the diazatriciclic nucleus is the closure of the piperidine ring A. This was obtained by conversion of the hydroxymethyl group, bound to C-9, into an ethylamine group, followed by a reaction of amino-hydroxylation of the carbon-carbon double bond present on the C ring of the *cis*-octahydroisoquinoline system[10].

B2.2.1 Synthesis of Enantiopure Lactam 27a

Even if the synthesis of the lactam **27a** is the same used for the preparation of madangamine D, the synthetic procedure is discussed in details.

The first goal to reach in the synthesis was represented by the construction of the chiral "*building block*" **27a**, starting from the commercially available (*R*)-(-)-2-phenylglycinol and a racemic δ-oxoester, through a process that involves the dynamic kinetic resolution (scheme 7).

Firstly the racemic intermediate 4-formyl-6-heptanoate **26** was obtained in 64% yield after treatment between metacrylate[10] and enamine **1**, obtained in turn from condensation of piperidine with 4-pentenal.

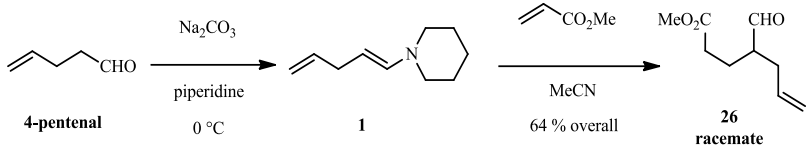

*Scheme 7 Synthesis of the **26** racemate.*

The cyclocondensation between **26** and the chiral inductor was carried out at 0 °C in presence of Na_2SO_4; the system was heated at 80 °C under *vacuum* (10-15 mmHg), and, in the end, were afforded the stereoselective lactames **27a** (kinetic product, 71% yield) and **27b** (10% yield), respectively (scheme 8).

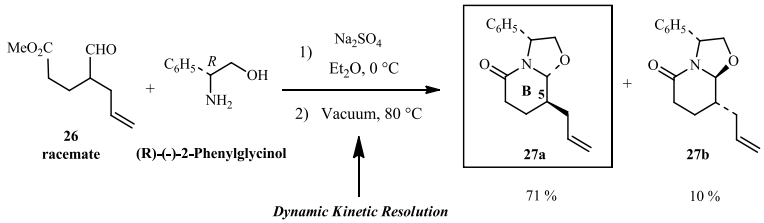

Scheme 8 B ring assembly.

The high stereoselectivity accomplished in the reaction can be exploited considering that the cyclocondensation proceeded through a Dynamic Kinetic Resolution (DKR) of the racemic substrate[12-16]. As shown in scheme 9, the mixture of the four oxazolidine diastereoisomers (a, b, c, d) generated from the reaction between **26** and (*R*)-phenylglycinol, is in equilibrium with the corresponding

imines/enamines (A-B-A'). The lactonization step occurred *via* a transition state in which the allylic substituent of the six-membered chair-like is equatorial (oxazolidines c and d). The isomer **27a** as major product denoted that the lactamization process occurred more quickly for the diastereoisomer c, in which the nucleophilic attack of the nitrogen on the carboxyl group took place on the less hindrance face, that one in *anti* than to the phenolic substituent (scheme 9).

This stereoselective process is an optimal route in order to assembly both the piperidinic ring B and to generate the first stereocenter C-5 of the alkaloid's scaffold.

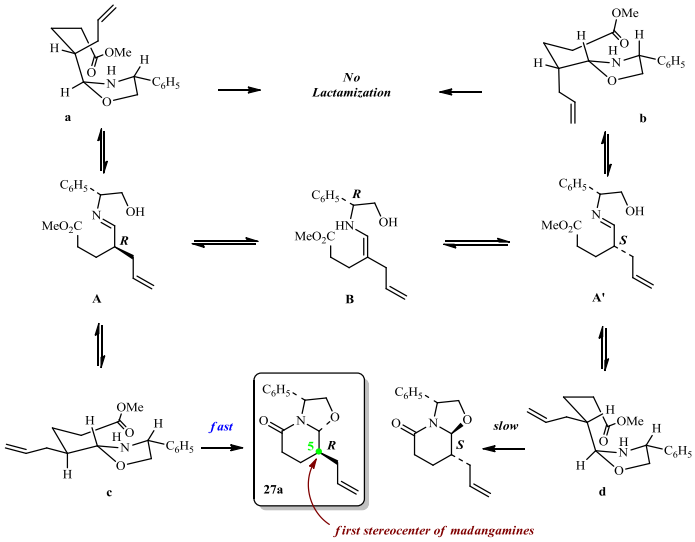

Scheme 9 Dynamic Kinetic Resolution process.

B2.2.2 Synthesis of Azabicyclic BC System

The azabicyclic BC system construction can be achieved following these main stages (scheme 10):

1. Stereoselective conjugate addition;
2. Ring Closing Metathesis (RCM) reaction;
3. Stereoselective alkylation at C-9.

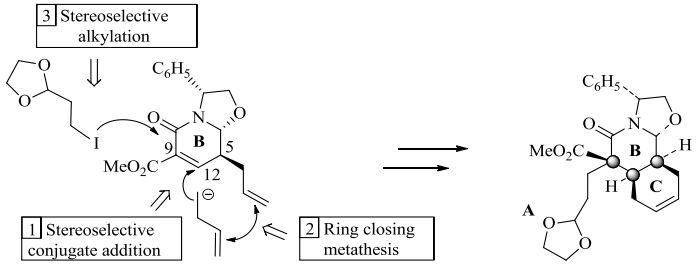

Scheme 10 Synthesis of functionalized azabicyclic system.

B2.2.3 Stereoselective Conjugate Addition

The key reaction in the synthesis of azabicyclic core was the stereoselective conjugate addition on the lactam **29**.

Since the α,β-unsaturated lactams are poor Michael acceptors, the addition of a withdrawing group at C-9 was necessary to improve the reactivity of the intermediate **29**[17, 18].The withdrawing group selected was the methoxycarbonyl.

Lactam **27a** was treated sequentially with lithium bis(trismethylsilyl)amide, methyl chloroformate and phenylselenyl

chloride; the resulting mixture of epimers **28a/b** was oxidized in presence of pyridine and H_2O_2 to afford compound **29**. The intermediate **29** was employed in the next reaction without further purification. Conjugate addition of the allyl group to the α,β-unsaturated lactam **29** was realized using allyl-magnesium bromide in presence of CuI, LiCl and TMSCl, yielding a mixture of epimers **30a/b** at C-9[19] (scheme 12).

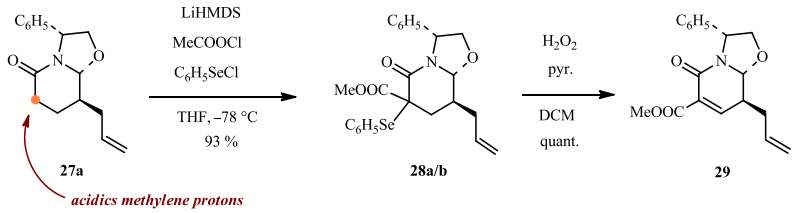

*Scheme 11 Preparation of unsaturated lactam **29**.*

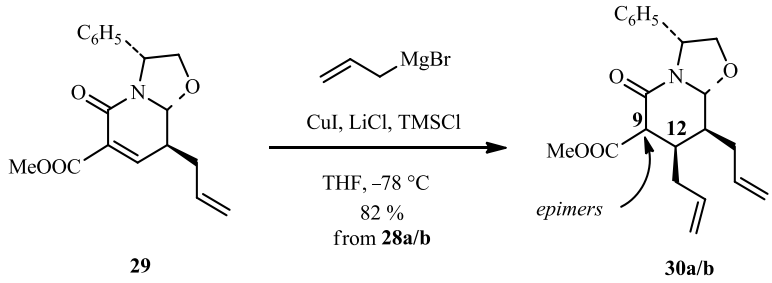

Scheme 12 Stereoselective conjugated addition.

The origin of this high stereoselectivity can be explain considering the rigid structure assumed by these compounds, due to

the presence of the amide bond, and to the conformation of the six membered ring, defined by the N-1 configuration. As a consequence, they adopt a *pseudo-chair* conformation (scheme 13) in which the allyl group is placed in *pseudo equatorial* position. The nucleophilic attack occurs under stereoelectonic control, leading to the formation of the kinetically favourite *cis* isomer.

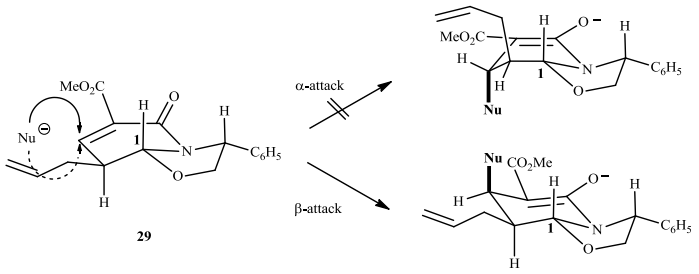

Scheme 13 Stereoelectronic control during the conjugate addition.

The intermediate obtained was really important, since it constitued the precursor of the azabicyclic system and brings to the introduction of the C-12 stereocenter.

B2.2.4 Olefin Metathesis

The synthesis of the azabicyclic intermediate **32** occurred *via* olefin RCM reaction on the diallyl compound **30**, which was converted in the tricyclic lactam **31** after treatment with second generation Grubbs catalyst in dichloromethane (DCM). The substituent present at the C-9 of the system activates the hydrogen in α-position of the carbonyl group, making it more acidic, and

represents the suitable precursor of the methyl-amino chain, necessary for the closure of the A ring of madangamines.

The alkylation of the mixture of C-9 epimers of compound **31** is totally stereoselective; in fact the product **32** is obtained as only isomer in high yield (scheme 14).

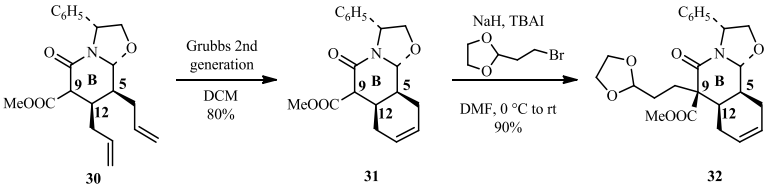

*Scheme 14 Synthesis of compound **32**.*

Olefin metathesis reactions have influenced the organic chemistry synthesis in the last 15 years[20-24].

Numerous synthetic transformations displayed by this reaction, when applied on suitable substrates, is until now still intriguing, since the same catalytic systems (initiators) can promote several reactions accordingly to the substrates and to the conditions' reaction used (scheme 15).

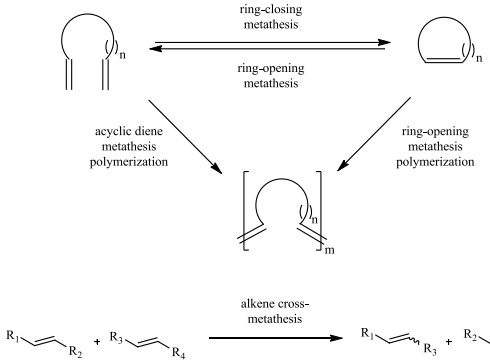

Scheme 15 Olefin metathesis reaction largely employed in organic chemistry.

B2.2.4.1 Catalysts

Nowadays, the ability to display success in a such surprising variety of reactions is due, partly, to the large amount of catalysts commercially available, all endowed by strong activity and tolerance towards different functional groups.

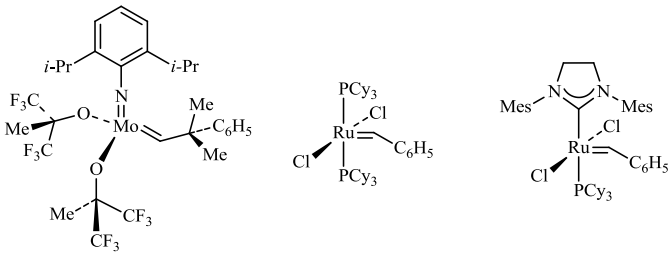

I **II** **III**

Figure 29 Olefin Metathesis catalysts.

The first catalysts employed in olefin metathesis, described by Katz *et al.*, were represented by tungsten-carbene units[25-29], until the

molybdenum based catalyst **I** come in vogue in 1990s by Schrock and co-workers, representing the first real innovation in field of catalysts[30]. Compound **I**, if on the one hand can be exerted in a wide range of reactions[31-34], on the other hand has drawbacks due to their sensitivity after exposure to oxygen, humidity and several polar functional groups[35]. Further, Grubbs and co-workers introduced the ruthenium-based catalyst **II**[36-39]. The first generation Grubbs catalyst (**II**) even if gifted of weaker activity than to the Schrock catalyst **I**, exhibited better tolerance towards different functional groups and high stability, once exposed to atmosphere conditions. With the aim to improve the catalytic activity of the catalysts, the ligands of ruthenium atom were modified; the substitution of a phosphine group with a *N*-heterocycle led to the second generation Grubbs catalyst **III**[40-43], which showed higher catalytic activity, higher thermic stability and more tolerance towards functional groups (figure 29). Despite these advances, the research for increasingly effective and selective catalysts continues[44-49].

B2.2.4.2 Mechanism

The explanation of the metathesis reaction mechanism was the culmination of nearly two decades of extensive research, and the subject of a lively debate among numerous research groups of that period. The mechanism originally proposed was the one by Hérisson and Chauvin in 1971[50], and the experimental proofs for its validity

were subsequently provided by Casey[51], Katz[52-54], and involving metal carbenes as propagators in the catalytic cycle. As shown in the scheme 16, in the initial phase (a) of the reaction the catalysts binds the olefinic substrate through a process [2+2] leading to a metal cyclobutene intermediate. A retro cycloaddition [2+2] to opposite direction defined the depletion of an olefin moiety (ethylene in that case) to form a new metal carbene specie (b), a suitable intermediate able to generate a new metallic cycle, after addition of an olefinic molecule. This cycle faced subsequently a disruption accomplished by the generation of a new olefinic product (d) and by the release of the initial catalyst, again available for further conversions (scheme 16).

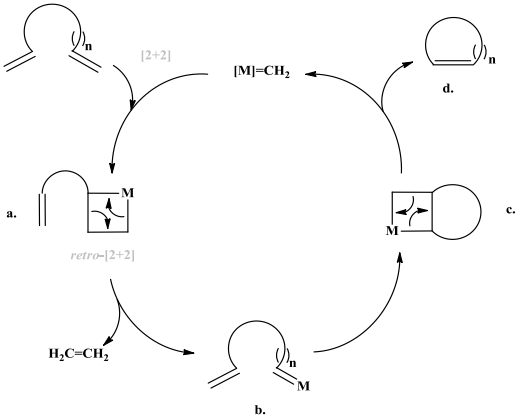

Scheme 16 General aspects of olefin metathesis.

B2.2.5 Formation of the Endocyclic Double Bond

The formation of the C ring of madangamines'system was accomplished by a ring closing metathesis reaction of the diallylic moieties using the second generation Grubbs catalyst **III**. Compound **31**, thus obtained, showed the azabicyclic system and an endocyclic double-bond, a fundamental requisite for the building of ABC nucleus of madangamines (scheme 17).

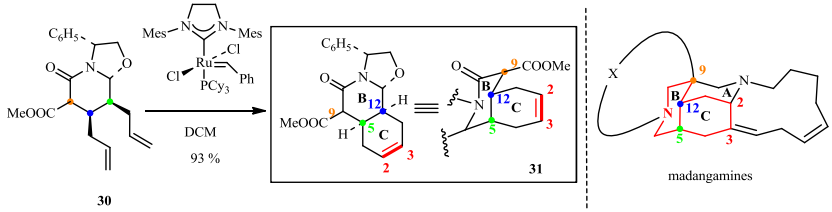

Scheme 17 C ring closure.

B2.2.6 Stereoselective Alkylation

With the availability of compound **31**, the generation of C-9 quaternary centre was performed by taking advantage of either the remaining methine proton and the convex conformation of the *cis*-hydroisoquinolone framework. The methoxycarbonyl works as precursor of the methylamino chain, fundamental for the A ring closure, improving the acidity of the H in α-position of carbonyl group (scheme 18).

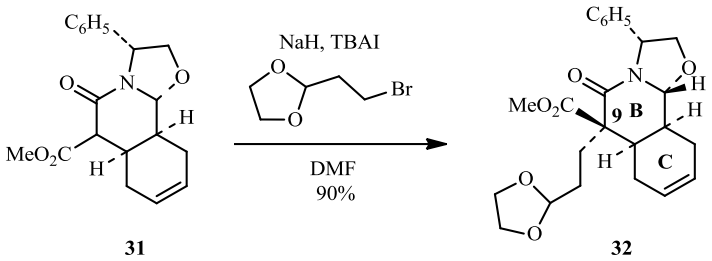

Scheme 18 Stereoselective alkylation: C-9 generation.

The alkylation was performed using the 2-(2-bromoethyl)-1,3-dioxolane in presence of NaH as base, and TBAI (scheme 19); the latter was used to promote the interchange bromide/iodine during the reaction and improve the reactivity of the alkylating group. The dioxolane was chosen because in the last step of the synthesis the acetale should be hydrolyzed in aldehyde, leading to the building of D ring and, in the end, of the whole macrocycle.

The reaction is highly stereoselective due to the geometry of the bicyclic system, which allowed an *exo*-alkylation.

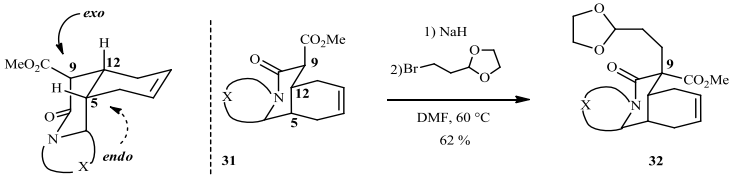

Scheme 19 Stereoselective alkylation.

B2.2.7 Removal of the Chiral Inductor

At this point, the removal of the phenylethanol moiety from the chiral auxiliary was achieved by successive treatment of **32** with Na in liquid NH_3 and $LiAlH_4$, to give an *N*-unsubstituted piperidine-3-methanol derivative, which was immediately protected as the *N*-Boc piperidine **37** (scheme 20).

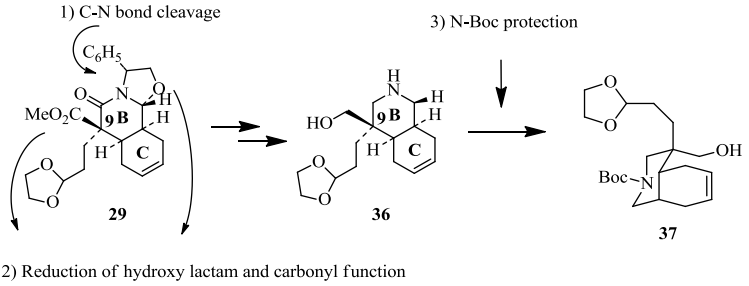

Scheme 20 C-N bond disruption.

The reduction of organic molecules with a "solution of electrons" in ammonia is known as "*dissolving metal reduction*". When alkali metals (lithium, sodium, potassium or calcium) are dissolved in liquid ammonia, the metal's atoms lose their electrons which impair a typical blue coloration to the solution. Unfortunately, even if these reductions are really effective, displayed poor selectivity.

As expected, this treatment led to the formation, at the same time, of the corresponding alkoxy- and hydroxylactam products and products deriving from reduction of the ester group.

Treatment of the mixture of products obtained after Na/NH_3 reduction with an excess of $LiAlH_4$ (15 eq.) in anhydrous dioxane allowed the reduction of both carbinolamine portion and two carbonyl groups (scheme 21). In the end, the amino function was protected with Boc- before proceeding with the next steps of the reaction.

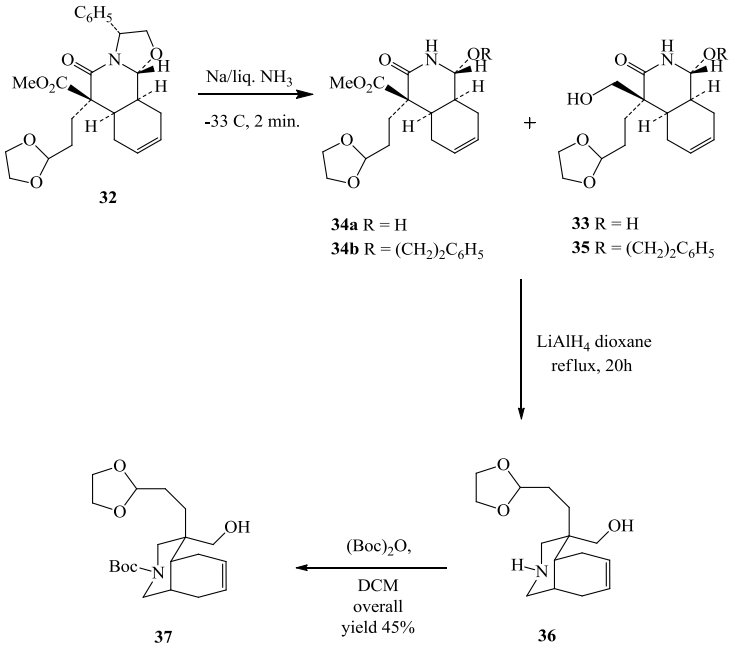

Scheme 21 Chiral inductor elimination: reduction.

This approach was really efficient for the synthesis of azabicyclic intermediate, providing the elimination of the chiral inductor.

B2.2.8 Synthesis of Tricycle ABC

Azabicyclic compound **37** owned two fundamental properties largely exploited for the synthesis of ABC system:

1. Primary alcohol in C-9, with a precise spacial arrangement, should be easly converted in amino function;
2. Double bond in C ring, should allow the reaction of epoxydation/intramolecular ring opening to form the diazatricyclic core and the two stereocenters C-2 and C-3.

The piperidine ring A was realized through an amino-hydroxylation on the double bond in the ring C (scheme 22).

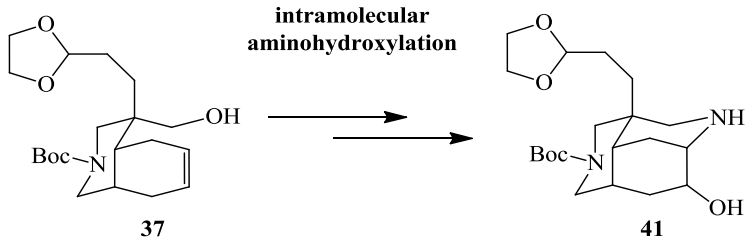

Scheme 22 Diazatricyclic nucleus assembly.

The synthetic strategy started with the transformation of the alcoholic moiety in **37** in an azide. The procedure envisaged first of all the transformation of the alcohol in a mesylate intermediate **38**, yielding the desired product **39** without effort and under drastic conditions of reaction (scheme 23).

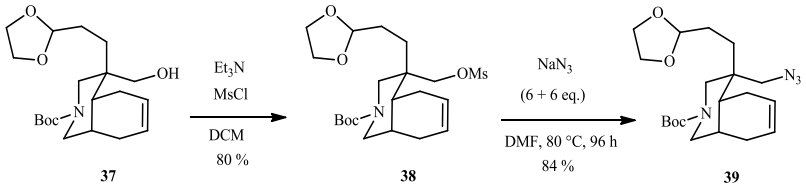

*Scheme 23 Synthesis of compound **39**.*

Treatment of azide intermediate **39** with *m*-chloroperbenzoic acid led to the non-isolable epoxide; further reaction proceeded with perfect selectivity affording only one isomer (scheme 24); this high selectivity should be explained considering that the reaction of epoxidation occurred on the less hindered face of the bicyclic system.

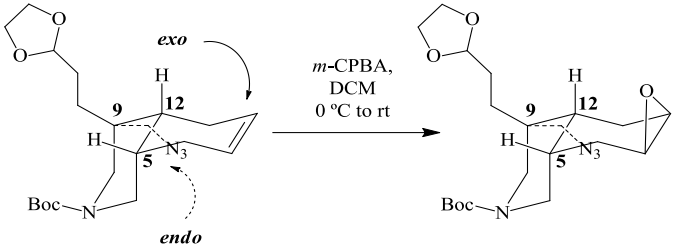

Scheme 24 Stereoselective epoxidation.

The resulting compound **40** was selectively reduced through the Staudinger reaction at the azide moiety. The amino epoxide derivative cycled spontaneously, leading to the diazatricyclic alcohol **41**. The analysis of the product **41** showed that the amino chain drives the *endo* nucleophilic attack on the epoxidic ring (scheme 25).

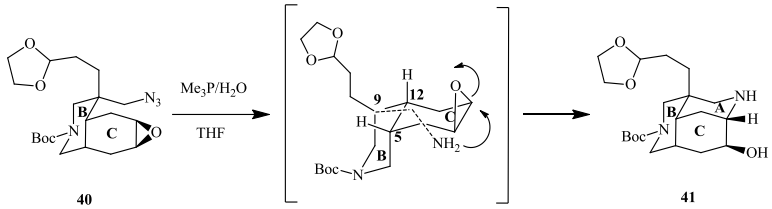

Scheme 25 A ring closure.

The free amino group was so protected with tosyl chloride, meanwhile the alcoholic residue in C-3 was oxidized in ketone through the use of Dess-Martin periodinane (scheme 26).

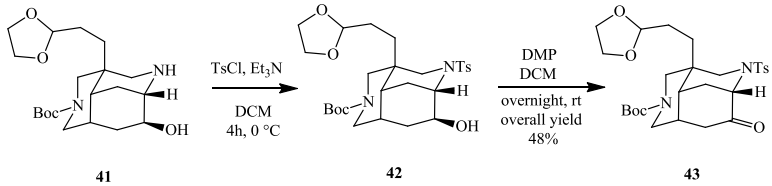

Scheme 26 ABC diazatricyclic core formation.

B2.3 Synthesis of C-13/C-20 Fragment

The synthesis of the fragment C-13/C-20 started with a *Z*-selective Wittig reaction between the phosphonium salt **49** and the methyl-5-oxo-heptanoate **46**. This fragment is really important for the construction of the E ring of madangamine B. It is an 8-membered chain presenting one *Z* unsaturation and a phosphonium salt moiety; that portion is fundamental to realize the anchorage by Wittig reaction between the diazatricycle core and this fragment.

The aldehyde was synthesized starting from the commercially available δ-valerolacton through these subsequential steps (scheme 27):

1. Hydrolysis/esterification in presence of H_2SO_4/MeOH;
2. Oxidation in presence of pyridinium chloro chromate (PCC).

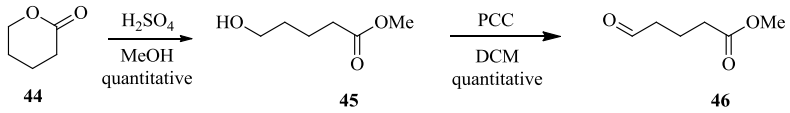

44 **45** **46**

*Scheme 27 Synthesis of aldehyde **46.***

Phosphonium salt was synthesized starting from 3-bromo propan-1-ol, previously protected with *tert*-butyldimethylsylil chloride, and triphenylphosphine (scheme 28).

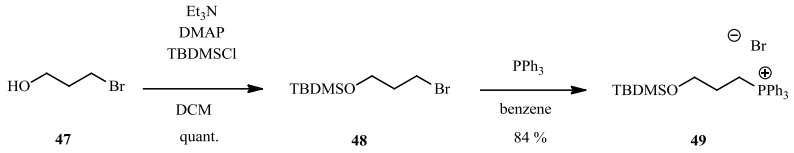

*Scheme 28 Preparation of phosphonium salt **49**.*

Reaction between the phosphonium salt **49** and the linear aldehyde **46**, in presence of NaHMDS as base[55, 56] afforded the compound **50** as unique *Z* isomer, with a 78% yield (scheme 29).

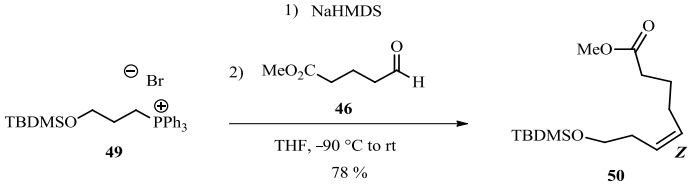

*Scheme 29 Wittig reaction to afford Z intermediate **50**.*

The synthesis of the chain was accomplished *via*:

1. *O*-deprotection;
2. Formation of bromo derivate **52**, occurred first of all through the formation of the mesylate intermediate, and secondly by bromination of the mentioned mesylate;
3. Final transformation in phosphonium salt **53** (scheme 30).

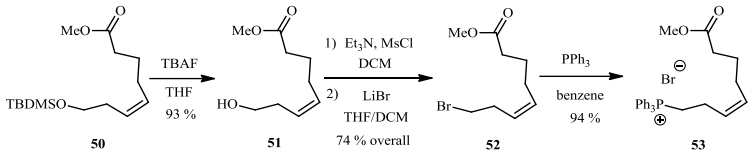

*Scheme 30 Synthesis of phosphonium salt **53**.*

The synthetic route to perform the assembly of the E ring should involve (i) the direct installation of the eight-membered carbon chain **53** at C-3 position and (ii) the subsequent annulation of the E ring through an intramolecular macrolactamization. So, the required *Z,Z* poliunsaturated system could be directly installed to the diazatricycle **43** using a *Z*-selective Wittig reaction with the corresponding phosphonium salt. Even if I didn't take part in that step of the synthesis, it is a key reaction in the total synthesis of madangamines, and I would like to evaluate the topic aspects of this reaction.

B2.3.1 Wittig Reaction

Fundamental to obtain good results in Wittig reaction is the presence of an anhydrous phosphonium salt. This effect was reached treating the phosphonium salt, strongly hygroscopic, with phosphorous pentoxide *under vacuum* for several days at 80 °C.

B2.3.1.1 Phosphorous Ylides

The Wittig reaction was realized between a phosphorous ylide and an aldehyde or a ketone (scheme 31). Since its discovery, this

reaction is nowaday still considered a really important reaction among the ones in organic chemistry, due to its simplicity and efficiency[57-63].

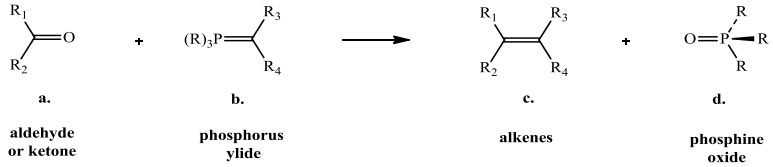

Scheme 31 Schematic Wittig reaction.

Initially, not much attention was paid to the stereochemistry of the reaction, since the products obtained were isolated as mixtures of Z/E isomers. More recently, however, it has been observed that depending on the ylide, on the carbonyl compound and on the reaction conditions it was possible to control the stereoselectivity of the reaction, favoring the formation of an isomer with respect to the other. The phosphorus ylides were classified (Figure 30) on the basis of their reactivity in:

i. "*stabilized*" ylides which have groups such as -COOMe, -CN, or -SO_2Ar on the carbon atom of the hylide and which give predominantly *E*-alkenes;

ii. "*semi-stabilized*" ylides which have slightly conjugated groups such as -Ph or allyl and which generally give a mixture of *E/Z* alkenes in a 1: 1 ratio;

iii. "*non-stabilized*" ylide which give mainly *Z*-alkenes[64, 65].

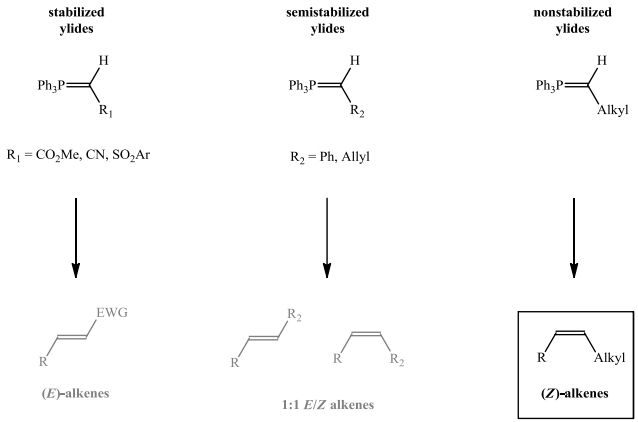

Figure 30 Different types of ylides.

Despite the promising progresses obtained for "stabilized" and "semi-satbilized" phosphonium salts, in this thesis we will treat the studies concerning the "non stabilized" ylides, since they are the ones used in this synthesis.

B2.3.1.2 About the Mechanism

In the original Wittig proposal, the nucleophilic addition of the ylide to the carbonyl compound led to the formation of the betainic intermediate, which will close to form a four-term cycle[66, 67] (1,2-oxyphosphethane).

Although the existence of betaine has not been fully verified, this hypothesis has gained wide acceptance.

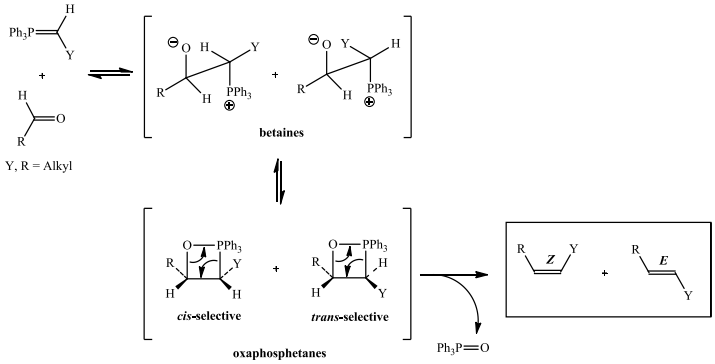

Scheme 32 Initial mechanism to explain the Wittig reaction.

However, in 1973 Vedejs revolutionized the reaction mechanism until that moment proposed. In fact, he observed, by means of spectroscopy ^{31}P NMR, that the only intermediates were the oxaphosphetanes[68, 69] (Scheme 32). Consequently, the *E/Z* ratio of the alkenes produced was established by the *cis/trans* ratio of the oxaphosphethanes, suggesting that the stereochemistry was controlled in the transition state of the reaction[70]. Taking into account these last results, the selectivity *Z* could be explained considering two distinct processes:

i. The irreversible addition of the ylide to the carbonyl compound, which produced two intermediates, oxyphosphetane diasteroisomers;

ii. The stereospecific decomposition of the oxaphosphetane in alkene (Scheme 33).

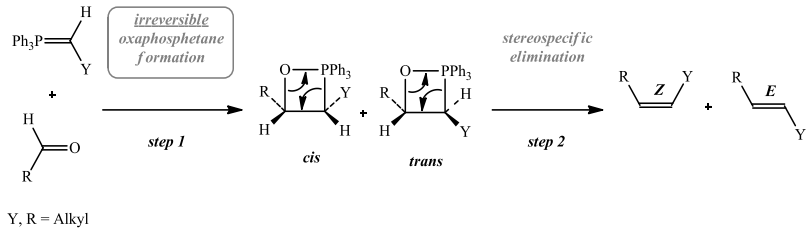

Scheme 33 Modification of the previous mechanism proposed.

The motivation for the preferential formation of *cis*-oxaphosphetane stimulated Vedejs and Marth to elaborate a theory. Without going into detail, it was sufficient to say that there was a good reason to believe that if the ylide and the carbonyl compound reacted together to give an oxaphosphetane compound, they will do it by approaching each other, keeping the large substituents as far away as possible from each other.

Furthermore, by playing on steric interactions it was clear how the *cis* geometry of the theory, above-mentioned, was favoured with respect to the *trans*, because of the smaller interactions 1,2 and 1,3, respectively between the Y substituent of the ylide and the larger substituent R of the carbonyl and between the phenyl and the smallest substituent H (scheme 34).

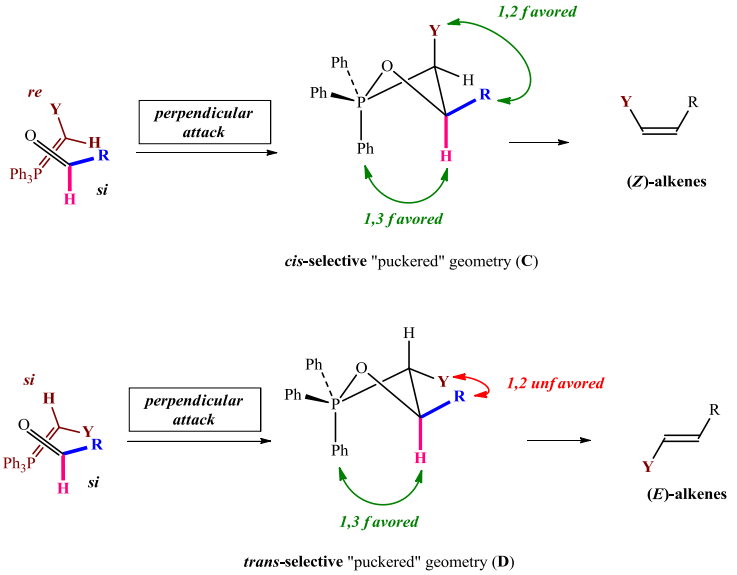

Scheme 34 Geometrical interactions.

The suggestions provided from these theoretical considerations helped us to understand the *Z* selective nature of the Wittig reaction, which conferred the desired product in the suitable stereochemical geometry.

B2.4 Synthesis of Fragment C-21/C-32

The fragment C-21/C-32 represents the chain of the D ring. This is an 11-membered chain, featuting three unsaturations, two in *Z* configuration and one in *E* configuration. The *Z* unsaturations derived from the synthesis of the fragment treated in this chapter, meanwhile the *E* unsaturation is going to be generated from the alkyl moiety already present in C-9 of the diazatricyclic core.

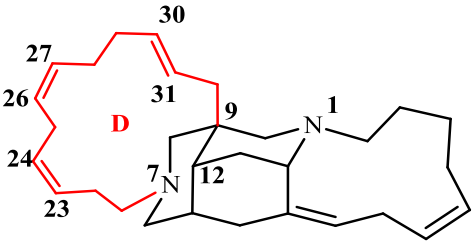

Figure 31 Madangamine B.

The synthesis of the fragment C-21/C-32 started with the protection of the 4-butyn-1-ol by treatment of **54** with TIPSCl protecting group. The presence of TIPS prooved be really useful in the D ring closure.

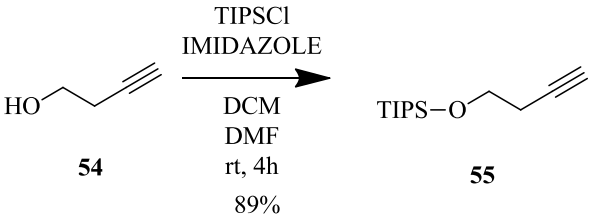

*Scheme 35 TIPS protection of 4-butyn-1-ol **54**.*

Tips protection of primary alcohol is a procedure used since 1974[71, 72] and was largely describe by Rucker[73]. The TIPS ether was easily obtained from but-3-yn-1-ol in DMF and DCM in the presence of imidazole. The reaction yielded product **55** in 89% (scheme 35).

The following step was fundamental for the introduction of a new primary alcoholic function, since it represented the suitable substrate for the further synthesis of the total 11-membered chain. The reaction was realized in presence of the intermediate **55**, *n*-BuLi and activated formaldehyde, and afforded after 5 hours the compound **56** in 87% yield (scheme 36).

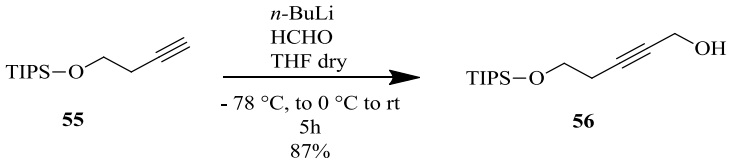

*Scheme 36 Synthesis of **56** molecule.*

Chain conjugation occurred after the treatment of tosylate intermediate **57** with NaI, CuI as catalysts, K_2CO_3 as base, yielding product **58** (86% overall yield of two steps, scheme 37). This

conjugated molecule was selectively reduced, affording the corresponding *cis* diene.

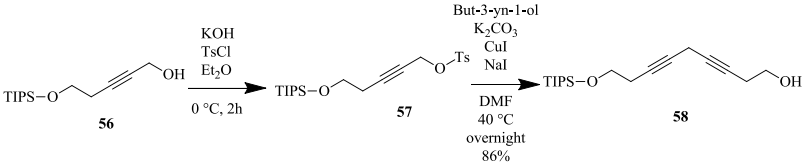

*Scheme 37 Synthesis of conjugate alkyne **58**.*

B2.4.1 Stereoselective Reduction

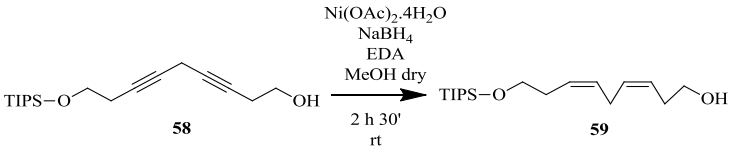

*Scheme 38 Synthesis of conjugate cis-alkene **59**.*

Conjugate alkyne was treated with Nickel acetate, in presence of solid $NaBH_4$, ethylendiammine in MeOH and, obviously, H_2 atmosphere; *cis* alkene **59** was obtained in high yield, due to the "reducing" system formed *in situ* from the above-mentioned reagents (scheme 38). Nickel (II) acetate was in fact reduced by borohydride, in MeOH, affording the P-2 nickel, a colloidal non-magnetic black catalyst (the formation of the colloid was well appreciated by observing the change of colour: from sea green to black). The presence

of ethylendiamine was really important to favor the production of *cis* alkenes. The reduction was completed once the atmosphere was fixed with hydrogen.

The precise methodology to follow was:

i. Addition of $Ni(OAc)_2 \cdot 4\ H_2O$ in anhydrous methanol;

ii. Addition of $NaBH_4$ portion wise (coloration of the solution from sea green to black);

iii. Addition of EDA and stirring for 20 minutes under Argon atmosphere;

iv. Addition of alkyne and replacement of the Ar atmosphere with the H_2 atmosphere.

B2.4.2 Iodination

Once the alcohol **59** was purified, the alcoholic residue was functionalized with mesyl chloride, in order to afford the iodine derivative, necessary for the D ring closure in madangamine system (Scheme 39). Different syntheses were elaborated, involving principally Br-, Cl- and I- as halogens; iodine derivate afforded the best results in term of yield.

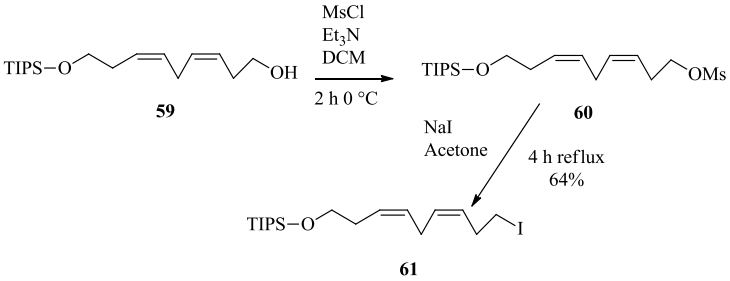

*Scheme 39 Iodination of bis-alkene **59**.*

B2.5 Closure of D Ring and E Ring of Madangamines: Synthesis of a Model

The synthesis of the 8-oxomorphan, a model largely used to study how to assemble the (*Z, Z*)-unsaturated 11-membered eastern E ring of madangamines, has been described below. The studies on that model were and are crucial, since the overall yield of the synthesis of the diazatricyclic core afforded really few amount of product. It is not rational use the ABC core for the different reactions employed to reach the total synthesis of madangamine B. In this context, a short and useful synthetic sequence was chosen to assembly the suitable functionalized morphan derivative **69**, which mimics rings A and C of the alkaloids from commercially available 4-vinylcyclohexene[75]. Synthetically speaking, the exocyclic double bond of the starting compound was selectively hydroborated by sequential treatment with disiamylborane. The following oxidative work-up yielded. the alcohol **64**, which was conveniently converted into the corresponding azide **66**. Further, epoxidation of the double bond, by treatment with *m*-chloroperbenzoic acid, and a Staudinger reduction of the azide functionality occurred (scheme 40). Notably, the synthesis of the azide required less drastic conditions than the ones employed towards the synthesis of ABC core. The amino epoxide intermediate underwent a smooth *in situ* cyclization, directly leading to an intermediate amino

alcohol, which was then N-protected with a tosyl chloride group and oxidized in presence of Dess-Martin periodinane (scheme 41).

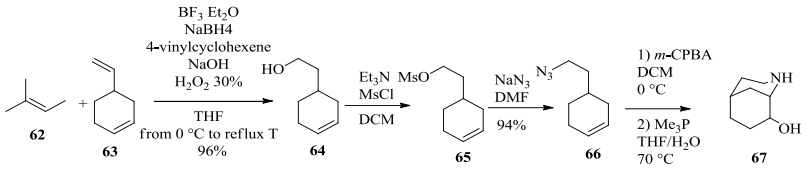

*Scheme 40 Synthetic strategy for the building of 8-bicyclic system **67**.*

According to the literature[75], even if the tosyl protecting group afforded the product endowed of less yield, it was considered the best intermediate for the further study of E ring closure.

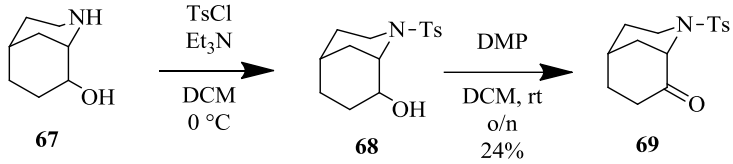

*Scheme 41 Synthesis of 8-oxomorphan **69**.*

Nowadays, the total synthesis of madangamine B is momentarily shelved to favor the pentacycle madangamine A. This change on focus is due to the fact that, even if the above-mentioned D chain accomplishes positive results on the synthesized model, it seems not working on the ABC tricycle core of madangamines, leading to negative results.

B2.6 Experiment al Section

B2.6.1 General Methods for UB project

All non-aqueous reactions were performed under an argon atmosphere using flame-dried and standard syringe/septa techniques.

All the reagents were purchased from Sigma-Aldrich or Alpha Aesar and used without further purification.

Reactions were magnetically stirred and monitored by TLC performed on Merck TLC alluminium sheets (silica gel 60 F245). Spots were visualized with UV light (λ= 254 nm) or through staining with $KMnO_4$ 1% aqueous solution.

Chromatographic purification of products (*Flash Chromatography*) was performed using SDS silica gel 60 ACC, 35-75 mm, 230-240 mesh ASTM.

Instrument FT-IR: Nicolet Avantar 320 FT-IR.

Optical rotations α: were measured on a Perkin-Elmer 241 and values are reported as follows $[\alpha]_D^{22}=10^{-1}$ deg cm^2 g^{-1}.

High Resolution Mass-Spectra (HMRS)were measured on a LC/MSD TOF Agilent Technologies, made at Centres Cientìfics i Tecnologics of Barcelona University.

NMR ^1H and ^{13}C spectra were recorder in $CDCl_3$ at 300 or 400 MHz (^1H) and at 75.4 o 100.6 MHz (^{13}C). Chemical shifts (δ) are reported in ppm and are referenced to $CDCl_3$ (δ=7.26 ppm for ^1H , δ=77.16 ppm for ^{13}C). All ^{13}C spectra were measured with complete proton

decoupling. TMS is used as internal standard. Data for NMR spectra are reported as follows: s = singlet, d = doublet, t = triplet, q = quartet, m = multiplet, br = broad signal, *J* = coupling constant in Hz.

B2.7 Synthesis of Tricycle ABC

Methyl-4-formyl-6-heptanoate (26)

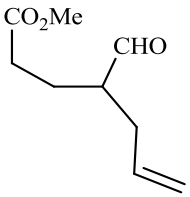

26

In a two-necked round-bottom flask, 4-pentanal (4.7 ml, 0.047 mol) was added dropwise to a dry solution of K_2CO_3 (2.0 g, 0.014 mol) in piperidine (12 mL, 0.1 mol) during 30 minutes, at 0 °C. The reaction was stirred for two days at room temperature, and filtered on sintered glass filter. The residue, carefully washed with Et_2O, contains the enamine.

To a solution of methyl-acrylate (7.5 mL, 0.0833 mol) in dry acetonitrile (75 mL), a solution of the enamine in dry acetonitrile (19 mL) was added at 5 °C. The reaction was stirred at room temperature overnight, and refluxed for 72 hours. After addition of glacial acetic acid (10.5 mL) in H_2O (75 mL) the reaction was refluxed for 72 hours. Et_2O was then added and the organic phase was washed with HCl 3N (100 mL), saturated solution of $NaHCO_3$ (100 mL) and NaCl saturated solution (100 mL). The combined organic extracts were dried on $MgSO_4$ and concentrated *in vacuo*. The residue methyl-4-formyl-6-

heptanoate was used in the next reaction without further purification (brown oil, 5.12 g, 0.030 mol, 64% yield).

^{1}H NMR (300 MHz, $CDCl_3$): δ_H 9.63 (d, *J* = 2.1 Hz, 1H, C*H*O), 5.76 (m, 1H, *H*- 6, m), 5.09 (m, 2H, *H*-7), 3.67 (s, 3H, CH_3), 2.51-2.21 (m, 5H, 2*H*-2, *H*-4, 2*H*-5), 1.98 (m, 1H, *H*-3), 1.80 (m, 1H, *H*-3). **^{13}C NMR** (100.6 MHz, $CDCl_3$): δ_C 203.7, 173.4, 134.3, 117.6, 51.7, 50.3, 32.9, 31.2, 23.2.

(3*R*, 8*S*, 8a*R*)-8-Allyl-5-oxo-3-phenyl-2,3,6,7,8,8a-hexahydro-5*H*-oxazolo[3,2-*a*]pyridine (27a)

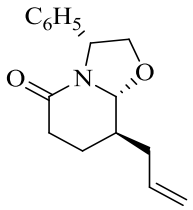

27a

In a two-necked round-bottom flask, a solution of racemic methyl-4-formyl-6-heptanoate (4.6 g, 29 mmol), (*R*)-(-)-2-phenylglicynol (3.97 g, 29 mmol) and dry Na_2SO_4 in Et_2O (115 mL) was stirred overnight at 0 °C. The resulting suspension was filtered on Celite. The organic mixture was concentrated *in vacuo* and the residue was heated at 80 °C for 18 h under *vacuum* (10.15 mmHg). The residual mixture of products was purified by FC (*n*-Hex/EtOAc 8:2 → 0:10) and afforded **27a** (5.3 g, 20.59 mmol, 71%) and (8*S*, 8a*S*)-diastereoisomer **27b** (2.9 g, 0.75 g, 10%).

Major isomer **27a**

^{1}H NMR (400 MHz, $CDCl_3$, COSY, gHSQC): δ_H 7.30-7.20 (m, 5H, C_6H_5), 5.86 (dddd, *J* = 16.5, 10.2, 7.8, 6.0 Hz, 1H, C*H*=), 5.12 (m, 2H, CH_2=), 4.92 (d, *J* = 6.6 Hz ,1H, *H*-3), 4.53 (d, *J* = 8.7 Hz, 1H, *H*-8a), 4.11 (dd, *J* = 9.0, 6.9 Hz 1H, *H*-2), 4.01 (dd, *J* = 9.0, 1.2 Hz, 1H, *H*-2), 2.62 (m, 1H, CH_2 allyl), 2.42 (ddd, *J* = 18.0, 7.2, 1.8 Hz, 1H, *H*-6),

2.30 (ddd, *J* = 18.0, 12.0, 6.6 Hz, 1H, *H*-6), 2.02 (m, 3H, H-7, H-8, CH_2 allyl), 1.45 (dddd, *J* = 13.8, 13.8, 12.0, 7.2 Hz 1H, H-7). **^{13}C NMR** (100.6 MHz, $CDCl_3$): δ_C 167.1, 141.4, 134.6, 127.4, 128.4, 126.2, 117.4, 91.9, 73.7, 58.9, 39.1, 35.4, 31.2, 23.6. $[\boldsymbol{\alpha}]_{\boldsymbol{D}}^{\mathbf{22}}$: -32.8 (*c* 1.0, EtOH). **IR** (film): 1655 (NCO) cm^{-1}.

Minor isomer **27b**

^{1}H NMR (400 MHz, $CDCl_3$, COSY, gHSQC): δ_H 7.34-7.25 (m, 5H, C$_6H_5$), 5.83 (dddd, *J* = 16.5, 10.2, 8.1, 6.0 Hz, 1H, C*H*=), 5.25 (t, 1H, *J* = 7.8 Hz *H*-3), 5.13 (m, 2H, CH_2=), 4.69 (d, *J* = 8.4 Hz, 1H, *H*-8a), 4.47 (dd, *J* = 9.0, 8.1 Hz 1H, *H*-2), 3.75 (dd, *J* = 9.0, 7.8 Hz, 1H, *H*-2), 2.56 (m, 1H, H-6, CH_2 allyl), 2.35 (ddd, *J* = 18.6, 12.0, 6.6 Hz, 1H, *H*-6), 2.07 (dt, *J* = 16.5, 8.4, 8.4 Hz, 1H, *CH*$_2$ allyl), 1.66 (m, 1H, H-8), 1.53 (m, 1H, H-7). **^{13}C NMR** (100.6 MHz, $CDCl_3$): δ_C 168., 139.4, 134.6, 127.4, 128.7, 126.0, 117.4, 92.0, 72.3, 58.3, 39.5, 35.8, 31.3, 22.7. $[\boldsymbol{\alpha}]_{\boldsymbol{D}}^{\mathbf{22}}$: -59.9 (*c* 1.0, EtOH). **IR** (film): 1658 (NCO) cm^{-1}.

(*3R,8S,8aR*)-methyl 8-allyl-5-oxo-3-phenyl-6-(phenylselanyl)hexahydro-2*H*-oxazolo[3,2-*a*]pyridine-6-carboxylate (28)

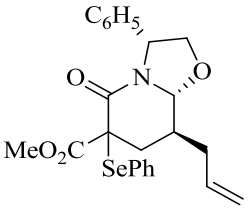

28

In two-neck round-bottom flask LiHMDS (1M in THF 10 mL) was slowly added at -78 ºC to a solution of lactam **27a** (2 g, 7.77 mmol) in dry THF (120 mL), and the resulting mixture was stirred for 90 minutes. Then, methyl chloroformate (0.6 mL, 7.78 mmol) is added at -78 ºC and was stirred for 90 minutes. In the end, phenyl selenium chloride (2.08 g, 10.8 mmol) was added dropwise and stirred for 1 h. Reaction was quenched by adding NH_4Cl saturated solution. The aqueous phase was extracted with EtOAc, and combined organic phases were dried over $MgSO_4$. The organic layers were concentrated *in vacuo* and the residue was purified by FC (*n*-Hex-EtOAc 9:1 → 1:1) affording product **28** (3.14 g, 6.68 mmol, 86%), as a mixture of epimers at C-6.

Epimer **28a**

^{1}H NMR (400 MHz, $CDCl_3$, COSY, gHSQC): δ_H 7.66-7.26 (m, 10H, Ar*H*), 5.17 (dddd, *J*= 16.8, 10.4, 7.6, 6.4 Hz 1H, C*H*=), 5.03 (m, 2H,

CH_2=), 4.87 (dd, *J*= 6.8, 2.0 Hz 1H, *H*-3,), 4.15 (d, *J*= 8.8 Hz, 1H, *H*-8a,), 4.05 (dd, *J*= 9.2, 6.8 Hz, 1H, *H*-2), 4.00 (dd, *J*= 9.2, 2.0 Hz, 1H, *H*-2), 3.58 (s, 3H, CH_3), 2.41 (m, 1H, *H*-7), 2.33 (dd, *J* = 14.0, 2.8 Hz, 1H, CH_2 allyl), 1.98 (m, 2H, *H*-7, *H*-8), 1.82 (dd, *J*=14.0, 12.4 Hz, 1H, CH_2 allyl). **^{13}C NMR** (100.6 MHz, $CDCl_3$): δ_C 170.8, 163.3, 140.5, 133.7, 138.2-126.4, 117.7, 91.8, 74.0, 59.4, 54.0, 53.0, 37.7, 36.6, 34.8. $[\boldsymbol{\alpha}]_{\boldsymbol{D}}^{\mathbf{22}}$:-99.3 (*c* 0.7, $CHCl_3$). **IR** (NaCl): 1667, 1725 cm^{-1}. **HRMS** (*m/z*): $[M+H]^+$ calcd for $C_{24}H_{25}NO_4Se$, 71.0948; found 471.0955.

Epimer **28b**

^{1}H NMR (400 MHz, $CDCl_3$, COSY, gHSQC): δ_H 7.47- 7.23 (m, 10H, Ar*H*), 5.59 (dddd, *J* = 16.0, 10.0, 8.0, 6.0 Hz, 1H, C*H*=), 4.97 (m, 3H, H-3, CH_2=), 4.63 (d, *J* = 9.2 Hz, 1H, *H*-8a,), 4.17 (dd, *J* = 9.2, 6.8 Hz 1H, *H*-2,), 4.10 (dd, *J* = 9.2, 1.2 Hz, 1H, *H*-2), 3.73 (s, 3H, CH_3), 2.52 (m, 1H, CH_2 allyl), 2.32 (m, 1H, *H*-8), 2.08 (dd, *J*= 15.2, 4.0 Hz, 1H, *H*-7), 2.00 (dd, *J* = 15.2, 11.6 Hz, 1H, *H*-7), 1.98 (m, 1H, CH_2 allyl). **^{13}C NMR** (100.6 MHz, $CDCl_3$): δ_C 171.0, 162.8, 140.5, 134.0, 138.3-126.8, 117.8, 91.6, 73.8, 59.6, 55.6, 53.3, 36.5, 35.0, 33.6. $[\boldsymbol{\alpha}]_{\boldsymbol{D}}^{\mathbf{22}}$: + 18.46 (*c* 0.5, $CHCl_3$). **HRMS** (*m/z*): $[M+H]^+$ calcd for $C_{24}H_{25}NO_4Se$, 471.0948; found 471.0946.

***(3R,8S,8aR)*-methyl-8-allyl-5-oxo-3-phenyl-3,5,8,8a-tetrahydro-2*H*-oxazolo[3,2-*a*]pyridine-6-carboxylate (29)**

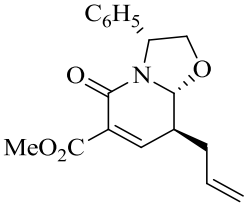

29

To a solution of a mixture of compounds **28a** and **28b** (1.6 g, 3.4 mmol), H_2O_2 30% (0.73 mL, 23.8 mmol) and pyridine (0.36 mL, 4.4 mmol) were added in DCM (231 mL); the resulting mixture was stirred for 2 h at room temperature. The two phases were separated and the organic layer was washed with water, dried over $MgSO_4$, and concentrated *in vacuum* to give the crude as oil, which was stored at -30 ºC and used in the next reaction without further purification.

^{1}H NMR (300 MHz, $CDCl_3$): δ_H 7.36-7.20 (m, 5H, Ar*H*), 5.86 (dddd, *J* = 15.3, 10.8, 8.7, 5.7 Hz, 1H, C*H*=), 5.27 (m, 2H, CH_2=), 5.03 (dd, *J* = 6.0, 2.4 Hz, 1H, *H*-3), 4.87 (d, *J* = 10.5 Hz, 1H, *H*-8a), 4.24 (dd, *J* = 9.0, 6.0 Hz, 1H, *H*-2), 4.20 (dd, *J* = 9.0, 2.4 Hz, 1H, *H*-2), 3.78 (s, 3H, CH_3), 2.91 (m, 1H, *H*-8), 2.7 (d, *J* = 14.4 Hz, 1H, CH_2 allyl), 2.31 (dt, *J* = 14.4, 8.7 Hz, 1H, CH_2 allyl). **^{13}C NMR** (75.4 MHz, $CDCl_3$): δ_C 164.3, 157.3, 147.6, 140.2, 133.3, 129.7, 127.7, 128.5-126.8, 119.0, 89.8, 74.4, 58.3, 52.3, 41.2, 33.5. **IR** (NaCl): 1673, 1741 cm^{-1}.

***(3R,7R,8S,8aR)*-Methyl-7,8-diallyl-5-oxo-3-phenylhexahydro-2*H*-oxazolo[3,2-*a*]pyridine-6-carboxylate (30)**

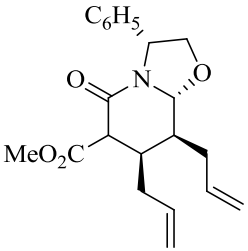

30

In a three-neck round-bottom flask of 250 mL LiCl (1.2 g, 28.4 mmol) was dried at 80 ºC for 1 h under *vacuum* (10-15 mmHg); in that flask, CuI (5.4 g, 28.4 mmol) and THF (150 mL) were added under inert atmosphere, and the mixture was stirred at rt for 5 minutes. The suspension was cooled at -78 ºC, and allyl magnesium bromide (28.4 mL, 28.4 mmol of a 1 M solution in Et_2O), TMSCl (3.6 mL, 28.4 mmol), and crude **29** (7.11 mmol) unsaturated lactam in THF (5 mL) were successively added. The resulting mixture was stirred at -78 ºC for 18 h. The reaction was quenched with NH_4Cl ss and filtered on Celite; followed an extraction of the aqueous layer with EtOAc , and dried on $MgSO_4$. The organic layers were concentrated *in vacuo* and the residue was purified by FC (*n*-Hex/EtOAc 9:1 → 7:3), affording **30** (2.1 g, 5.75 mmol, 81%) as a mixture of epimers at C-6.

Major epimer **30a** (6*S*)

^{1}H NMR (300 MHz, $CDCl_3$, COSY, gHSQC): δ_H 7.33-7.26 (m, 5H, C_6H_5), 5.84 (dddd, *J* = 15.3, 9.9, 8.7, 5.1 Hz, 1H, C*H*=), 5.68 (dddd, *J* = 15.0, 10.2, 9.0, 4.8 Hz, 1H, C*H*=), 5.14 (m, 4H, CH_2=), 4.91 (dd, *J* = 7.2, 1.8 Hz, 1H, H-3), 4.62 (d, *J* = 9.6 Hz, 1H, *H*-8a), 4.15 (dd, *J* = 9.3, 7.2 Hz, 1H, H-2), 4.02 (dd, *J* = 9.3, 1.8 Hz, 1H, H-2), 3.60 (s, 3H, CH_3O), 3.43 (d, *J* = 1.5 Hz, 1H, H-6), 2.70-2.44 (m, 3H, H-8, CH_2 allyl), 2.34 (d, *J* = 12.0 Hz, 1H, H-7), 2.16 (dt, *J* = 14.1, 9.3, 9.3 Hz, 1H, CH_2 allyl,), 1.80 (1 H, CH_2 allyl, ddd, *J* = 14.1, 12.0, 9.0 Hz. **^{13}C NMR** (75.4 MHz, $CDCl_3$): δ_C 170.6, 162.3, 140.5, 134.8-134.4, 128.2, 127.4, 116.5, 117.4, 89.4, 73.9, 59.6, 52.3, 51.5, 38.5, 36.9, 31.8, 31.6. **IR** (film): 1665, 1736 (CO) cm^{-1}. **HRMS** (*m/z*): $[M+H]^+$ calcd. for $C_{21}H_{25}NO_4$, 356.1783; found 356.1779.

***(3R,6aR,10aS,10bR)*-Methyl-5-oxo-3-phenyl-3,5,6,6a,7,10,10a,10b-octahydro-2*H*-oxazolo[2,3-*a*]isoquinoline-6-carboxylate (31)**

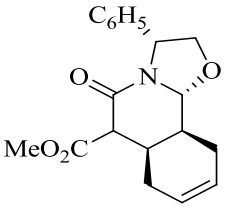

31

In a two-neck round-bottom flask, second generation Grubbs catalyst (642 mg, 0.78 mmol) was added to a solution of lactam **6** (3.58 g, 10.1 mmol) in DCM (1400 mL). The mixture was stirred at rt for 18 h and concentrated under reduced pressure. The crude of the reaction was purified by FC (*n*-Hex/EtOAc 4:1 → 3:2) affording product **31** (3.1 g, 9.39 mmol, 93%) as a mixture of epimers at C-6.

Major Epimer **31a** (6*R*)

^{1}H NMR (400 MHz, $CDCl_3$, COSY, gHSQC): δ_H 7.35-7.22 (m, 5H, C_6H_5), 5.69 (m, 2H, *H*-8, *H*-9), 4.92 (dd, *J* = 6.9, 1.2 Hz, 1H, *H*-3), 4.85 (d, *J* = 9.9 Hz, 1H, *H*-10b), 4.12 (dd, *J* = 9.0, 6.9 Hz, 1H, *H*-2), 3.96 (dd, *J* = 9.0, 1.2 Hz, 1H, H-2), 3.60 (s, 3H, CH_3O), 3.18 (s, 1H, *H*-6), 2.70 (m, 1H, *H*-10a), 2.50 (m, 1H, *H*-6a), 2.43 (m, 2H, *H*-10), 2.20 (m, 1H, *H*-7), 2.00 (m, 1H, H-7). **^{13}C NMR** (100.6 MHz, $CDCl_3$): δ_C 170.2, 162.0, 140.6, 127.2, 128.0-126.8, 124.8-124.4, 87.1, 73.6, 59.4, 53.9, 52.2, 33.5, 32.6, 28.0, 25.1. **IR** (film): 1667, 1738 (CO) cm^{-1}.

***(3R,6R,6aR,10aS,10bR)*-Methyl-6-(2-(1,3-dioxolan-2-yl)ethyl)-5-oxo-3-phenyl-3,5,6,6a,7,10,10a,10b-octahydro-2*H*-oxazolo[2,3-*a*]isoquinoline-6-carboxylate (32)**

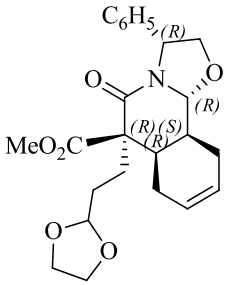

32

In a two-neck round-bottom flask, a solution of isoquinoline **31** (880 mg, 2.69 mmol) in dry DMF (2 mL) was added to a cooled (0 ºC) suspension of NaH (60% dispersion in mineral oil, 161 mg, 4.03 mmol) in anhydrous DMF under an inert atmosphere; the resulting mixture was stirred at 0 ºC for 1 h. 2(2-bromoethyl)-1,3-dioxolane (1.59 mL) and TBAI (198 mg, 0.54 mmol) were added at 0 ºC, and the mixture was stirred overnight at rt.The reaction was quenched by addition of NH_4Cl saturated solution, and the mixture was extracted firstly with Et_2O and then with DCM. The organic phases were dried on $MgSO_4$, and the resulting phase was concentrated *in vacuo*. The crude was purified by FC (*n*-Hex/EtOAc 7:3 → 1:1) and afforded the product **32** (920 mg, 2.15 mmol, 80%).

^{1}H-NMR (400 MHz, $CDCl_3$): δ_H 7.20-7.10 (m, 5H, Ar*H*), 5.67 (m, 2H, *H*-8, *H*-9), 4.92 (dd, *J* = 6.8, 1.6 Hz, 1H, *H*-3'), 4.90 (d, *J* = 9.6 Hz, 1H, *H*-10b), 4.61 (t, *J* = 4.8 Hz, 1H, $CH_2CH_2CHO_2$), 4.13 (dd, *J* = 9.2, 6.8 Hz, 1H, *H*-2), 4.05 (dd, *J* = 9.2, 1.6 Hz, 1H, *H*-2), 3.80-3.75 (2m, 4H, OCH_2CH_2O), 3.71 (s, 3H, CH_3O), 2.58 (dd, *J* = 9.6, 4.8 Hz, 1H, *H*-10a), 2.46 (m, 2H, *H*-10), 2.27 (ddd, *J* = 11.6, 5.6, 3.6 Hz, 1H, *H*-6a), 2.16 (tm, *J* = 17.2 Hz, 1H, *H*-7) 1.99 (m, 2H, $CH_2CH_2CHO_2$), 1.85 (dm, *J* = 17.2 Hz 1H, *H*-7), 1.44 (m, 2H, $CH_2CH_2CHO_2$). **^{13}C-NMR** (100.6 MHz, $CDCl_3$): δ_C 171.8, 165.1, 141.5, 128.3, 127.4, 126.6, 124.6-124.3, 104.1, 87.0, 73.5, 64.6, 59.7, 58.4, 51.9, 40.0, 33.4, 31.4, 29.4, 25.7-25.6. **$[\alpha]^{22}_D$**= – 35.2 (*c* 0.7, $CHCl_3$). **HRMS** (*m/z*): $[M+H]^+$ calcd for $C_{25}H_{33}NO_5$, 427.24; found 428.37.

***(4R,4aR,8aS)*-tert-butyl-4-(2-(1,3-dioxolan-2-yl)ethyl)-4-(hydroxymethyl)-3,4,4a,5,8,8a-hexahydroisoquinoline-2(1H)-carboxylate (37)**

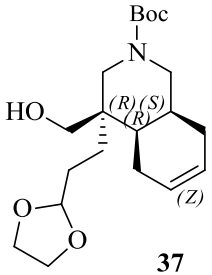

37

First step: liquid ammonia was condensed at -78 ºC in a three-necked, 100 mL round-bottomed flask, equipped with a coldfinger condenser and charged with dry-ice acetone; a solution of lactam **32** (200 mg, 0.454 mmol) in THF (10 mL) was added. The temperature was raised at -33 ºC for 2 minutes and sodium metal was added in small portions until the blue color persisted. The mixture was stirred at -33 ºC for 2 minutes. After this time, the reaction was quenched with solid NH_4Cl until the blue color disappeared, and the solution was leave stirring at rt for about 2h. The residue was digested at rt with DCM and the resulting suspension was filtered on celite. The organic solvent was evaporated at reduced pressure and the crude afforded was employed for the next reaction without further purification.

Second step: $LiAlH_4$ (235 mg, 6.21 mmol in dioxane) was added dropwise under inert atmosphere at 0 °C to a solution of the previous reaction in anhydrous dioxane (14 mL), and the mixture was stirred at

reflux temperature overnight. After cooling the reaction at 0 ºC, it was quenched with distilled water (x3) and NaOH at 5%. Take care during this process and add water only when argon flux is open; Na_2SO_4 is added as solid in the reaction flask. The crude was filtered through celite and the solvent was reduced *in vacuo*. The yellow oil obtained was used in the next step without any further purification.

Third step: Di-*tert*-butyl-dicarbonate (98 mg, 0.455 mmol) was added dropwise to a solution of the previous amino alcohol in anhydrous DCM (7 mL) at rt under inert atmosphere, and the resulting mixture was stirred for 20 h. Saturated aqueous NH_4Cl was added. The aqueous phase was extracted with DCM and the organic phases were collected and washed with a saturated aqueous solution of NaCl, dried on $MgSO_4$.

The crude was purified by FC (*n*-Hex/EtOAc 9:1 → 1:1) and afforded the molecule **37** in 45% (75 mg, 0.204 mmol) overall yield.

^{1}H NMR (400 MHz, $CDCl_3$): δ_H 5.60 (m, 2H, *H*-6 *H*-7), 4.87 (t, *J* = 4.8 Hz, 1H, $CH_2CH_2CHO_2$), 3.98 -3.85 (2m, 4H, OCH_2CH_2O), 3.62-3.59 (m, 2H, *H*-1, *H*-3), 3.42 (s, 2H, CH_2OH), 2.77-2.67 (m, 2H, *H*-1, *H*-3), 2.30-1.98 (m, 4H, *H*-5, *H*-8, *H*-8a), 1.96-1.78 (m, 2H, *H*-8, *H*-4a), 1.76-1.58 (4H, $CH_2CH_2CHO_2$, m), 1.45 (s, 9H, $(CH_3)_3C$)**. ^{13}C NMR (**100.6 MHz, $CDCl_3$): δ_C 124.8, 104.7, 79.5, 68.2, 64.9, 45.4, 34.2, 28.4, 27.9, 27.21, 24.0, 21.6. $[\boldsymbol{\alpha}]_{\boldsymbol{D}}^{\mathbf{22}}$: -8.34 (*c* 0.44, DCM). **HRMS** (*m/z*): $[M+Na]^+$ calcd for $C_{20}H_{33}NO_5$, 390.2251; found 390.2263.

***(4R,4aR,8aS*)-tert-butyl-4-(2-(1,3-dioxolan-2-yl)ethyl)-4-(azidomethyl)-3,4,4a,5,8,8a-hexahydroisoquinoline-2(1H)-carboxylate (39)**

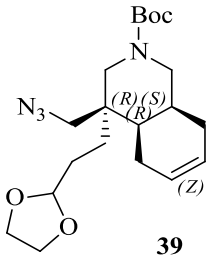

39

First step: in a two-neck round-bottom flask, anhydrous Et_3N (2.18 mL, 15.6 mmol) and MsCl (1.21 mL, 15.6 mmol) were added at 0 ºC under inert atmosphere to a stirred solution of alcohol **37** (1.98 g, 5.21 mmol) in dry DCM (86 mL), and the resulting mixture was stirred at rt for 4h. The reaction was quenched adding aqueous saturated NH_4Cl solution, and extracted with DCM/H_2O; the collected organic phases were dried on $MgSO_4$ and the volume reduced *in vacuo*. The resulting mesylate **38** was obtained as yellow oil and was used in the next step without purification.

Second step: NaN_3 (2.03 g, 31.2 mmol) was added to a solution of the previous mesylate **38** in dry DMF (15 mL), and the mixture was heated to 90 ºC. After 48 h, more NaN_3 (2.03 g, 31.2 mmol) was added and the resulting mixture was stirred at 90 ºC for an additional 24 h. The reaction was quenched by adding distilled water. The aqueous layer was extracted with DCM and the organic layers were dried on $MgSO_4$;

solvent volume was reduced *in vacuo*. The mixture was purified by FC (*n*-Hex → *n*-Hex/EtOAc 1:1) yielding azide **39** (1.6 g, 4.12 mmol, 79%).

^{1}H NMR (400 MHz, $CDCl_3$): δ_H 5.48 (m, 2H, *H*-6, *H*-7), 4.72 (t, *J* = 4.8 Hz, 1H, *H*-3',), 3.85- 3.72 (2m ,4H, O*CH*$_2$*CH*$_2$O), 3.62-3.59 (m, 2H, *H*-1, *H*-3), 3.10 (m, 2H, *CH*$_2$N$_3$), 2.63-2.49 (m, 2H, *H*-1, *H*-3), 2.08-1.88 (m, 4H, *H*-5, *H*-8, *H*-8a), 2.08-1.44 (m, 10H, *H*-1', *H*-2' *H*-8, *H*-4a, *H*-5, *H*-8a), 1.35 (s, 9H, (*CH*$_3$)$_3$C). **^{13}C NMR** (100.6 MHz, $CDCl_3$): δ_C 124.5, 123.9, 104.6, 79.6, 64.8, 44.1, 43.3, 39.7, 34.7, 28.3, 27.7, 25.7, 21.5. $[\boldsymbol{\alpha}]_{\boldsymbol{D}}^{\mathbf{22}}$: -35.18 (*c* 0.595, CH_2Cl_2). **HRMS** (*m/z*): $[M+Na]^+$ calcd for $C_{20}H_{32}N_4O_4$, 415.2316; found 415.2334.

***(4S,4aS,6S,8aS)*-tert-butyl-4-(2-(1,3-dioxolan-2-yl)ethyl)-7-hydroxy-9-tosyloctahydro-6,4-(epiminomethano)quinoline-1(2*H*)-carboxylate (42)**

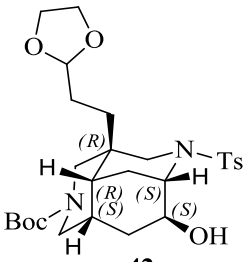

42

First step: in a two-neck round-bottom flask, *m*-chloroperoxybenzoic acid (317 mg, 1.84 mmol) was added to a cold solution (0 ºC) of azide **39** (327 mg, 0.83 mmol) in DCM (12 mL); the mixture was allowed to warm slowly to rt. After 5 h the reaction was quenched adding an aqueous solutions of 1:1 $NaHCO_3$ and saturated $Na_2S_2O_3$, than extracted firstly with Na_2SO_3 10% and secondly with DCM. The organic extracts were dried on $MgSO_4$ and concentrated *in vacuo*, to yield the azido epoxide **40**, used in the next step without purification.

Second step: Me_3P (1.33 mL, 1.33 mmol) was added to a solution of the azido epoxide **40** in THF (16 mL) and H_2O (16 mL), and the mixture was stirred at rt overnight. The diazatricyclic intermediate **41** was obtained after evaporation of the organic phase *in vacuo.*

Third step: Et_3N (0.12 mL, 0.83 mmol) was added dropwise to a stirring solution of the aminoalcohol **41** in dry DCM (14 mL) at 0 ºC.

A solution of *p*-toluensulfonyl chloride (158 mg, 0.83 mmol) in dry DCM was transferred *via* cannula and the stirring continued at 0 ºC for about 2.5/3 h. The reaction was quenched by adding saturated aqueous NH_4Cl solution and the aqueous layer was extracted with DCM. The combined organic extracts were dried on $MgSO_4$ and concentrated *in* vacuo. The raw material was purified by FC (*n*-Hex/EtOAc 9:1 → 1:1) to afford the protected tricyclic compound **42** (89 mg, 0.166 mmol, 20%).

^{1}H NMR (400 MHz, $CDCl^3$, COSY, HSQC): δ_H 7.64 (d, *J* = 8.2 Hz, 2H, *H-o* Ts), 7.22 (d, *J* = 8.1 Hz, 2H, *H-m* Ts), 4.60 (s, 1H, *H*-3'), 3.96 (s, 1H, *H*-6), 3.90 (hidden signal, 2H, *H*-1, *H*-3), 3.86 (m, 2H, CH_2O), 3.83 (hidden signal, 1H, *H*-7), 3.76 (m, 2H, CH_2O), 3.24 (d, *J* = 12.9 Hz, 1H, *H*-10), 3.03 (d, *J* = 12.5 Hz, 1H, *H*-10), 2.78-2.60 (m, 2H, H-1, H-3), 2.33 (s, 3H, CH_3Ts), 1.97 (m, 1H, H-8a), 1.92 (d, *J* = 16.0 Hz, 1H, *H*-5), 1.64-1.59 (m, 3H, 2*H*-8, *H*-5), 1.45 (m, 1H, *H*-4a), 1.41-1.35 (m, 13H, (CH_3)$_3$C, H-1', H- 2'). **^{13}C NMR** (100.6 MHz, $CDCl_3$): δ_C 155.3, 143.3, 137.6, 129.9, 127.2, 104.4, 80.0, 67.3, 64.8, 50.8, 49.6-48.4, 46.8, 35.2, 32.4, 32.3, 30.7, 29.4, 28.2, 27.3, 21.9, 21.1. $[\boldsymbol{\alpha}]_{\boldsymbol{D}}^{\mathbf{22}}$: = +24.01 (*c* 1.5, $CHCl_3$). **HRMS** (*m/z*): $[M+H]^+$ calcd for $C_{27}H_{40}N_2O_7$, 537.2629; found 537.2613.

***(4S,4aS,6S,8aS)*-tert-butyl-4-(2-(1,3-dioxolan-2-yl)ethyl)-7-oxo-9-tosyloctahydro-6,4-(epiminomethano)quinoline-1(2*H*)-carboxylate (43)**

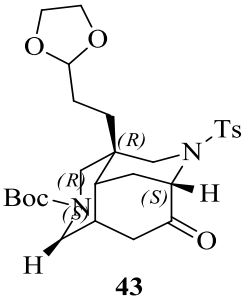

43

In a two-neck round-bottom flask, Dess-Martin periodinane (840 mg, 1.98 mmol) was added to a solution of alcohol **42** in DCM at 0 °C. The reaction was stirred overnight at rt. After this time aqueous saturated solutions 1:1 of $NaHCO_3$ and NaS_2O_3 were added, and the resulting mixture was extracted with DCM. The organic layer was dried on $MgSO_4$ and concentrated under reduced pressure. The crude was purified by FC (*n*-Hex → *n*-Hex:EtOAc 1:1) and afforded oxidized product **43** (910 mg, 1.70 mmol, 86%).

^{1}H NMR (400 MHz, $CDCl_3$, COSY, HSQC): δ_H 7.70 (d, *J* = 8. Hz, 2H, *H-o* Ts), 7.70 (d, *J* = 8. Hz, 2H, *H-o* Ts), 7.23 (d, *J* = 8.0 Hz, 2H, *H-m* Ts), 4.85 (s, 1H, *H*-3'), 4.35 (s, 1H, H-6), 3.98 (m, 2H, C*H*$_2$O), 3.86 (m, 2H, C*H*$_2$O), 3.76-3.55 (br, 3H, *H*-1, *H*-3, *H*-10), 2.78-2.59 (br, 3H, *H*-1, *H*-3, *H*-10), 2.48-2.42 (m, 1H, H-5), 2.37 (s, 3H, C*H*$_3$Ts),

2.35-2.29 (m, 1H, H-8), 2.11 (s, 1H, H-8a), 1.72- 1.63 (m, 3H, *H*-4a, *H*-8, *H*-5), 1.58-1.54 (2H, H-2', m), 1.41-1.32 (m, 11H, (CH_3)$_3$C, H-1'). **^{13}C NMR** (100.6 MHz, $CDCl_3$): δ_C 205.1, 155.0, 143.5, 134.4, 129.8, 127.0, 104.1, 80.1, 64.9, 56.9, 50.8-47.2, 47.0, 43.1, 36.3, 34.1, 29.4, 29.1, 28.2, 27.5, 21.4. **IR** (film): 1715 (C=O) cm^{-1}, 1688 (C=O) cm^{-1}. $[\boldsymbol{a}]_{\boldsymbol{D}}^{\mathbf{22}}$: +12.46 (*c* 3.15, $CHCl_3$). **HRMS** (*m/z*): $[M+NH_4]^+$ calcd for $C_{28}H_{40}N_2O_7S$, 566.2894; found 566.2894.

B2.8 Synthesis of Fragment C-13/C-20

3-Bromo-1-(tert-butyl)dimethylsilyloxy)propane (48)

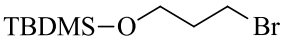

48

In a two-neck round-bottom flask, Et_3N (3,6 mL, 26.0 mmol), DMAP (122 mg, 1.0 mmol), and TBDMSCl (3.6 g, 26.0 mmol) were added to a solution of 3-brome-1-propanol (1.8 mL, 20 mmol) in dry THF (30 mL). After stirring for 18 h at rt, aqueous saturated solution of NH_4Cl was added. The aqueous phase was extracted with DCM, the organic layer collected dried on $MgSO_4$ and, in the end, concentrated under reduced pressure. The mixture of products was purified by FC (*n*-Hex → *n*-Hex/EtOAc 8:2) and yielded the product **48** (4.86 g, 19.2 mmol, 96%).

^{1}H NMR (400 MHz, $CDCl_3$): δ_H 3.73 (t, *J* = 5.4 Hz, 2H, *H*-3), 3.51 (t, *J* = 6.6 Hz, 2H, H-1), 2.03 (m, 2H, H-2), 0.90 (s, 9H, $(CH_3)_3C$), 0.07 (s, 6H, $(CH_3)_2Si$). **^{13}C NMR** (100.6 MHz, $CDCl_3$): δ_C 60.4, 35.5, 30.7, 25.9, 18.3, 5.4.

(3-((Tert-butyldimethylsilyl)oxy)propyl)triphenylphosphonium bromide (49)

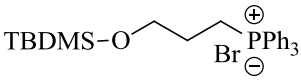

49

In a two-neck round-bottom flask, solid PPh_3 was added, in inert atmosphere, to a solution of protected alcohol **48** (4.0 g, 15.9 mmol) in dry benzene (3 mL); the resulting mixture was stirred at 85 °C for 18 h. The reaction was allowed to cool at rt, and Et_2O was added; the volume of the solvent was reduced *in vacuo*. The crude was purified by FC (*n*-Hex → DCM/MeOH 9:1) and afforded the phosphonium salt **49** (7.9 g, 15.26 mmol, 96%).

Mp: 216 °C.

^{1}H NMR (300 MHz, CDCl3): δ_H 7.90-7.69 (m, 15H, C_6H_5), 3.98 (m, 4H, *H*-1, *H*-3), 1.95 (m, 2H, *H*-2), 0.85 (s, 9H, (CH_3)3C), 0.04 (s, 6H, CH_3Si).

13C NMR (100.6 MHz, CDCl3): δ_C 134.9, 133.7-130.3, 118.8-118, 61.8-61.6, 2.1-26.0, 25.9, 19.2-18.7, 18.2, 5.3. **HRMS** (*m/z*): $[M+H]^+$ calcd for $C_{21}H_{22}OP$–TBDMSi, 321.1403; found 321.1398.

Methyl-*(Z)*-8-((tert-butyldimethylsilyl)oxy)oct-5-enoate (50)

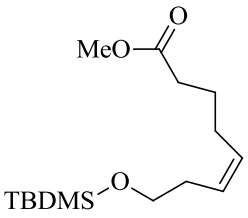

50

In a two-neck round-bottom flask, NaHMDS (21.36 mL of a 1 M solution in THF, 21.36 mmol) was added dropwise, under inert atmosphere at -30 ºC, to a solution of the phosphonium salt **49** (10 g, 19.42 mmol) in THF (240 mL) and toluene (48 mL). The orange reaction was stirred for 5h and 30' at -30 ºC. A solution of the aldehyde **46** (5.05 g, 38.83 mmol) in THF (20 mL) was added at -78 ºC; the reaction was allowed to warm at rt and was leave stirring overnight. Aqueous saturated NH_4Cl was added and the mixture was extracted with EtOAc. The organic phase was dried on $MgSO_4$ and was evaporated under reduced pressure. Product **50** (4.7 g, 16.5 mmol) was afforded after FC purification (*n*-Hex → *n*-Hex:EtOAc 8:2) in 85% yield.

^{1}H NMR (400 MHz, $CDCl_3$, COSY, gHSQC): δ_H 5.40 (m, 2H, *H*-5, *H*-6), 3.67 (s, 3H, CH_3O), 3.60 (t, *J* = 6.4 Hz, 2H, CH_2OSi), 2.31 (t, *J* = 8.0 Hz, 2H, H-2), 2.25 (m, 2H, *H*-7), 2.08 (m, 2H, H-4), 1.69 (m, 2H, H-3), 0.89 (s, 9H, $(CH_3)_3CSi$), 0.05 (s, 6H, $(CH_3)_2Si$). **^{13}C NMR**

(75.4 MHz, $CDCl_3$): δ_C 174.1, 130.3-126.9, 62.9, 51.5, 33.5, 31.1, 26.7, 25.9, 24.8, 18.3, 5.3. **IR** (film): 1742 (COO) cm^{-1}. **HRMS** (*m/z*): $[M+H]^+$ calcd for $C_{15}H_{30}O_3Si$, 287.2000; found 287.2042.

Methyl-*(Z)*-8-bromooct-5-enoate (52)

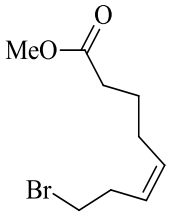

52

Mesylation step: in a two-neck round-bottom flask, Et_3N (190 μL, 1.35 mmol) and MsCl (130 μL, 1.8 mmol) were added at 0 °C, to a solution of alcohol **50** (135 mg, 0.9 mmol) in dry DCM (12 mL). The reaction was allowed to warm at rt and was stirred for 2 h. Aqueous saturated NH_4Cl was added to quench the reaction, and the phase was extracted with DCM. The organic layer was dried on $MgSO_4$ and evaporated *in vacuum*. The mesylate intermediate was obtained in 99% yield after FC purification (n-Hex-EtOc 8:2 → 6:4).

Bromination step: under inert atmosphere, a solution of LiBr (2.9 g, 33.3 mmol) in THF (13 mL) was added to a solution of previous mesylate (818 mg, 3.33 mmol) in DCM (9.3 mL) at 0 °C. The reaction was stirred overnight at rt. The reaction was quenched by addiction of distilled H_2O and the aqueous phase was extracted with DCM. The organic layer was dried on $MgSO_4$ and the volume reduced *in vacuo*. Derivative **52** was yielded (587 mg, 2.5 mmol, 75%) after FC purification (*n*-Hex → *n*-Hex/EtOAc 3:7).

^{1}H NMR (300 MHz, $CDCl_3$): δ_H 5.56 (m, 1H, CH=), 5.41 (1H, CH=, m), 4.21 (t, *J* = 6.8 Hz, 2H, *H*-8), 3.67 (s, 3H, C*H*$_3$O), 2.55 (qd, *J* = 7.2, 1.2 Hz 2H, *H*-7), 2.36 (t, *J* = 7.2 Hz, 2H, *H*-2), 2.14 (m, 2H, *H*-4), 1.71 (m, 2H, *H*-3). **^{13}C NMR** (100.6 MHz, $CDCl_3$): δ_C 173.8, 132.6, 69.0, 51.5, 37.4, 32.2, 27.3-26.6, 24.5. **IR** (film): 1730 (COO) cm^{-1}.

***(Z)*-[(8-Methoxycarbonyl)-3-octen-1-yl]triphenylphosphonium bromide (53)**

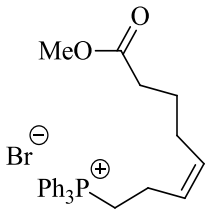

53

In a two-neck round-bottom flask, PPh_3 (113 mg, 0.43 mmol) was added under inert atmosphere to a solution of **52** (100 mg, 0.43 mmol) in dry benzene (1.2 mL). Reaction was stirred for 18 h at 85 °C, then allowed to cool at room temperature. After removal of organic phase under reduced pressure, the crude was purified by FC (*n*-Hex → DCM:MeOH) yielding the phosphonium salt **53** (201 mg, 0.40 mmol, 94%). Once this product was obtain, before its use in the further reaction, was dried under *vacuum* connected to a P_2O_5 system.

^{1}H NMR (400 MHz, $CDCl_3$): δ_H 7.92-7.67 (m, 15H, C_6H_5), 5.65 (m, 1H, C*H*=), 5.38 (m, 1H, C*H*=), 4.00 (m, 2H, *H*-8), 3.60 (s, 3H, CH_3O), 2.43 (m, 2H, *H*-7), 2.21 (t, *J* = 7.2 Hz, 2H, *H*-2), 1.85 (2H, H-4, q, *J* = 7.6 Hz), 1.57 (m, 2H, H-3). **^{13}C NMR** (100.6 MHz, $CDCl_3$): δ_C 173.9, 135.0-134.9, 131.0, 133.8-133.7-130.5-130.4, 127.4-127.2, 118.8-117.9, 51.4, 33.2, 26.5, 24.4, 23.2, 20.3.

B2.9 Synthesis of Fragment C-21/C-32

(Triisopropyloxy)-3-butane (55)

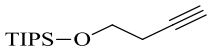

55

In a two-neck round-bottom flask under inert atmosphere, TIPSCl (8.2 g, 42.8 mmol) was added at 0 °C to a stirred solution of imidazole (3.3 g, 48.5 mmol) and but-3-yn-1-ol (2 g, 28.53 mmol) in dry DMF (7 mL). The mixture was then allowed to warm at rt and stirred for 4 h. An aqueous saturated solution of NH_4Cl was added to quench the reaction. The aqueous phase was extracted with DCM and the organic layer was dried on $MgSO_4$ and the volume reduced *in vacuo*. Purification by FC (*n*-Hex → *n*-Hex/EtOAc 9:1) afforded the protected alcohol **55** (5.75 g, 25.39 mmol) in 89% yield.

^{1}H NMR (400 MHz, $CDCl_3$): δ_H 3.80 (t, 2H, *H*-1), 2.42-2.38 (m, 2H, *H*-2), 1.92 (s, 1H, H-4), 1.11-1.03 (m, 21H, TIPS-H). **^{13}C NMR** (100.6 MHz, $CDCl_3$): δ_C 81.30, 69.24, 62.03, 31.62, 22.90, 17.90, 11.97.

5-((Triisopropylsilyl)oxy)pent-2-yn-1-ol (57)

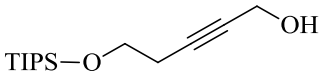

57

In a two-neck round-bottom flask, under inert atmosphere at -78 °C, *n*-BuLi (11.1 mL, 27.66 mmol) was added to a solution of protected alcohol (5.68 g, 25.25 mmol) in dry THF (72 mL). The reaction was stirred for 15' and was allowed to warm at 0 °C. HCHO was added (830 mg, 27.66 mmol) and reaction was warmed at rt and stirred for 5 h. HCl 1 M was added and the mixture was extracted with Et_2O. The crude was purified by FC (*n*-Hex → *n*-Hex/EtOAc 8:2) and afforded product **57** (5.63 g, 21.96 mmol) in 87% yield.

^{1}H NMR (400 MHz, $CDCl_3$): δ_H 4.25-4.23 (m, 2H, *H*-5), 3.80 (t, 2H, *H*-1), 2.49-2.45 (tt, 2H, *H*-2), 1.12-1.07 (m, 21H, TIPS-*H*). **^{13}C NMR** (100.6 MHz, $CDCl_3$): δ_C 83.18, 62.05, 51.13, 23.13, 17.86, 11.91.

9-((Triisopropylsilyl)oxy)nona-3,6-diyn-1-ol (58)

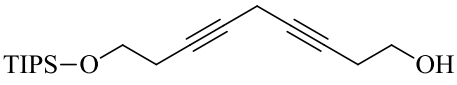

58

First step: in a two-neck round-bottom flask, TsCl (4.145 g, 21.77 mmol) was added to a solution of the alcohol **57** (4.65 g, 18.14 mmol) in Et_2O (91 mL) at 0 °C. KOH (5.08 g, 90.12 mmol) was added and the reaction was stirred for 2 h. Aqueous saturated solution of NH_4Cl was added and the mixture was extracted with EtOAc/brine and the organic phase was dried on $MgSO_4$. Solvent was evaporated under reduced pressure. Tosylated product was used in the next reaction without further purification.

Second step: to a solution of the protected intermediate in dry DMF (91 mL), K_2CO_3 (3.76 g, 27.21 mmol), CuI (3.45 g, 18.14 mmol), NaI (2.72 g, 18.14 mmol) and, in the end, but-3-yn-1-ol (1.32 g, 18.09 mmol) were added, and the mixture was stirred overnight at 40 °C. The reaction was quenched by addiction of aqueous saturated solution of NH_4Cl. The mixture was firstly filtered on celite, and once the two phases were separated they were extracted with Et_2O. The resulting organic layer was evaporated *in vacuo*. Product **58** (4.80 g, 15.55 mmol) was afforded through FC (*n*-Hex → *n*-Hex/EtOAc 85:15) in 86% yield.

^{1}H NMR (400 MHz, $CDCl_3$): δ_H 3.76 (t, 2H, *H*-1), 3.67 (t, 2H, *H*-9), 3.11 (m, 2H, *H*-5), 2.44-2.37 (m, 4H, *H*-2, *H*-8), 1.10-1.02 (m, 21H, TIPS-*H*). **^{13}C NMR** (100.6 MHz, $CDCl_3$): δ_C 75.18, 70.97, 62.15, 61.04, 23.12-23.05, 17.90, 11.93, 9.71.

***(3Z,6Z)*-9-((Triisopropylsilyl)oxy)nona-3,6-dien-1-ol (59)**

59

In a three-neck round-bottom flask, $NaBH_4$ (425 mg, 11.24 mmol) was added portionwise to a stirred solution of $Ni(OAc)_2$ x 4 H_2O (2.4 g, 9.55 mmol) in dry MeOH (191 mL) at rt under inert atmosphere. Argon atmosphere was replaced with H_2 and a purple coloration was appreciated. EDA was added and the mixture was stirred for 30'. After addition of starting material (1.73 g, 5.62 mmol) in anhydrous MeOH (14 mL), other 2 h passed before quenching the reaction. The mixture was filtered on celite and washed with Et_2O. The volume of the organic phase was reduced and re-extracted with brine and DCM. The intermediate was used in the next two reaction without further purification.

^{1}H NMR (400 MHz, $CDCl_3$): δ_H 5.55-5.31 (m, *J* = 9.15, 5.76, 4.34, 1.66 Hz, 4H, *H*-3, *H*-4, *H*-6, *H*-7), 3.71 (t, 2H, *H*-1), 3.14 (t, 2H, *H*-9), 2.82 (t, 2H, *H*-5), 2.67 (q, 2H, *H*-2), 2.31 (q, 2H, *H*-9), 1.13-1.04 (m, 21H, TIPS-*H*). **^{13}C NMR** (100.6 MHz, $CDCl_3$): δ_C 130.57, 128.90, 128.14, 126.67, 63.01, 31.47-31.29, 25.94, 18.08, 11.99.

([(3Z,6Z)-9-Iodo-1-[(triisopropylsilyl)oxy]-3,6-nonadien (61)

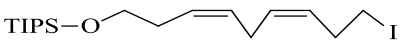

61

First step: in a two-neck round-bottom flask, the reduced alcohol (1.73 g, 5.62 mmol) was cooled at 0 °C in DCM (14 mL). Et_3N (295 mg, 7.87 mmol) was added, followed by MsCl (269 mg, 6.74 mmol). After stirring 2 h, an aqueous saturated solution of NH_4Cl was added and the mixture was extracted with DCM, dried over $MgSO_4$ and the volume reduced *in vacuo*. The crude was used in the next reaction without further purification.

Second step: in a solution of the mesylate intermediate in dry acetone (34 mL), NaI (3.37 g, 22.48 mmol) was added and the mixture was stirred at reflux temperature for 2 h. The reaction was allowed to cool at room temperature, and after addition of brine and a saturated solution of tiosulphate the aqueous layer was extracted with hexane. Purification of the crude by FC (*n*-Hex → *n*-Hex/EtOAc 95:5) afforded the iodine derivate **61** (1.52 g, 3.60 mmol) in 64% overall yield.

^{1}H NMR (400 MHz, $CDCl_3$): δ_H 5.43-5.37 (m, *J* = 9.15, 5.76, 4.34, 1.66 Hz, 4H, *H*-3, *H*-4, *H*-6, *H*-7), 3.83 (t, 2H, *H*-1), 3.17 (t, 2H, *H*-9), 2.63 (t, 2H, *H*-5), 2.53 (q, 2H, *H*-2), 2.15 (q, 2H, *H*-9), 1.13-1.04 (m,

21H, TIPS-*H*). **^{13}C NMR** (100.6 MHz, $CDCl_3$): δ_C 131.3, 128.8, 125.67, 64.10, 31.7, 25.6, 22.10, 17.90, 5.20.

B2.10 Synthesis of the model

2-(3-Cyclohexenyl)ethanol (64)

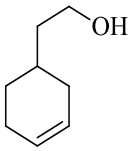

64

In a two-naked round-bottom flask, $BF_3{\cdot}Et_2O$ (7.5 mL, 61 mmol) was added dropwise over 30 minutes under inert atmosphere, to a cooled (0 ºC) solution of 2-methyl-2-butene (61 mL of a 2 M solution in THF, 122 mmol) and $NaBH_4$ (1.2 g, 44.4 mmol) in anhydrous THF (28 mL), and the resulting mixture was stirred at 0 ºC for 1 h. 4-vinylcyclohexene (6 g, 55.5 mmol) was then added dropwise over a 5 minutes and the solution was stirred at rt for 2 h. The borane intermediate was oxidized by slowly addition at 0 ºC of NaOH 3N (50 mL) and H_2O_2 30% (50 mL), and the resulting solution was stirred overnight at 70 ºC. The resulting mixture was extracted with Et_2O and combined organic extract were dried over Na_2SO_4, filtered, and concentrated under reduced pressure affording alcohol **64** in 95% yield (6.65 g, 52.7 mmol).

^{1}H NMR (400 MHz, $CDCl_3$, COSY, gHSQC): δ_H 5.65 (m, 2H, *H*-1, *H*-2), 3.71 (t, *J* = 6.8 Hz, 2H, *H*-2'), 2.11 (dm, *J* = 14.8 Hz, 1H, *H*-3), 2.05 (m, 2H, *H*-6), 1.72 (m, 2H, *H*-4, *H*-5), 1.69 (dm, *J* = 14.8 Hz, 1H,

H-3), 1.54 (m, 2H, H-1'), 1.26 (m, 1H, *H*-5). **^{13}C NMR** (100.6 MHz, $CDCl_3$): δ_C 127.0-126.0, 60.8, 39.4, 31.7, 30.1, 28.8, 25.0. **IR** (film) 3400 (OH) cm^{-1}. **HRMS** (ESI): $[M+H]^+$ calcd for $C_8H_{14}O$, 127.1117; found: 127.1114.

4-(2-Azidoethyl)cyclohexene (66)

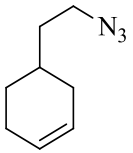

66

In a two-neck round-bottom flask, Et_3N (1.0 mL, 7.0 mmol) and MsCl (680 μL, 9.26 mmol) were added dropwise to a stirring solution of alcohol (584 mg, 4.63 mmol) in anhydrous DCM (58 mL) cooled to 0 ºC under inert atmosphere. After the end of addition, the mixture was allowed to heat slowly to rt and was stirred for additional 2 h. Aqueous saturated solution of NH_4Cl was added as quenching and the mixture was extracted with DCM. The combined organic layers were dried over anhydrous Na_2SO_4, filtered and the solvent was concentrated *in vacuo*. The crude was purified by FC (*n*-Hex/EtOAc 99:1 → 95:5) and the azide **66** (658 mg, 4.35 mmol, 94%) was obtained as colourless oil.

^{1}H NMR (400 MHz, $CDCl_3$): δ_H 5.66 (m, 2H, H-1, H-2), 3.33 (t, *J* = 6.9 Hz, 2H, H-2'), 2.05 (m, 3H, 2*H*-6, *H*-3), 1.80-1.53 (m, 5H, *H*-5, *H*-4, *H*-3, 2*H*-1'), 1.29 (m, 1H, *H*-5). **^{13}C NMR** (100.6 MHz, $CDCl_3$): δ_C 126.9-125.8, 49.1, 35.1, 31.3, 30.8, 28.4, 24.8.

8-Hydroxy-2-*(p*-toluenesulfonyl)-2-azabicyclo[3.3.1]nonane (68)

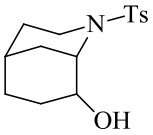

68

First step: in a two-neck round-bottom flask, *m*-chloroperoxybenzoic acid (5 g, 29 mmol) was added to a cold solution (0 ºC) of azide (1.5 g, 10 mmol) in DCM (102 mL); the mixture was allowed to warm slowly to rt. After 4 h the reaction was quenched adding an aqueous solution of 1:1 $NaHCO_3$ and saturated $Na_2S_2O_3$, then extracted firstly with Na_2SO_3 10% and secondly with DCM. The organic extracts were dried on Na_2SO_4 and concentrated *in vacuo*, to yield a mixture of epoxides, used in the next step without purification.

Second step: Me_3P (12.5 mL, 12.55 mmol) was added to a solution of the azido epoxide (10.0 mmol) in THF/H_2O (170 mL, 6:1), and the mixture was stirred at rt overnight. The diazatricyclic intermediate was obtained as a pale oil after evaporation of the organic phase *in vacuo.*

Third step: Et_3N (2.4 mL, 17.2 mmol) was added dropwise to a stirring solution of the aminoalcohol (15.6 mmol) in dry DCM (156 mL) at 0 ºC. A solution of *p*-toluensulfonyl chloride (3.87 g, 20.3 mmol) in dry DCM was transferred *via* cannula and the stirring continued at 0 ºC for about 4 h. The reaction was quenched by adding saturated aqueous NH_4Cl solution and the aqueous layer was extracted with DCM. The combined organic extracts were dried on $MgSO_4$ and

concentrated *in* vacuo. The raw material was purified by FC (*n*-Hex →*n*-Hex/EtOAc 1:1) to afford the protected tricyclic compound **68** (2.95 g, 8.58 mmol, overall yield 55%).

^{1}H NMR (400 MHz, $CDCl_3$): δ_H 7.70 (d, *J* = 8.1 Hz, 2H, *H*-o Ts), 7.30 (d, *J* = 8.1 Hz, 2H, *H*-m Ts), 4.10 (br. s, 1H, *H*-8), 3.75 (m, 1H, *H*-1), 3.50 (q, *J* = 6.3 Hz, 1H, *H*-3), 3.18 (q, *J* = 6.3 Hz, 1H, H-3), 2.43 (s, 3H, C*H*$_3$Ts), 1.26-2.05 (m, 9H, 2*H*-4, 2*H*-9, *H*-5, 2*H*-6, 2*H*-7). **^{13}C NMR** (100.6 MHz, $CDCl_3$): δ_C 143.2, 136.8, 129.6, 127.1, 68.7, 53.3, 40.9, 27.6, 25.8, 24.1, 23.3, 21.4. **IR** (film) 3600 (OH) cm^{-1}.

8-Oxo-2-(*p*-toluenesulfonyl)-2-azabicyclo[3.3.1]nonane (69)

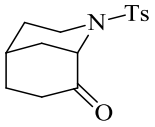

69

In a two-neck round-bottom flask, Dess-Martin periodinane (604 mg, 1.42 mmol) was added at the temperature of 0 °C, to a solution of the above alcohol (171 mg, 0.58 mmol) in DCM (19.5 mL). The reaction was allowed to reach rt and was stirred overnight. After this time aqueous saturated solutions 1:1 of $NaHCO_3$ and $Na_2S_2O_3$ were added, and the resulting mixture was extracted with DCM. The organic layer was dried on $MgSO_4$ and concentrated under reduced pressure. The crude was purified by FC (*n*-Hex → *n*-Hex:EtOAc 1:1) and afforded oxidized product **69** (41 mg, 0.139 mmol, 24%).

^{1}H NMR (400 MHz, $CDCl_3$): δ_H 7.65 (d, *J* = 8.0 Hz, 2H, *H*-o Ts), 7.28 (dd, *J* = 8.0, 0.8 Hz, 2H, *H*-m Ts), 4.21 (t, *J* = 2.8 Hz, 1H, *H*-1), 3.65 (dt, *J* =12.4, 6.0 Hz, 1H, *H*-3), 3.27 (m, 1H, *H*-3), 2.41 (s, 3H, C*H*$_3$ Ts), 2.28 (m, 2H, *H*-7), 2.12 (m, 3H, *H*-5, *H*-4, *H*-9), 1.95 (m, 1H, *H*-6), 1.84-1.89 (m, 3H, H-4, H-9, H-6). **^{13}C NMR** (100.6 MHz, $CDCl_3$): δ_C 207.7, 143.5, 129.5, 127.6, 59.2, 40.6, 38.1, 33.1, 30.6, 29.8, 23.6, 21.5. **IR** (film) 1716 (C=O) cm^{-1}. **HRMS** (*m/z*): $[M+H]^+$ calcd for $C_{15}H_{19}NO_3S$, 294.1158, found: 294.115.

Chapter B3

Bibliography

1. J. M. Kornprobst, *Encyclopedia of Marine Natural Products*, Wiley-VCH: Weinheim, 2010.
2. J. W. Blunt, B. R. Copp, R. A. Keyzers, M. H. G Munro and M. R. Prinsep, *Nat. Prod. Rep.*, 2013, **30**, 237–323 and previous reviews in this series.
3. J. C. Morris, *Nat. Prod. Rep.*, 2013, **30**, 783–805 and previous reviews in this series.
4. K. Fangming, I. E. Graziani and R. J. Andersen, *J. Nat. Prod.*, 1998, **61**, 267-271.
5. M. Amat, M. Pérez, R. Ballette, S. Proto and J. Bosch, *The Alkaloids*, 2015, **74**, 159-199.
6. J. H. H. L. de Oliveira, A. M. Nascimento, M. H. Kossuga, B. C. Cavalcanti, C. O. Pessoa, M. O. Moraes, M. L. Macedo, A. G. Ferreira, E. Hajdu, U. S. Pinheiro and R. G. S. Berlinck, *Journal of Natural Products*, 2007, **70**, 538-543.
7. F. Kong, R. J. Andersen and T. M. Allen, *J. Am. Chem. Soc.*, 1994, **116**, 6007−6008.
8. F. Kong, E. I. Graziani and R. J. Andersen, *J. Nat. Prod.*, 1998, **61**, 267−271.
9. F. Diaba, C. Pujol-Grau, A. Martínez-Laporta, I. Fernández and J. Bonjoch, *Org. Lett.*, 2015, **17**, 568−571.

10. M. Amat, R. Ballette, S. Proto, M. Pérez and J. Bosch, *Chem. Commun*., 2013, **49**, 3149-3151.
11. R. Ballette, M. Pérez, S. Proto, M. Amat and J. Bosch, *Angew. Chem. Int. Ed*., 2014, **53**, 6202-6205.
12. M. Amat, M. Cantó, N. Llor, V. Ponzo, M. Pérez, and J. Bosch, *Angew. Chem.*, 2002, **114**, 345–348.
13. M. Amat, M. Cantó, N. Llor, V. Ponzo, M. Pérez, and J. Bosch, *Angew. Chem. Int. Ed.*, 2002, **41**, 335–338.
14. M. Amat, M. Cantó, C. Escolano, E. Molins, E. Espinosa, and J. Bosch, *J. Org. Chem*., 2002, **67**, 5343–5351.
15. M. Amat, O. Bassas, M. Pericàs, M. Pastó, and J. Bosch, *Chem. Comm.*, 2005, **0**, 1327–1329.
16. H. Pellissier, *Tetrahedron*, 2003, **59**, 8291–8327.
17. H. Nagashima, N. Ozaki, M. Washiyama and K. Itoh, *Tetrahedron Lett.*, 1985, **26**, 657-660.
18. T. J. Hagen, *Synlett*, 1990, **1**, 63-66.
19. M. Amat, M. Pérez, A. T. Minaglia, N. Casamitjana, and J. Bosch, *Org. Lett*., 2005, **7**, 3653–3656.
20. R. H. Grubbs and S. Chang, *Tetrahedron*, 1998, **54**, 4413–4450.
21. (a) A. Fürstner, *Angew. Chem.*, 2000, **112**, 3140–3172; (b) *Angew. Chem. Int. Ed.* **2000**, *39*, 3012–3043.
22. B. Schmidt and J. Hermanns, *Top. Organomet. Chem.*, 2004, **7**, 223–267.

23. S. J. Connon and Blechert, *Top. Organomet. Chem.,* 2004, **7**, 93–124.
24. J. Prunet and L. Grimauld, L. *Comprehensive Organic Functional Group Transformations II*; A. R. Katritzky, R. J. K. Taylor, Eds.; Elsevier: Oxford, 2005, Vol. **1**, 669–722.
25. J. McGinnis, T. J. Katz and S. Hurwitz, *J. Am. Chem. Soc.*, 1976, **98**, 605–606.
26. T. J. Katz, J. McGinnis and C. Altus, *J. Am. Chem. Soc.*, 1976, **98**, 606–608.
27. T. J. Katz, S. J. Lee, and N. Acton, *Tetrahedron Lett.,* 1976, **17**, 4247–4250.
28. T. J. Katz and N. Acton, *Tetrahedron Lett.*, 1976, **17**, 4251–4254.
29. S. J. Lee, J. McGinnis and T. J. Katz, *J. Am. Chem. Soc.*, 1976, **98**, 7818–7819.
30. R. R. Schrock, J. S. Murdzek, G. C. Bazan, J. Robbins, M. DiMare, and M. O'Regan, *J. Am. Chem. Soc.,* 1990, **112**, 3875–3886.
31. R. R. Schrock, *Top. Organomet. Chem.*, 1998, **1**, 1–36.
32. R. R. Schrock, *Tetrahedron*, 1999, **55**, 8141–8153.
33. R. R. Schrock and A. H. Hoveyda, *Angew. Chem.*, 2003, **115**, 4740–4782.
34. R. R. Schrock and A. H. Hoveyda, *Angew. Chem. Int. Ed.*, 2003, **42**, 4592–4633.

35. R. Toreki and R. R. Schrock, *J. Am. Chem. Soc.*, 1990, **112**, 2448–2449.
36. S. T. Nguyen, L. K. Johnson, R. H. Grubbs and J. W. Ziller, *J. Am. Chem. Soc.*, 1992, **114**, 3974–3975.
37. P. Schwab, M. B. France, J. W. Ziller and R. H. Grubbs, *Angew. Chem.*, 1995, **107**, 2179–2181.
38. P. Schwab, M. B. France, J. W. Ziller and R. H. Grubbs, *Angew. Chem. Int. Ed. Engl.* 1995, **34**, 2039–2041.
39. P. Schwab, R. H. Grubbs and J. W. Ziller, *J. Am. Chem. Soc.*, 1996, **118**, 100–110.
40. For reviews of the utility of *N*-heterocyclic carbene ligands in transition-metal catalysis, see: W. A. Herrmann and C. Köcher, *Angew. Chem.*, 1997, **109**, 2257–2282.
41. W. A. Herrmann and C. Köcher, *Angew. Chem. Int. Ed. Engl.*, 1997, **36**, 2162–2187.
42. W. A. Herrmann, *Angew. Chem.*, 2002, **114**, 1342–1363.
43. W. A. Herrmann and C. Köcher, *Angew. Chem. Int. Ed.*, 2002, **41**, 1290–1309.
44. For examples of the development of novel catalysts for metathesis, see: H. Wakamatsu, and S. Blechert, *Angew. Chem.*, 2002, **114**, 2509–2511.
45. H. Wakamatsu, and S. Blechert, *Angew. Chem. Int. Ed.*, 2002, **41**, 2403–2405.

46. S. J. Connon, A. M. Dunne, and S. Blechert, *Angew. Chem.*, 2002, **114**, 3989–3993.
47. S. J. Connon, A. M. Dunne, and S. Blechert, *Angew. Chem. Int. Ed.*, 2002, **41**, 3835–3838.
48. J. J. van Veldhuizen, S. B. Garber, J. S. Kingsbury and A. H. Hoveyda, *J. Am. Chem. Soc.*, 2002, **124**, 4954–4955.
49. A. Fürstner, L. Ackermann, B. Gabor, R. Goddard, C. W. Lehmann, C. W. Mynott, F. Stelzer and O. R. Thiel, *Chem. Eur. J.*, 2001, **7**, 3236–3253.
50. J. L. Hérisson and Y. Chauvin, *Makromol. Chem.*, 1971, **141**, 161–176.
51. C. P. Casey and T. J. Burkhardt, *J. Am. Chem. Soc.*, 1974, **96**, 7808–7809.
52. T. J. Katz and J. McGinnis, *J. Am. Chem. Soc.*, 1975, **97**, 1592–1594.
53. R. H. Grubbs, P. L. Burk and D. D. Carr, *J. Am. Chem. Soc.*, 1975, **97**, 3265–3267.
54. R. H. Grubbs, D. D Carr, C. Hoppin and P. L. Burk, *J. Am. Chem. Soc.*, 1976, **98**, 3478–3483.
55. J. Sandri and J. Viala, *J. Org. Chem.*, 1995, **60**, 6627–6630.
56. J. Viala and R. Labaudinière, *J. Org. Chem.*, 1993, **58**, 1280–1292.

57. For general reviews of the Wittig reaction or selected aspects of it, see: L. D. Bergelson, and M. M. Shemyakin, *Angew. Chem., Int. Ed. Engl.*, 1964, **3**, 250–260.
58. S. Trippett, *Pure Appl. Chem.*, 1964, **9**, 255–270.
59. M. Schlosser, *Top. Stereochem.*, 1970, **5**, 1–30.
60. Y. Le Bigot, M. Delmas and A. Gaset, *Inform. Chim.*, 1984, **251**, 123–131.
61. H. J. Bestmann, *Pure Appl. Chem.*, 1979, **51**, 515–533.
62. I. Gosney and A. G. Rowley, *Organophosphorus Reagents in Organic Synthesis;* Cadogan, J. I. G., Ed.; Academic Press: New York, 1979, 7–153.
63. H. G. Bestmann and S. V. Ley, *Pure Appl. Chem.*, 1980, **52**, 771–788.
64. B. E. Maryanoff and A. B. Reitz, *Chem. Rev.*, 1989, **89**, 863–927.
65. E. Vedejs, M. J. Peterson, *Top. Stereochem.*, 1994, **21**, 1–215.
66. G. Wittig and G. Geissler, *Liebigs Ann. Chem.*, 1953, **580**, 44–57.
67. G. Wittig and W. Haa, *Chem. Ber.*, 1955, **88**, 1654–1666.
68. E. Vedejs and K. A. J. Snoble, *J. Am. Chem. Soc*., 1973, **95**, 5778–5780.
69. E. Vedejs, G. P. K. Meier, A. J. Snoble, *J. Am. Chem. Soc*. 1981, **103**, 2823–2831.

70. E. Vedejs and C. F. Marth, *J. Am. Chem. Soc*., 1990, **112**, 3905–3909.
71. K. K. Ogilvie, K. L. Sadana, E. A. Thompson, M. A, Quilliam and J. B. Westmore, *Tetrahedron Lett*., 1974, 2861.
72. K. K. Ogilvie, E. A. Thompson, M. A.; Quilliam and J. B. Westmore, *Tetrahedron Lett*., 1974, 2865-2868.
73. C. Ruecker, *Chemical Reviews*, 1995, **95**, 1009-1064.
74. C. A. Brown and V. Ahuja, *J.Chem .Soc. Chem. Commun*., 1973, **0**, 553-554.
75. S. Proto, M. Amat, M. Pérez, R. Ballette, F. Romagnoli, A. Mancinelli, and J. Bosch, *Org. Lett*., 2012, **14**, 3916-3919.

Curriculum Vitae

Date of Birth: May 2nd 1990

ELISA DE PAOLIS

Place of Birth: Rome, RM, Italy

Hometown: Rome, RM, Italy

Nationality: Italian

List of Publications

Quaglio, D.; Zappia, G.; De Paolis, E.; Balducci, S.; Botta, B.; Ghirga, F. Olefin metathesis reaction as a locking tool for macrocycles and mechanomolecules construction. Org. Chem. Front. 2018, Org. Chem. Front., 2018,5, 3022-3055 (doi 10.1039/c8qo00728d).

Berardozzi, S.; Bernardi, F.; Infante, P.; Ingallina, C.; Toscano, S.; De Paolis, E.; Alfonsi, R.; Caimano, M.; Botta, B.; Mori, M.; Di Marcotullio, L.; Ghirga, F. Synergistic inhibition of the Hedgehog pathway by newly designed Smo and Gli antagonists bearing the isoflavone scaffold. Eur. J. Med. Chem. 2018, 156, 554−562 (doi 10.1016/j.ejmech.2018.07.017).

Krasilnikova, J.; Lauberte, L.; Stoyanova, E.; Abadjieva, D.; Chervenkov, M.; Mori, M.; De Paolis, E.; Mladenova, V.; Telysheva, G.; Botta, B.; Kistanova, E. Oregonin from Alnus incana bark affects DNA methyltransferases expression and mitochondrial DNA copies in mouse

embryonic fibroblasts. J. Enzyme Inhib. Med. Chem. 2018, 33, 1055−1063 (doi 10.1080/14756366.2018.1476504).

List of Oral Presentations

Elisa De Paolis, Deborah Quaglio, Federica Aiello, Federica Balzano, Ilari D'Acquarica, Gloria Uccello Barretta, Silvia Balducci, Francesca Ghirga; "Snapshot of Ruthenium-Carbene-Resorc[4]arene Complex in an Olefin Metathesis reaction". **IASOC 2018,** Naples, Italy.

De Paolis, E.; Quaglio, D.; Mori, M.; Tottone, L.; Ingallina, C.; Corradi, S.; Screpanti, I.; Botta, B.; Palermo, R.; Ghirga; F. Inhibition of Notch signaling in T-cell acute lymphoblastic leukemia: a challenge posed by a novel chalcone derivative. **2nd Training School COST Action CM1407**, Universidade Lusófona de Humanidades eTecnologias in Lisbon, Portugal.

List of Poster Presentations

De Paolis, E.; Quaglio, D.; Aiello, F.; Balzano, F.; D'Acquarica, I.; Uccello Barretta, G.; Botta, B.; Balducci, S.; Ghirga, F.; "Snapshot of Ruthenium-Carbene-Resorc[4]arene Complex in an Olefin Metathesis reaction". **IASOC 2018**, Naples, Italy.

Mangiardi, L.; Ingallina, C.; Berardozzi, S.; De Paolis, E.; Ghirga, F.; Quaglio, D.; Mori, M.; Di Marcotullio, L.; Infante, P.; Alfonsi, R.; Botta, B. Inhibition of Hedgehog Pathway: a challenge posed by the isoflavone GlaB and its new derivatives. **VII European Workshop in Drug Synthesis**. Siena, Italy.

De Paolis, E.; Ghirga, F.; Ingallina, C.; Tortolini, C.; Mangiardi, L.; Mazzei, F.; Botta, B.; Quaglio, D.; Corradi, S. Synthesis of a new artificial linker resorc[4]arene-based system for immunosensors development. **Nanotech Middle East 2017** Conference and Exhibition, Dubai, Arabian Emirates.

Corradi, S.; Ghirga, F.; Mori, M.; Ingallina, C.; Berardozzi, S.; De Paolis, E.; Di Marcotullio, L.; Alfonsi, R.; Botta, B.; Quaglio, D. Identification of novel natural products chemotypes of Hedgehog-dependent tumors inhibitors. **2nd Training School of Cost Action 1407**, Lisbon, Portugal.

De Paolis, E.; Quaglio, D.; Mori, M.; Tottone, L.; Ingallina, C.; Corradi, S.; Screpanti, I.; Botta, B.; Palermo, R.; Ghirga, F. Inhibition of Notch signaling in T-cell acute lymphoblastic leukemia: a challenge posed by a novel chalcone derivative. **XLII A. Corbella, International Summer School**, Gargnano, Italy.

Corradi, S.; De Paolis, E.; Ingallina, C.; Berardozzi, S.; Ghirga, F.; Quaglio, D.; Mori, M.; Di Marcotullio, L.; Infante, P.; Alfonsi, R.; Botta, B. Gli1/DNA interaction is a druggable target for Hedgehog-dependent tumors. **XLII A. Corbella, International Summer School**, Gargnano, Italy.

Ghirga, F.; Mori, M.; Ingallina, C.; Berardozzi, S.; De Paolis, E.; Di Marcotullio, L.; Alfonsi, R.; Botta, B.; Quaglio, D. Inhibition of Hedgehog-dependent tumors and cancer stem cells by a newly identified naturally occurring chemotype. **3rd Meeting of COST Action CM1407, Challenging**

organic syntheses inspired by nature - from natural products chemistry to drug discovery, Cracovia, Poland.

De Paolis, E.; Quaglio, D.; Botta, B.; Ingallina, C.; Menta, S.; Pierini, M.; Ghirga, F. Synthesis of a basket-resorc[4]arene via metathesis reaction and encapsulation studies of fullerenes C60 and C70. **Young Chemists Symposium**, Rimini, Italy.

Ingallina, C.; Ghirga, F.; Quaglio, D.; Berardozzi, S.; De Paolis, E.; Mori, M.; Di Marcotullio, L.; Marianecci, C.; Botta, B. A new anticancer agent for Hedgehog-dependent tumors: from drug discovery to drug delivery. **Nanoscience & Nanotechnology**, Frascati, Italy.

De Paolis, E.; Ingallina, C.; Berardozzi, S.; Ghirga, F.; Quaglio, D.; Mori, M.; Di Marcotullio, L.; Infante, P.; Alfonsi, R.; Botta, B. Gli1/DNA interaction is a druggable target for Hedgehog-dependent tumors. **VI European Workshop in Drug Synthesis.** Siena, Italy.